Doctoral Dissertation (Censored)
博士論文（要約）

The advancement of alkenone paleothermometry: applications to coastal, lake, and subaerially exposed sediments

（アルケノン古水温計の新展開―沿岸・湖沼堆積物と堆積岩への適用―）

A Dissertation Submitted for the Degree of Doctor of Philosophy
December 2020
令和 2 年 12 月博士（理学）申請

Department of Earth and Planetary Science, Graduate school of Science
The University of Tokyo
東京大学大学院理学系研究科地球惑星科学専攻

Hiroto Kajita
梶田展人

Abstract

Long Chain alkenones (LCAs) are a class of C_{37}–C_{42} unsaturated ketones synthesized by a specific group of haptophyte algae (Isochrysidales). In the open ocean, both in vitro experiments and ocean observational analysis indicated there is a linear relationship between the alkenone unsaturation ratio and sea surface temperature (SST). Therefore, LCAs in marine sediment cores have been widely used as a quantitative paleo-SST proxy since the 1990s. In this doctorate dissertation, after summarizing the development history of alkenone paleothermometry (Chapter I), I first present applicational studies of this method to coastal shallow-sea sediments to understand the relationship between climate change and human civilization flourished in coastal East Asia (Chapter II). Next, I present proxy developments on alkenone paleothermometry for further advances in the field, in particular for enabling applications to on-land geological sections and lake sediments (Chapter III). Finally, I proposed the potential for further development of LCAs as a reliable paleothermometer (Chapter IV).

In Chapter II, I reconstructed paleoclimate changes during the Holocene to investigate the influence of climatic events on the human histories in coastal East Asia. The coastal marine sediment cores are useful to reconstruct the paleoclimate because of the strong correlations of SST with atmospheric temperature (AT) in the shallow coastal area. In the first part, I investigate the estuary region of the Yangtze River (China), the oldest Neolithic civilization, well-known for paddy rice cultivation that flourished during the mid-Holocene (ca. 5500–2200 BCE). However, although it is known that this Neolithic civilization collapsed at around 4.2 ka BP, the reason behind the collapse

remains controversial. Sedimentary cores (MD06-3039 and 3040) collected from the inner shelf of the East China Sea, off the southeast coast of China, provide an excellent insight into estimating the regional paleoenvironment since ca. 5500 BCE. We analyzed the alkenone unsaturation ratios and our data indicated abrupt cold episodes (i.e., 3–4°C drop in SST) occurred frequently in the Yangtze delta region during 2600–1900 BCE. These episodes could have been related to the global climatic transition called the "4.2 ka event", when the dynamic of the East Asian monsoon might have been altered. These cold episodes could be sufficiently severe to damage rice cultivation and constitute a plausible explanation for the demise of the Yangtze Neolithic civilization. In the second part, I investigate the offshore of Tokyo area, central Japan, to enrich our understanding of climate change in East Asia and its impact on Japanese civilizations during the Holocene. Previous studies already reported paleo-SST records measured on midden shells along the coast of Tokyo Bay. However, continuous, high time-resolution and quantitative paleotemperature records were still lacking. A piston core was retrieved from Tokyo Bay from which 22 mollusk shells were extracted. An age model for the core, determined via accelerator mass spectroscopy (AMS) ^{14}C dating of the shells and a scoria layer from the Hoei eruption (1707 CE), showed that the sediment core recovered the period from ca. 2400 BCE to the present. We analyzed the alkenone unsaturation ratios to reconstruct the variations in the SST. The SST during the Meghalayan was generally warmer than the present exhibiting a declining trend, which roughly matches with the orbital-forcing changes in summer insolation and with the millennial-scale southward shift of the subarctic front in the northeastern Pacific Ocean. The largest cold period, which occurred ca. 2300 BCE and had a minimum temperature of 19.5 °C, interrupted the warm conditions. This cold period may correspond to the 4.2 ka event.

Our results also revealed that several cold periods occurred, which may have been caused by decreases in solar activity or large volcanic eruptions. Particularly, large decadal to centennial-scale cold periods were observed ca. 440 BCE and 100CE during the Yayoi era, which might be related to the occurrence of the large civil war and the decrease in the Jomon population, respectively. The coldest period after the establishment of a governmental centralized system was recorded ca. 1050 SE, which may have been caused by the combination of a strong El-Niño mode and reduced solar activity. These climate change events may eventually lead to major shifts in Japanese social systems.

In Chapter III of the doctorate dissertation, I reported my works about the developments of LCAs as a paleotemperature proxy. I applied alkenone paleothermometer to previously unstudied geological materials, i.e., a terrestrial outcrop and lacustrine sediment. I detected that LCAs and the other biomarkers are preserved in the rock outcrop of the Kazusa Group exposed in central Japan, the most continuous sedimentary succession in the world, covering almost the entire Pleistocene. The alkenone unsaturation ratios and *n*-alkane-based proxies appeared to reflect the glacial-interglacial changes in the SST and terrestrial climate, respectively. LCAs-based paleo-SSTs during 1.1–1.0 Ma were significantly higher than present-day SSTs in the same area, as supported by foraminiferal Mg/Ca-based SSTs, and thus possibly reflects a direct intrusion of the warm Kuroshio Current. Applying these biomarkers, which might be circumstantially preserved owing to their immunity to high temperature and consolidation stress during burial and uplift, we expect that the Kazusa Group should reveal detailed oceanic and atmospheric changes of the Kuroshio region.

I also discovered LCAs in sediment from the brackish Lake Takahoko, in northern Japan. Identifying the lacustrine haptophyte species that produce LCAs is essential for LCAs-based paleotemperature reconstruction because the haptophytes inhibiting lakes are largely diversified and have different temperature calibrations. The identity of LCA-producing species in Lake Takahoko was investigated using 18S ribosomal DNA and organic geochemical analysis. Two distinct genetic groups, termed as Tak-A and Tak-B, were identified within the Group II haptophyte phylotype. Tak-A was closely related to Hap-A, which was obtained from Lake George, USA; and Tak-B was identified as *Isochrysis galbana*. Hap-A and *Isochrysis galbana* have similar temperature calibrations because they are closely related species. Therefore, Tak-A and Tak-B were expected to share similar calibrations and the changes of their relative abundances in the lake should not significantly disturb the paleotemperature reconstructions. The alkenone temperature recorded in the surface sediment corresponds to the lake temperature observed in early to late summer. This is likely related to the haptophyte bloom season in Lake Takahoko. Considering the haptophyte bloom season, Lake Takahoko may be a viable location for reconstructing an LCAs-based paleotemperature record.

Contents

第Ⅲ-A 章については、5 年以内に雑誌等で刊行予定のため、非公開

第Ⅲ-B 章については、5 年以内に雑誌等で刊行予定のため、非公開

Chapter I.
General Introduction

I−1. The importance of quantitative paleotemperature reconstructions

Currently, global warming and increasing natural disasters related to the high atmospheric CO_2 concentration have become world problems. How will climate changes affect our societies? Studies on causal analysis of historical human civilizations collapses as well as recent conflicts revealed that climate change can seriously damage human civilizations (e.g., Kelley et al., 2015; McConnell et al., 2020). Therefore, we human beings need to know the controlling mechanisms climate changes and assess the future climate change with its possible impacts on our society. For that, the unique way to do it is to understand the mechanism of past climate changes.

Especially, quantitative and high-time resolution paleoenvironmental data are needed to put recent global warming trends into the context of natural climate variability (IPCC Assessment Report, 2014). The climate of the Holocene (11.5 ka BP to the present) is relatively warm and stable compared to those of the last glacial period, which has promoted the human settlement and the growth and development of modern societies (Grove et al., 2015). However, there is some evidence that the Holocene climate includes some episodic variations and there are regional disparities in the amplitude of these climatic variations as well as in their synchronicity (Mayewski et al., 2004; Wanner et al., 2008). Therefore, it is very important to analyze a wide area with widely distributed sites and to obtain high-time resolution paleoenvironmental data to avoid risks of extrapolation. It is also necessary to improve our systematic knowledge about the Holocene climate variability, which must be controlled by multiple factors.

Sea surface temperature (SST) and air temperature (AT) are two of the most important factors that control global atmosphere and ocean

circulations (Stocker et al., 2013). Temperature changes will cause global- to regional-scale climate changes, which have large influence on the primary industries such as agriculture, forestry, and fisheries (Kirilenko et al., 2007; Lobell and Burke, 2008; Sumaila et al., 2011; Hatfield et al., 2011). In order to reconstruct long, continuous, and quantitative paleotemperature records, paleoceanographers and paleoclimatologists have developed many types of proxies applicable for marine and lake sediments. The requirements for a reliable paleotemperature proxy are that 1) it has been confirmed at the laboratory level to work under ideal conditions; 2) it is clear what season and range of temperature it reflects; 3) it can reproduce the current observed temperatures, and 4) it hardly changes due to diagenesis. Many kinds of paleothermometers have been developed and each has its advantages and disadvantages.

I-2. Paleotemperature proxies

In this chapter, I represent the major quantitative paleotemperature (SST and/or AT) proxies with their advantages and weakness that are widely applicable to sediment cores. The ratio of magnesium to calcium (Mg/Ca) of surface-dwelling planktonic foraminifera is the most established paleo-SST indicator (Nürnberg et al., 1996). Mg forms the most important solid solution with calcite, and Mg substitutes directly for Ca in the foraminiferal calcite structure during foraminifera shell precipitation (Branson et al. 2013). Culture experiments indicate that Mg/Ca ratios of planktonic foraminifera increase at a higher temperature. This effect can be explained by the substitution of Mg^{2+} into calcite associated with a change in enthalpy or heat of reaction, which is sensitive to temperature (Rosenthal et al. 1997). The sensitivity of Mg/Ca ratio to

temperature depends on the species, which can be explained by a biologically mediated precipitation process. To date, a lot of species-specific culture calibrations have been developed, and the reproductivity of these formulas has been confirmed by sediment trap calibration and core-top calibrations (Lea et al., 1999; Elderfield and Ganssen, 2000; Anand and Elderfield, 2003; Tierney et al., 2019). The long residual time of Mg and Ca guarantee the availability of this paleothermometer as far back as approximately 15 Ma (Broecker, 2013). However, the post-depositional dissolutions and contaminations by adherent sediments, organic matter, and Fe-Mn oxides on the shell can influence the analysis of trace element concentrations in the foraminifera shells. Therefore, the paleotemperature estimates should be obtained with proper cleaning methods (Barker et al., 2003).

Reef-building corals living in the surface ocean can provide high-time resolution (weeks to a month) paleo-SST records based on the geochemical records (Sr/Ca, Mg/Ca, and U/Ca) in coral skeletons (Beck et al., 1992; Min et al., 1995; Watanabe et al., 2001). Massive corals (e.g., *Porites* spp) are especially useful to reconstruct seasonal-scale SST variations, which enable to know monthly- to annual-scale environmental changes such as the El-Niño Southern Oscillation and Indian Ocean Dipole (Watanabe et al., 2011; Watanabe et al., 2019). Based on the culture experiments, Mg/Ca and U/Ca are considered to be biased by the skeletal growth rate, and ambient pH, respectively (Inoue et al., 2007, 2011). However, Sr/Ca has been widely accepted and used as a paleo-SST proxy (Hayashi et al., 2013). Monthly-scale analysis for modern corals enables to make rigorous calibration between the Sr/Ca and the current measured SSTs, which enhances the reliability of the temperature

calibrations (e.g., Kajita et al., 2017). The weakness of this method is that it can be applied to assess paleo-SST changes only in subtropical to tropical regions where corals live. It is difficult to obtain long-term records because *Porites* spp. lives for only approximately 400 years at the maximum (DeLong et al., 2014; Kawakubo et al., 2019). Therefore, the coral records recovered from sediments cores are usually fragmented, only provide snapshots of the target periods (e.g., Felis et al., 2014; Asami et al., 2020).

Ocean environments, including sea surface temperature, affect the spatial distribution of marine microfossils. Therefore, the relationship between modern environmental factors and these faunas can be used to reconstruct past environmental conditions. This statistical approach referred to as “transfer functions”, and the assemblages of planktonic foraminifera and radiolarians have been developed for SST indicators since the 1970s (Nigrini, 1970; Imbre and Kipp, 1971; Climap Project Members, 1976). Transfer function methods are essentially based on the assemblage data from the modern datasets; therefore, its application to, for example, down-core analysis, is largely limited to 1) regional-scale, 2) well-preserved microfossils, and 3) the relatively recent (usually younger than Quaternary) samples (Schiebel and Hemleben, 2017). Species selected for transfer function differ upon regions because regionalities of key species of each microfossils group, thus geographical coverage of modern dataset should be selected carefully (e.g., Matsuzaki and Itaki, 2017). The selected species dissolution and extinction in down core samples can affect the results; therefore, statistical analysis of the data consisting of several steps are needed when applying transfer functions to the old era (e.g., Miocene: Matsuzaki et al., 2019, 2020). The additional weakness of transfer function model is that they are based on several

assumptions; 1) the relationship between fossil species and environmental factor is linear through time, 2) modern observation enclose all the necessary information to explain the fossil data, and 3) changes in fossil fauna is controlled by only environmental parameters, SST in instance.

Few indicators can restore the ambient paleotemperature from the lake sediment cores. Pollen data is nearly the only applicable proxy for quantitative temperature reconstruction. Nakagawa et al. (2002) has reconstructed the paleo-AT changes over the past 40 ka using the pollen record from sediment core retrieved in Lake Mikata, central Japan. It relied on the modern analogue technique established by the statistical correlation between the distributions of vegetation types and surface pollen assemblages covering the whole of Japan. Although this method is considered to be applicable for the other lakes with similar vegetation around (e.g., Nakagawa et al., 2005; 2008), those quality is highly dependent on the current reference pollen dataset. For example, to properly reconstruct the AT in glacial periods when the flora was significantly different from the present, it is necessary to extend the modern reference dataset to the colder regions of the Russian Far East (Tarasov et al., 2011). When restoring the climate of Hokkaido island northern Japan, the dataset covering the whole Japan is not appropriate for paleo-AT reconstructions. To limit the reference sites in cold conifer dominant regions are necessary to reduce the error (Leipe et al., 2013). Therefore, the pollen-based paleothermometer was not a versatile method that can be applied uniformly to various periods and regions.

Until a few years ago, the relative abundance of isoprenoid Glycerol Dialkyl Glycerol Tetraether (GDGT) lipids in marine and lake sediments had often been used for paleotemperature reconstructions (Castañeda and Schouten, 2011; Schouten et al., 2013). The core top calibrations between the TEX_{86} (tetraether index of tetraethers consisting of 86 carbons) indexes and SSTs have been established (Schouten et al., 2002; Kim et al., 2010). Although some studies proposed the lacustrine TEX_{86} calibrations using several data from medium to large lakes (Powers et al., 2010; Tierney et al., 2010). However, there are a lot of lakes where the single TEX_{86}-based temperature calibrations cannot be applied (Blaga et al., 2009; Powers et al., 2010), probably because of the intrusion of allochthonous GDGTs. The fateful flaw in TEX_{86} paleothermometer is that the synthesizers of GDGTs have not been identified. GTGTs are long thought to be biosynthesized by Thaumarchaeota; however, recent analysis of environmental samples has shown that their structural diversity and sources are much wider than those predicted and that they occur ubiquitously in a wide range of environments including deep sea water and soils (Weijers et al., 2006; Schouten et al., 2013). Due to the ambiguous origin of isoprenoid GDGTs, it is ambiguous to discuss accurately TEX_{86}-based temperature paleoceanographic and paleoclimatic meaning.

I-3. Long Chain alkenones as a proxy for paleo-SST

In this thesis, I focused on the Long Chain Alkenones (LCAs) biolipids, a class of C_{35}–C_{42} unsaturated ketones, that are synthesized by a very restricted group of haptophyte algae (Isochrysidales) living in surface euphotic waters (Fig. I-1). It has been confirmed that cellular alkenone composition is directly correlated with

haptophyte species and their growth temperature (Marlowe et al., 1984b; Brassell et al., 1986; Brassell, 1993). Formulae for alkenone indices used in this thesis are shown in Table I-1.

Since the 1980s, C_{37}–C_{39} LCAs have been widely detected from marine sediments (Volkman et al., 1980a; Marlowe et al.1984a). It was confirmed that they were produced by universal marine haptophyte species, *Emiliania huxleyi* and *Gephyrocapsa oceanica* (Family Noëlaerhabdaceae; coccolith-bearing taxa) (Volkman et al., 1980b; Marlowe et al., 1984b). The good proportional correlation between C_{37} alkenone unsaturation ratios (U^{K}_{37} and $U^{K'}_{37}$; each definition is shown in Table I-1) and water temperatures was confirmed by numerous culture experiments for both species (Prahl and Wakeham, 1987; Prahl et al., 1988; Volkman et al., 1995; Conte et al., 1995; Sawada et al., 1996) (Fig. I-2). In marine settings, $U^{K'}_{37}$ is more often used than U^{K}_{37} because of the better correlation of $U^{K'}_{37}$ with temperature than that of U^{K}_{37} (Prahl et al., 1988). The culture calibrations between $U^{K'}_{37}$ and temperature presented in these studies differed each other, even though some of them used the same strain, which might be due to the differences in cell physiological state and growth phase of haptophytes in each chemostat (Conte et al., 1995; Herbert, 2006). Among these culture calibrations, the following conversion formula (1) proposed by Prahl et al. (1988) is very good agreement with the global core top calibration (2) between $U^{K\prime}_{37}$ in surface marine sediments and in-situ SSTs (Muller et al., 1988).

$$U^{K'}_{37} = 0.034T + 0.039 \quad (R^2 = 0.994)$$

$$U^{K'}_{37} = 0.033T + 0.044 \quad (R^2 = 0.958)$$

The good agreement between the culture and in-situ calibrations increases the reliability of $U^{K'}_{37}$ as an SST proxy, which may be due to the low genetic diversity of Noëlaerhabdaceae family species in marine settings (Bendif et al., 2014, 2015). There is an error of approximately 1.5 °C (± 1σ) between the temperatures restored by equation (4) from surface sediments and the actual SSTs, but the difference is due to the seasonality of alkenone production and the difference in blooming water depth (Conte et al., 2006). LCAs are likely less decomposed than other lipids, and even if it is decomposed, the degree of unsaturation hardly changes because of the decomposition rates of diunsaturated C_{37} alkenone ($C_{37:2}$) and triunsaturated C_{37} alkenone ($C_{37:3}$), which are almost equal (Prahl et al., 1989). Therefore, $U^{K'}_{37}$ recorded in marine sediment cores have been widely used as one of the most quantitative well-established proxies for paleo- SST (e.g., Liu et al., 2018; McGregor et al., 2018). LCAs could be detected in a wide range of marine sediments, including coastal shallow seas and deep seas over the carbonate compensation depth where planktonic foraminifera are rarely preserved (e.g. Conte et al., 2006).

I-4. Development of the LCAs-based proxies for on-land geological settings

The success of the LCAs-based SST proxy is largely due to their high resistance to degradation. The unusual trans-bond configuration of the carbon-carbon double bounds in LCAs should be an important factor in their resistance to early diagenesis (Rechka and Maxwell, 1988), as many bacteria lack in the enzymes required to break down such type of double bond (Brassell, 1983). Today, LCAs have been detected from marine sediments as old as ca. 120 Ma (Farrimond et al., 1986; Brassell et al., 2004), and thus

indicated their high stability in marine sedimentary deposits. Although the LCAs distributions in Cretaceous sediments are completely different from those of modern marine sediments, LCAs recorded in the sediments younger than the Eocene are very similar to those of the present, and reasonable paleotemperatures comparable with foraminiferal Mg/Ca-paleotemperatures can be calculated using the temperature calibration applicable to modern settings (Müller et al., 1997; McClymont et al., 2005).

Although LCAs are more stable than many other lipid classes, they can be decomposed under the oxidative and/or high temperature conditions. The concentrations of LCAs in marine sediments usually decrease with an increasing burial depth (Simoneit et al., 1994), because of large losses in post-depositional diagenesis (Prahl et al., 1989). In hydrous pyrolysis experiments, LCAs are decomposed rapidly when they are exposed to temperatures above 120℃ at short-time scale (several hours) (Rabinowitz et al., 2017). According to field observations of the sediments deposited around the hydrothermal, LCAs seemed to disappear after a long-time (hundreds of years) exposure to environments of 20–80 °C (Simoneit et al., 1994). Therefore, LCAs are often completely decomposed in the subaerially exposed sedimentary rocks subjected to diagenesis during the burial and/or uplift processes (e.g., Sampei et al., 2003). However, many studies have previously confirmed that the concomitant changes of U^{K}_{37} and $U^{K'}_{37}$ values with LCAs degradations are minor (Prahl et al., 1989, 2003; Hoefs et al., 1998) due to the similar tolerance to diagenesis of di-, tri-, and tetra unsaturated C_{37} alkenones. Therefore, alkenone paleothermometry, if LCAs are preserved, has the potential to be available in subaerially exposed sedimentary rocks.

I-5. Development of the LCAs-based proxies for lacustrine settings

LCAs are also detected in some specific lake sediments (Cranwell, 1985). The relative abundances of LCAs in lake sediments are completely different from those in marine sediments, by being abundant in $C_{37:4}$ alkenones (Volkman et al., 1988, Li et al., 1996, Wang and Zheng 1998, Thiel et al., 1997). Amplicon sequencing-based detection revealed that LCAs in brackish lakes are mainly biosynthesized by Isochrysidaceae family of haptophytes, which are genetically diversified compared to Noëlaerhabdaceae family of haptophytes (Theroux et al., 2010). It also revealed the existence of another clade of haptophytes that differs from Isochrysidaceae and Noëlaerhabdaceae at the family level. They were often called "Greenland haptophyte" or "Group I haptophyte", because they were first discovered in the lakes of Greenland (Anderson and Leng, 2004; D'Andrea et al., 2016). Greenland haptophytes are detected in freshwater to oligohaline lakes; however, no studies have succeeded in isolating their strains.

In the 2000s, the linear relationships between $U^{K'}_{37}$ in surface lake sediment and ATs were observed in some locations (Zink et al., 2001; Chu et al., 2005), which suggested that lake alkenones could also be used as an AT paleothermometer (Fig. I-2). In the 2010s, several Isochrysidaceae family of haptophytes were isolated from brackish environments and confirmed that their U^{K}_{37} and their growth temperatures were highly correlated (Fig. I-2). Unlike the Noëlaerhabdaceae family of haptophytes, U^{K}_{37} often correlates with temperature better than $U^{K'}_{37}$. To date, several U^{K}_{37}-T calibrations based on culture experiments have been published for three species, *Ruttnera lamellosa*, *Isochrysis galbana*, and *Tisochrysis lutea* (Theroux et al., 2013, Nakamura et al., 2014, 2016, Zheng et al., 2016, Araie et al., 2018), which completely differ from those of the

Noëlaerhabdaceae family of haptophytes. The large diversities observed among their U^{K}_{37}-T calibrations might reflect genetic differences because closely related species at genus level generally share the similar equations (Fig. I-3).

These achievements in culture experiments suggest that different conversion formulas must be applied to each lake depending on the inhabiting haptophyte species. However, Isochrysidaceae family of haptophytes are very small (<10μm) and are rarely dominant in lakes, making it difficult to isolate the strains. It is also difficult to morphologically distinguish the species because they do not form characteristic carbonate shells like Noëlaerhabdaceae family of haptophytes (Theroux et al., 2010).

The relative distribution of LCAs (chemical taxonomic features) can be used for estimating those potential synthesizers in the environment (Table I-2). Greenland (Group I) haptophytes have the conserved alkenone characteristics, synthesizing C_{37} and C_{38} tri-unsaturated isomers. Based on the culture experiments, it has been confirmed that Noëlaerhabdaceae family of haptophytes contain both C_{38Et} and C_{38Me}, while the Isochrysidaceae family of haptophytes does not have C_{38Me} (Marlowe et al., 1984b; Rontani et al., 2004; Longo et al., 2016; Nakamura et al., 2016). The relative contents of $C_{37:4}$ and C_{40} also differ at the genus to family level (Table I-2). Although these characteristics are useful for revealing family-level diversity of haptophytes in coastal area and marginal lakes (e.g., Kaiser et al., 2019; Salacup et al., 2019), it is necessary at least genus level to determine the selection of U^{K}_{37}-T calibrations applicable for lakes inhabited by the Isochrysidaceae family of haptophytes. Since the technology of environmental DNA analysis using the Next-generation sequencer has recently improved, it becomes possible to estimate inhabiting species of haptophytes even if the

strains cannot be isolated (e.g., Theroux et al., 2010), which can help in the selection of conversion formula applicable for the lake sediments.

Based on these recent achievements on the genetic diversity of haptophytes, our interpretations for the classical alkenone based SST reconstructions in marine settings should be partly revised. In marginal seas with high freshwater supply, the contributions of Greenland haptophytes and Isochrysidaceae family of haptophytes to total alkenone production cannot be ignored (e.g., Salacup et al., 2019). For example, it was confirmed that those haptophytes inhabit a significant amount in Baltic sea especially in the low-salt environment in the inner part of the bay (Kaiser et al., 2019), which should be the cause of the uncorrelation between $U^{K'}_{37}$ and in situ SSTs (Blanz et al., 2005). The contribution of Greenland haptophytes and family Isochrysidaceae of haptophyts are estimated from the abundance of $C_{37:4}$ and $C_{38:4}$, which is rarely synthesized from the family Noëlaerhabdaceae of haptopytes living in the environment above 15 degrees (Prahl et al., 1988). Unreasonable temperatures are often calculated from marine sediments where a significant amount of $C_{37:4}$ is detected in marine sediments, such as Okhotsk sea and Japan Sea during the last glacial maximum (Seki et al., 2004; Fujine et al., 2006; Lee et al., 2008). We should carefully consider the applicable temperature calibration for such marine sediments, taking into account the possible variability of haptophyte species.

I-6. The Aims of the doctorate dissertation

The doctoral research has two purposes; one is to reconstruct the paleoclimate changes in coastal areas of East Asia during the Holocene and reveal their impacts on the evolution of human civilizations. I aimed to provide higher time resolution and a more quantitative paleotemperature record compared to previous studies using terrestrial archives. Those results are presented in Chapter II. Chapter II-A focused on the Yangtze delta area, where the relationship between the evolution of the Neolithic Yangtze civilizations and climate change has long been debated (Kajita et al., 2018). In Chapter II-B, I studied the sedimentary core recovered from Tokyo Bay for reconstructing local paleotemperature record and compared it with the climate changes previously suggested by historical documents for understand how climate changes affected the human civilization of Japan (Kajita et al., 2020b).

The other purpose is to expand the suitability of alkenone paleothermometry to on land section and lakes sediments. LCAs are often selectively preserved in sediments relative to other planktonic lipids because the molecular chains are very long and the intervals between double bonds are extended. Despite its tolerance to diagenesis, LCAs-based proxies have rarely been applied to subaerially exposed sedimentary rocks for paleotemperature studies. In Chapter III-A, I report that I discovered that multiple biomarkers, including LCAs, are contained in the outcrops of the Kazusa Groups exposed in central Japan. I carefully examined the signals of these biomarkers and investigated their availability for paleoenvironmental studies (Kajita et al., under review).

The culture-based temperature calibrations for LCAs biosynthesized by Isochrysidaceae haptophytes settings have been established since the 2010s. However, the methods of applying alkenone paleothermometry to the lacustrine sediments are not well established because the number of LCAs containing lake sediments is extremely limited. In Chapter III-B, I discovered that estuarine lake Takahoko, northern Japan, contained LCAs. Combining the environmental-DNA technique, I investigated how the LCA-based paleotemperature reconstruction can suit to this lake (Kajita et al., 2020a).

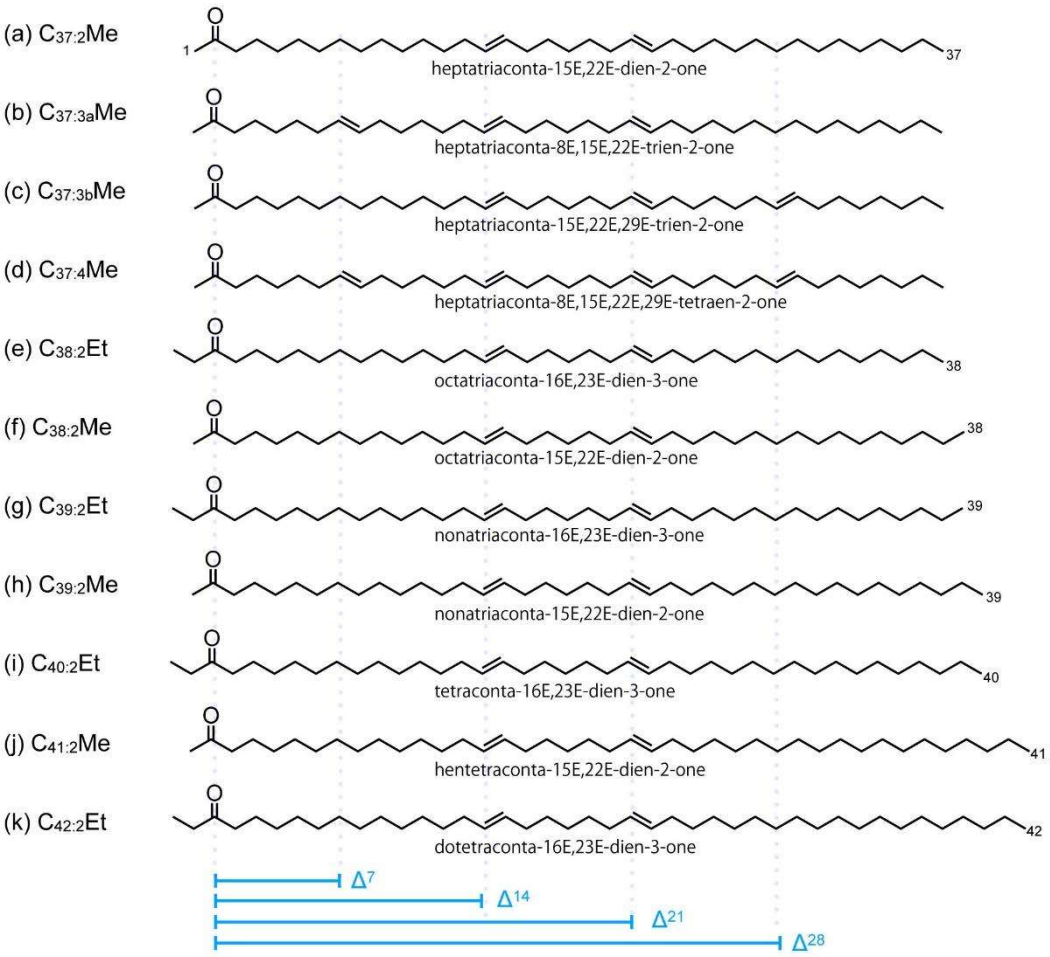

Fig. I-1 Chemical structures, abbreviated notations, and chemical names of selected LCAs mentions in this thesis.

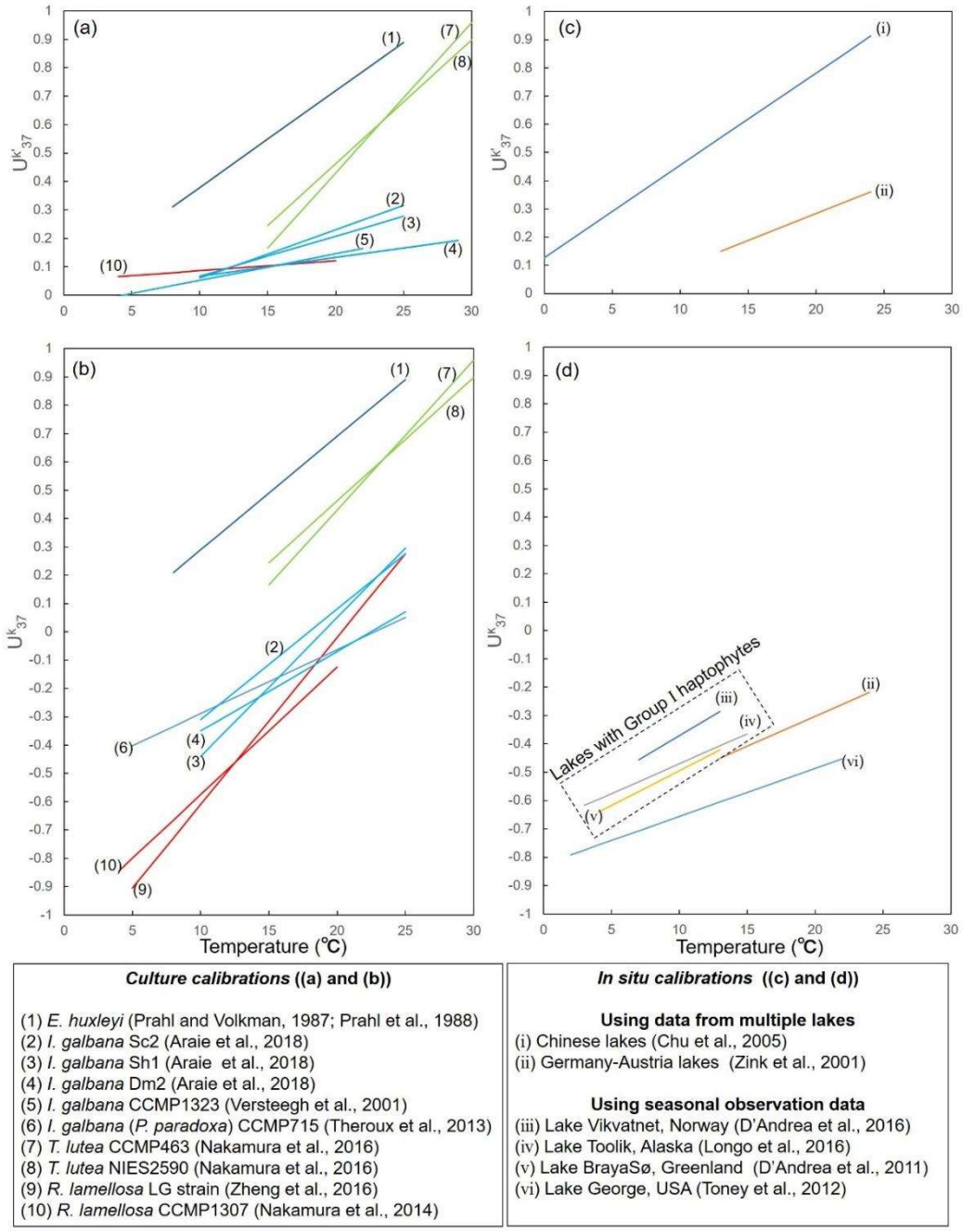

Fig. I-2 (a) $U^{K'}_{37}$-T and (b) U^{K}_{37}-T conversion formula derived from the culture experiment of haptophytes under the controlled temperatures summarized in Kajita and Nakamura (2020). (c) $U^{K'}_{37}$-T and (d) U^{K}_{37}-T in situ temperature calibrations.

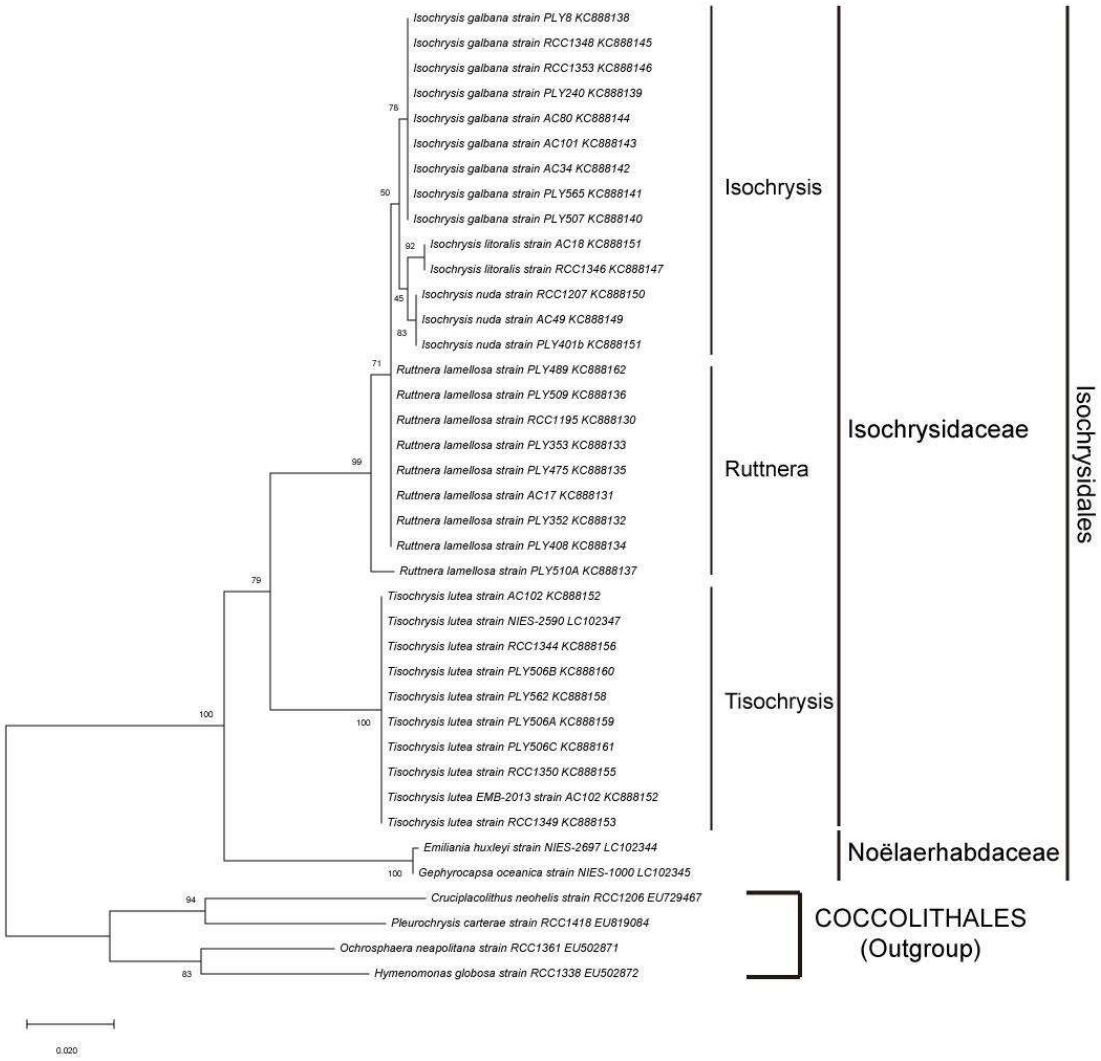

Fig. I-3 Maximum likelihood tree of strains in Isochrysidales and 4 strains in Coccolithales based on DNA sequences using 28S rRNA gene. The values on each note are bootstrap percentage. GenBank accession numbers follows all species names.

Table I-1

Formulae for alkenone indices used in this doctorate dissertation. Shorthand notation is carbon number: number of double bounds. Me = methyl ketone, Et = ethyl ketone, LCA = long chain alkenones.

Index	Equation	Reference
U_{37}^{K}	$([C_{37:2Me}]-[C_{37:4Me}]) / ([C_{37:2Me}]+[C_{37:3Me}]+[C_{37:4Me}])$	Brassell et al., 1986
$U_{37}^{K'}$	$[C_{37:2\ Me}] / ([C_{37:2\ Me}]+[C_{37:3\ Me}])$	Prahl and Wakeham, 1987
C_{37}/C_{38}	$\Sigma C_{37}LCA/\Sigma C_{38}LCA$	Rosell-Mele et al., 1994
$C_{38}Et/C_{38}Me$	$([C_{38:2Et}]+[C_{38:3Et}]) / ([C_{38:2Me}]+[C_{38:3Me}])$	Conte et al., 1998

Table I-2

Chemotaxonomic characteristics and calibration equations of alkenone-producing haptophyte species summarized in Kajita and Nakamura, 2020. A: Absence, P: Presence, -: Not reported in the paper, †: data of environmental samples （uncultured haptophytes）, ※1: depends on strains (absent or minor amount), ※2: minor amount (<2%), ※3: relatively low correlation of determination (R^2<0.5), ※4: *in-situ* calibration of Toolik lake.

Family (Clade)	Genus	Species	$C_{37:4}$	C_{38}Mt	C_{40}	$C_{37:3}$b	Calibration formula ($U^{K'}_{37}$-T)	Calibration formula (U^{K}_{37}-T)	Cultured temperature (℃)	References
(Group I)†	-	-	P	P	A	P	-	U^{K}_{37}=0.021T-0.68※4	-	Longo et al., 2016; 2018
Isochrysida-ceae (Group II)	*Isochrysis*	*I. galbana* Sc2	P	A	P※2	A	$U^{K'}_{37}$=0.017T-0.11	U^{K}_{37}=0.039T-0.70	5~25	Araie et al., 2018
		I. galbana Sh1					$U^{K'}_{37}$=0.014T-0.073	U^{K}_{37}=0.049T-0.93	5~26	Araie et al., 2018
		I. galbana Dm2					$U^{K'}_{37}$=0.0066+0.0005	U^{K}_{37}=0.028T-0.63	5~27	Araie et al., 2018
		I. galbana CCMP1323					$U^{K'}_{37}$=0.0093T-0.041	-	7~22	Versteegh et al., 2001
		I. galbana CCMP715					$U^{K'}_{37}$=0.0047T-0.0071 ※3	U^{K}_{37}=0.0226-0.5149	5~24	Theroux et al., 2013
	Tisochrysis	*T. lutea* CCMP463	A	P※2	P※2	A	$U^{K'}_{37}$=0.053T-0.63	U^{K}_{37}=0.053T-0.63	15~35	Nakamura et al., 2016
		T. lutea NIES2590					$U^{K'}_{37}$=0.044T-0.41	U^{K}_{37}=0.044T-0.41	15~35	Nakamura et al., 2016
	Ruttnera	*R. lamellosa* LG strain	P	A	P※2	A	$U^{K'}_{37}$=0.014T-0.07※3	U^{K}_{37}=0.059T-1.20	5~25	Zheng et al., 2016
		R. lamellosa CCMP1307					$U^{K'}_{37}$=0.0035T+0.051	U^{K}_{37}=0.045T-1.025	4~20	Nakamura et al., 2014
Noëlae-rhabdaceae (Group III)	*Gephrocapsa* and *Emiliania*	*E. huxleyi* 55a	A※1	P	A	A	$U^{K'}_{37}$=0.034T+0.039	U^{K}_{37}=0.04T+0.11	8~25	Prahl et al., 1988
		E. huxleyi EH2					$U^{K'}_{37}$=0.063T-0.762	-	10~20	Sawada et al., 1996
		G. ocenaica JB02					$U^{K'}_{37}$=0.049T-0.52	-	11.1~29	Volkman et al., 1995
		G. oceanica GO1					$U^{K'}_{37}$=0.044T-0.204	-	15~28	Sawada et al., 1997

Chapter II

Quantitative and high time resolution alkenone paleotemperature reconstructions during the Holocene: relationship between the climate change and human history in East Asia

Chapter II-A

Extraordinary cold episodes during the mid-Holocene in the Yangtze delta: interruption of the earliest rice cultivating civilization

II-A-1. Introduction

The Holocene, an epoch of the late Quaternary period is known for its warm and stable climate and millennial-scale climatic perturbations (Bond et al., 2001; Mayewski et al., 2004). Currently, global warming and climate-related disasters related to the increase in atmospheric CO_2 concentration are of great concern (IPCC Assessment Report, 2014). Recently, investigations of Holocene climatic variability and its socioeconomic impacts have received increasing attention with regard to the prediction of future climatic change and the evaluation of its impact on human society. However, despite much effort, knowledge of the climatic and environmental systems that affect the Earth's surface on local and regional scales, their spatial patterns, and the causal factors behind them remain incomplete.

It has been found that environmental and climatic changes have influenced the rise and fall of human civilizations (Cullen et al., 2000; deMenocal et al., 2001; Stanley et al., 2003; Staubwasser et al., 2003; Haug et al., 2003; Wu and Liu, 2004; Kawahata et al., 2009, 2017a). In the downstream area of the Yangtze River, Neolithic developments began around 7.0 cal. kyr BP. Yangtze Neolithic civilizations were based on paddy rice cultivation, whereas millet or wheat featured predominantly in most other Neolithic civilizations around the world (Chang, 1986). The Hemudu site, which was first excavated in 1973–1974, is considered one of the birthplaces of rice cultivation because of the discovery of enormous quantities of rice hulls dated at 6.0–7.0 cal. kyr BP. Yangtze Neolithic civilizations, which developed remarkably based on paddy rice, fisheries, and livestock domestication, collapsed abruptly at around 4.2 cal. kyr BP, after which there followed a period of about 300

years without a trace of human settlement (e.g. Stanley et al., 1999; Itzstein-Davey et al., 2007a, b) (for details, see Section 3, “Archaeological information”).

The change in climate known as the 4.2 ka event, which is estimated to have occurred at around 2500–2000 BCE, has been proposed as one of the several large regional-/global-scale climatic events during the Holocene (Walker et al., 2012), and was ratified as the boundary of the mid-Holocene (Northgrippian) and late-Holocene (Meghalayan) by the International Commission on Stratigraphy in July 2018. The 4.2 ka event was accompanied by the weakening of monsoon systems and brought severe cold and dry episodes over large sections of the Eurasian Continent (e.g., Chen et al., 1999; Xiao et al., 2004; Wang et al., 2005; Drysdale et al., 2006; Berkelhammer et al., 2012; Nakamura et al., 2016), which has been cited as a plausible explanation for the collapse of ancient major civilizations in Egypt, the Indus Valley, and Mesopotamia (Cullen et al., 2000, Stanley et al., 2003, Staubwasser et al., 2003). In China, several archaeological sites located in the middle of the Yellow River basin were abandoned at around 2000 BCE because of reduced agricultural productivity due to dry events (Wu et al., 2004; An et al., 2005). In addition, sudden abandonment of a settlement at the Sannai-Maruyama site in northern Japan (Fig. IIA-1a) was reported, following 1,700 years of reasonable prosperity, which was attributed to a rapid decrease in atmospheric temperature (AT) by 2.0 °C at around 2200 BCE (Kawahata et al., 2009). As rice is one of the most important staple foods in present day Asia, it is important to reveal the response of rice cultivating cultures to climate change. The paleoclimatic patterns of the Yangtze delta have been reconstructed based on qualitative environmental parameters, such as pollen assemblages and grain size analyses of terrestrial or lacustrine sediments.

However, the details concerning the climate around the time of the 4.2 ka event remain controversial (Liu et al., 1992; Stanley et al., 1999; Yu et al., 2000; Chen et al., 2005; Itzstein-Davey et al., 2007a, b; Atahan et al., 2007; Li et al., 2010; Zong et al., 2011; Innes et al., 2014; Wang et al., 2017; Wang et al., 2018).

In this study, in order to evaluate the effect of the environment on the human activity of the Yangtze Neolithic civilizations, I collected coastal marine sediments from near the Yangtze delta, which present a continuous record of both marine and terrestrial environments in their sedimentary sequence. It was particularly advantageous to be able to estimate terrestrial AT quantitatively based on the high positive correlation between monthly mean SSTs and ATs in summer in the coastal region (Kawahata et al., 2009, 2017a, 2017b). The purpose of this study was to reconstruct paleo-SSTs (or paleo-ATs) quantitatively to permit discussion on the possible effects on human activity of climatic/environmental change, especially at around the time of the 4.2 ka event.

II-A-2. Study areas and materials

II-A-2.1. East China Sea

The East China Sea (ECS) is located to the east of China and extends to the Okinawa Trough, covering an area of approximately 1,450,000 km^2 (Fig. IIA-1a). The depth of the water in the ECS is mostly <200 m (Fig. IIA-1b). Therefore, most of today's sea floor of the ECS had dried up in the last glacial maximum period due to lower sea levels (Lambeck et al., 2014). The Yangtze and Yellow rivers, two of the largest rivers in China, lower the salinity of the ECS to <34.0 (Zweng et al., 2013). As the sea level has been raised close to its present level since 6.5–7.5 kyr BP (Lambeck et al., 2014), the ECS continental shelf has been continuously accumulating the silty clays and silty-clayey sands derived from both the Yangtze and Yellow rivers (Liu et al., 2007).

II-A-2.2. The Yangtze River

The Yangtze River is one of the largest rivers in the world. Its length and the area of its drainage basin are 6,300 km and 1.8×10^6 km^2, respectively. The mean water discharge of the Yangtze River is ~30,000 $m^3\ s^{-1}$ with a mean suspended-sediment concentration of 540 mg L^{-1} (Milliman, 1985). About 70% of the annual discharge and 87% of the annual sediment load occur during the flood season (May–October) because the drainage basin is affected strongly by the East Asian Summer Monsoon (EASM). Most sediment derived from the Yangtze River is deposited in and around the estuarine area, developing the delta region, while the remainder is transported into the ECS.

Today's Yangtze delta formed after the mid-Holocene sea level high stand (HHS) at around 7.5 kyr BP (Hori et al., 2002). The delta topography is extremely flat with an elevation of only 0–5 m above mean sea level. In the southern part of the Yangtze delta, a large freshwater lake (Lake Taihu) covers an area of 2,250 km^2 with a mean depth of 2 m. The climate of the Yangtze River drainage is characterized as a subtropical monsoon climate (Tada and Murray, 2016). Today, mixed deciduous and evergreen forests are typical of the vegetation within the region. Climate information for the area around Shanghai, located in the northern part of the Yangtze delta, can be accessed from the China Meteorological Administration (http://www.cma.gov.cn/en2014/) and Japan Meteorological Agency (http://www.data.jma.go.jp/gmd/cpd/monitor/index.html). The mean annual AT is 17.1 °C. The region is influenced primarily by the Subtropical High in summer with a maximum AT of 28.6 °C and by the Siberian High in winter with a minimum AT of 4.8 °C. The mean annual precipitation is 1,157 mm yr^{-1}. Summer and winter rainfall account for 54% and 18% of the annual total, respectively. In particular, the EASM plays an important role in flood damage, from which the Yangtze delta region has suffered many times.

II-A-2.3. Oceanographic setting

The ECS Coastal Current (ECSCC) carries freshwater from the Yangtze River with suspended particles southward along the coast, creating an inner shelf mud belt (Fig. IIA-1b). The inner shelf mud belt extends ~800 km from the Yangtze River estuary southward to the Taiwan Strait (Liu et al., 2007). Conversely, the warm and saline Taiwan Warm Current flows northward along the 50 m depth contour line.

The Taiwan Warm Current is one of the branches of the Kuroshio Current (KC), which flows northward along the continental shelf break (Fig. IIA-1a).

Based on SST data available at 27°52'30"N, 121°22'30"E from 2005 to 2016 from the Advanced Very High Resolution Radiometer (Reymonds et al., 2007), the annual mean SST is 21.1 °C, with maximum and minimum SSTs of 28.0 °C (August) and 13.4 °C (February), respectively. The AT data collected on Daichin Island (28°29'N, 121°55'E) near the core site (Fig. IIA-1b) showed maximum and minimum values of 28.3 °C (August) and 7.1 °C (January), respectively. The monthly mean AT is closely correlated with the monthly mean SST ([AT] = −10.8 + 1.35 × [SST]; $r^2 = 0.90$, $p < 0.001$), which allowed us to reconstruct the AT quantitatively from the SST. The coastal environment is highly correlated with SST because the heat capacity of seawater is much larger than that of the atmosphere. Sea surface salinity measurements at 27°30'N, 121°30'E are also available from 2005 to 2012 from the World Ocean Atlas Select 2013 (Zweng et al., 2013). Monthly mean sea surface salinity has a minimum value of 33.2 in April, maximum value of 34.3 in January, and an annual mean value of 33.8. The decrease during summer is caused by increased freshwater discharge from the Yangtze River.

II-A-2.4. Cores MD06-3040 and -3039

Two giant piston cores (MD06-3040 and MD06-3039: depths 19.39 m and 8.11 m, respectively) were recovered at approximately the same location in the inner shelf mud belt at a water depth of 47 m (MD063040: 27°43'36"N, 121°46'88"E; MD06-3039: 27°43'36"N, 121°46'91"E; Fig. IIA-1) during the IMAGES MD155-Marco Polo cruise (Zheng et al., 2010; Wang et al., 2014). Both cores primarily

consist of sediment derived from the Yangtze River, comprising yellow to olive-gray homogeneous muddy sediment with sporadic thin sandy layers.

Core MD06-3040 can be divided into three lithological units based on visual observation and grain size variation (Zheng et al., 2010; Wang et al., 2014) (Fig. IIA-2). Unit A (0.00–15.86 m) is principally composed of yellow to dark-gray medium silt (10–63 μm) interbedded with fine sand layers. Grain size variation is relatively constant except for minor disconformities between 3.00–3.18 and 3.20–3.23 m. The top 1–2 cm of Unit A was lost due to disturbances on the seafloor during the coring process. Unit B (15.86–18.30 m) consists of dark-gray medium silt interbedded with fine sand. Wavy and lenticular bedding are typical of the depositional structures, and many bivalve shell fragments are scattered within the beds. Unit C (18.30–19.39 m) is mainly composed of dark-gray coarse silt interbedded with thin layers of coarse sand and it is rich in bivalve shell fragments. An age model for the cores has been determined in previous studies (Zheng et al., 2010; Wang et al., 2014) (for details, see Table IIA-1). They established that core MD06-3040 was continuously deposited and could provide a continuous environmental record back to 10.4 cal. kyr BP. The concentrations of major elements (Al, Ca, Fe, Mg, Na, K, Mn, P, and Ti) and trace elements (Li, Sc, Rb, Y, Zr, Ba, Th, U, Nb, Hf, and rare earth elements) of core MD06-3040 have already been analyzed using inductively coupled plasma-atomic emission spectrometry (ICP-AES) and inductively coupled plasma-mass spectrometry (ICP-MS) at Tongji University, China (Shao, 2012; Yang et al., 2015; Bi et al., 2017). The results of clay mineral analysis of core MD06-3040 using X-ray diffraction (XRD) were also published in Fang et al. (2018).

II-A-3. Archaeological information

For better discussion on the relation between the natural environment and human activity, I provide a brief outline of the archaeological information pertaining to the Yangtze delta region. Thanks to the benefits offered by the fertile soil and the freshwater of Lake Taihu and the Yangtze River, the Yangtze delta region has a long history of human settlement, including numerous sites of Neolithic cultures. Hundreds of sites of Neolithic cultures have been found in the Yangtze delta region, which can be categorized into three stages: Majiabang/Hemudu (ca. 5500–3900 BCE), Songze (ca. 3900–3200 BCE), and Liangzhu (ca. 3200–2200 BCE) (Stanley et al., 1999; Chen et al., 2005; Zhang et al., 2005; Itzstein-Davey et al., 2007a, b). Kuahuqiao, Tianluoshan, and Hemudu archaeological sites indicate that the Majiabang/Hemudu prospered around the Hangzhou Bay, and show evidence of the earliest paddy rice cultivation (e.g., Zong et al., 2007; Zheng et al., 2009; Fuller et al., 2009; Liu et al., 2016). The villagers survived by farming, hunting, fishing, and gathering. Many types of animal bone have also been found, including those of domesticated animals. The fauna indicated riverine and lacustrine plains and an environment that was more humid than today. Some artifacts of wood, bone, and bamboo, such as arrowheads, needles, and knives, have been recovered (Chang, 1986). The Songze was a development from the Majiabang, which was characterized by social stratification, ceramic technology, and decorative sophistication. Stone implements became more common and bone artifacts were used less than during the time of the Majiabang. Stonework became thinner and neater, and the shape and function of pottery diversified (Chang, 1986). The Songze was followed by the

Liangzhu, which was well developed both technologically and socially. Artifacts from the Liangzhu occupation, such as semilunar knives with holes, sickles, and something similar to a grain-pounding apparatus, have provided evidence of advanced rice cultivation. This culture also had diverse and sophisticated jade articles and advanced architectural technology (Chang, 1986; Liu et al., 2017).

The Liangzhu terminated mysteriously around 2200 BCE, after which time there followed a period of about 300 years without a trace of human settlement (the so-called "cultural interruption") until the beginning of the Bronze Age, Maquiao culture (1900–1200 BCE). The number of Neolithic cultural sites and population dramatically decreased during this period (Chen et al., 2005) (Fig. IIA-4g). The origin of the Maquiao culture might not have been related to the Liangzhu people because the Maquiao materials were less sophisticated than those of the Liangzhu (Stanley et al., 1999). At the time of the cultural interruption, other Neolithic settlements located around the upper reaches of the Yangtze River were also abandoned, e.g., the Shijiahe and the Longmagucheng Baodun (Yasuda et al., 2004).

II-A-4. Methods

II-A-4.1. Age determination

The age model for both sediment cores has already been constructed based on nine AMS ^{14}C dates of bivalve shells: five from core MD06-3040 and four from core MD06-3039 (Zheng et al., 2010; Wang et al., 2014). Stratigraphic correlation between the two cores was achieved by comparing magnetic susceptibility records, which allowed us to associate the stratigraphic depth of core MD06-3039 to that of core MD06-3040 (Zheng et al., 2010; Wang et al., 2014). To evaluate the chronological model for core MD06-3040 more accurately, I analyzed an additional four well-preserved shells from core MD06-3040 using ^{14}C-accelerator mass spectrometry at Paleo-Labo Co., Ltd. All ^{14}C age results were calibrated to calendar years using OxCal ver. 4.2.4 software (Ramsey et al., 2013) with the Marine 13 dataset (Reimer et al., 2013), which includes a constant average global reservoir age of 400 yr.

II-A-4.2. Alkenone analysis

Sediment samples were dried and crushed into a fine powder for organic matter analysis. The lipids contained in the powdered sediment (approximately 5 g) of each sample were extracted by sonication with dichloromethane/methanol (70:30, v/v) and then saponified with 0.5 mol L^{-1} KOH in MeOH. The saponified sample was then extracted with *n*-hexane to obtain the neutral components (Ohkouchi et al., 2005). The neutral lipids were separated into four subfractions by silica gel column chromatography. The N-1 fraction (hydrocarbons) was extracted with *n*-

hexane/dichloromethane (95:5, v/v), and the N-2 fraction (ketones, esters, and aldehydes) was collected with *n*-hexane/dichloromethane (4:6, v/v). Then, the N-2 fraction was introduced into a gas chromatograph with a flame ionization detector (GC-FID) equipped with a VF-5ms fused silica capillary column (30 m × 0.25 mm internal diameter, Agilent) at the Japan Agency for Marine-Earth Science and Technology. The oven temperature was programmed as follows: maintained at 40 °C for 2 min, raised to 120 °C at 30°C min^{-1}, raised to 300 °C at 6 °C min^{-1}, and maintained at 300 °C for 20 min. Several procedural blanks, which were analyzed parallelly to the same analysis, showed no C_{37} alkenone contamination.

It has been confirmed that the alkenone unsaturation index $U^{K'}_{37}$, defined as $[C_{37:2}]/([C_{37:2}] + [C_{37:3}])$ ($[C_{37:2}]$ and $[C_{37:3}]$ indicates the relative abundance of di-unsaturated C_{37} alkenone and tri-unsaturated C_{37} alkenone, respectively) and recovered from marine sediments are highly correlated with SST (Brassell et al., 1986; Prahl et al., 1988; Muller et al., 1998; Herbert et al., 2001; Conte et al., 2006). In this study, I applied the following relationship, which has been widely applied for the alkenone paleo-SST reconstructions in the ECS (e.g., Xing et al., 2013; Yuan et al., 2018), and was proposed by Tao et al. (2012) based on the $U^{K'}_{37}$ data collected from 30 sediment samples covering most of the southern Yellow Sea (YS) near the core site.

Annual mean SST (°C) = $(U^{K'}_{37} + 0.350)/0.059$

($R = 0.912$; $1\sigma = 0.41$°C; $n = 30$)

The analytical errors for $U^{K'}_{37}$-SST and alkenone content were ±0.3% (±1σ) and ±20.1% (±1σ) based on 12 replicated analyses.

II-A-4.3. Measurement of organic carbon and nitrogen content

I measured the content (wt.%) of total organic carbon (TOC) and total nitrogen (TN) using a Flash 2000 CHNS elemental analyzer at the Geological Survey of Japan (National Institute of Advanced Industrial Science and Technology) using analytical methods similar to those of Maeda et al. (2002). For TOC determination, 1 M HCl was added to approximately 20 mg of powdered sediment until all $CaCO_3$ was dissolved. The analytical error was within ±1% based on seven replicated analyses.

II-A-4.4. Identification of coccolithophores

Samples of sediment at depths of 9, 424, 709, 723, 843, and 1,193 cm were prepared as smear slides for examination of calcareous nannofossils at ×1500 magnification under a cross-polarized light microscope. At least 300 coccoliths were counted in each sample, and the species were identified using a scanning electron microscope. The classification of *Gephyrocapsa* spp. coccoliths followed that of Bollman et al. (1998).

II-A-5. Results

II-A-5.1. Radiocarbon dating and depositional environment

The calendar age–depth profile based on the AMS ^{14}C dates shows that core MD06-3040 provides a continuous record from the present day to 10.4 cal. kyr BP (Fig. IIA-2; Table IIA-1). The mean sedimentation rate was approximately 2.0×10^2 cm kyr^{-1}.The sedimentation rate of Units B and C was 1.1×10^2 cm kyr^{-1}, i.e., lower than that of Unit A. The boundary between Units A and B (15.86 m) corresponds to the age 7.5 cal. kyr BP, when the postglacial rise of sea level decelerated (Liu et al., 2004; Lambeck et al., 2014). The relatively low sedimentation rate and fluctuating grain size of Units B and C could be attributed to a reduction of the sediment supply and an unstable sedimentary environment during the formation of a transgressive systems tract before the HHS. The relatively homogeneous grain size of Unit A indicates that water circulation and the sedimentary environment were similar throughout this time, which is consistent with the stable marine conditions at the core site after the HHS (Fig. IIA-3h).

II-A-5.2. Alkenone SST

C_{37} methyl alkenones ($C_{37:2}$ and $C_{37:3}$) and C_{38} methyl and ethyl alkenones ($C_{38:2Me}$, $C_{38:3Me}$, $C_{38:2Et}$, and $C_{38:3Et}$) were found in core MD06-3040. Total alkenone content ranged from 1.41 to 213 ng g^{-1} (average: 51.4 ng g^{-1}). The entire alkenone record of core MD06-3040 can be classified into three periods (I, II, and III) based on the characteristics of the $U^{K'}_{37}$-SST variations (Fig. IIA-3a). From 3.8 cal. kyr BP to the present day (Period I), the $U^{K'}_{37}$-SST values were relatively high and constant

(20.9–22.5 °C), except for during a short period of decline from 1700 to 1850 CE. From 2600 to 1900 BCE (Period II), the $U_{37}^{K'}$ values dropped remarkably and fluctuated considerably (17.9–21.9 °C). From 6800 to 2600 BCE (Period III), the $U_{37}^{K'}$ values were relatively high and moderately stable (20.3–22.4 °C). All of the $U_{37}^{K'}$ data are shown in Table IIA-2.

II-A-5.3. Organic carbon and nitrogen content

TOC and TN constituted 0.39–0.59 wt.% (average: 0.50 wt.%) and 0.045–0.090 wt.% (average: 0.072 wt.%) of the sediments, respectively (Fig. IIA-3d, e). Both values increased continuously from 9.0 cal. kyr BP to the present day, being noticeably low in Unit B and highest at the top of Unit A. The C/N ratios ranged from 6.2 to 8.8 (average: 7.0); they were moderate in Unit A and increased conspicuously in Unit B (Fig. IIA-3f). C/N ratios can be used to distinguish the source of organic matter. Typical marine phytoplankton organic matter has a C/N ratio of 6–7, whereas the C/N ratio of terrestrial organic matter is >12 (Meyers et al., 1994). The C/N ratios in this study indicated that most organic matter was of marine origin after the sea level stabilized at around 5500 BCE, whereas there was greater contribution from terrestrial organic matter before the HHS. All of the data are shown in Table IIA-3.

II-A-5.4. Coccolith assemblages

Coccoliths were recognized in six sediment samples from core MD06-3040 (Fig. IIA-3g). *Gephyrocapsa oceanica*, *Emiliania huxleyi*, *Helicosphaera carteri*, and *Calcidiscus leptoporus* were identified in each sediment sample. Some

Noëlaerhabdaceae coccoliths that could not be identified at the species level due to partial dissolution were classified as Noëlaerhabdaceae gen. et sp. indet. The coccolith assemblages of all the observed samples were dominated by *G. oceanica*, which represented 70%–80% of the total; *E. huxleyi* accounted for 5%–10%, and the relative abundances of the other minor species represented <5%. These characteristics of coccolith assemblages of core MD06-3040 are consistent with the results of Tanaka (2003) and Yang et al. (2004), who reported the coccolith fluxes and species assemblages at the shelf edge of the ECS.

II-A-6. Discussion

II-A-6.1. Assessment of alkenone SST time series record

As described above, I obtained remarkably low $U^{K'}_{37}$-SSTs in Period II, which is unique as a Holocene climate change record. Before discussing the results for SST fluctuations, I need to establish the reliability of the $U^{K'}_{37}$-SST reconstruction for this core.

II-A-6.1.1. Effects of alkenone production depth and season

The $U^{K'}_{37}$ value can sometimes be disturbed by changes in alkenone production depth (e.g. Ohkouchi et al., 1999). However, $U^{K'}_{37}$ variations of core MD06-3040 might not reflect the change of habitat depth of alkenone producers because the depth around the coring site is only 40–50 m and the annual mean water temperature variation in the water column is less than 1 ºC according to the World Ocean Atlas 2013 (Locarnini et al., 2013). As discussed by Chapman et al. (1996) and Dowsett et al. (2011), the shift in the season of maximal coccolith production could also produce $U^{K'}_{37}$-SST's anomalies. Although it is difficult to rule out such potential anomalies, I have no evidence to suggest they are important for the remarkably low $U^{K'}_{37}$-SSTs in Period II because no changes in nutrient supply, primary productivity, freshwater flux, and sediment source were suggested by the TOC, TN, C/N ratio (Fig. IIA-4d–e), clay mineral assemblage (Fang et al., 2018), and other major and trace element concentrations (Shao, 2012; Yang et al., 2015; Bi et al., 2017) in the relevant part of core MD06-3040. The $U^{K'}_{37}$ values represent annual mean SST based on several core-

top sediment $U_{37}^{K'}$ data points in the ECS and southern YS, where the marine environmental factors, including nutrient supply, salinity, and temperature, are significantly diversified (Tao et al., 2012; Kim et al., 2015). Therefore, I believe that the $U_{37}^{K'}$ values of core MD06-3040 would most closely reflect annual mean SSTs.

II-A-6.1.2. Effects of haptophyte species

G. oceanica and *E. huxleyi*, known as coccolith-bearing taxa belonging to the family Noëlaerhabdaceae, are distributed in the oceans around the world (Volkman et al., 1980; Marlowe et al., 1984). C_{37} and C_{38} alkenones produced in the ocean are derived mainly from these two species. However, there are other haptophytes that also produce alkenones with much lower $U_{37}^{K'}$ values than those of *G. oceanica* and *E. huxleyi*. Some of the haptophytes belonging to family Isochrysidaceae, such as *Isochrysis galbana* and *Ruttnera lamellose* (revised from *Chrysotila lamellosa*; Andersen et al., 2014), form no coccoliths and live in low-salinity seawater or saline lakes (Versteegh et al., 2001; Sun et al., 2007; Nakamura et al., 2014; Araie et al., 2018). These species have been considered minor contributors in marine settings. However, I evaluate their contributions to $U_{37}^{K'}$ in the sediments because our study site is close to the mouth of the Yangtze River. The relative contributions of the alkenone producers among these two types of haptophytes were generally evaluated based on the C_{37}/C_{38} ratio or the absence/presence of $C_{37:4}$ and C_{38Me} (Marlowe et al., 1984; Chu et al., 2005). Based on culture experiments, the C_{37}/C_{38} ratio of *G. oceanica* and *E. huxleyi* was found to range between 0.4 and 2.5, whereas the ratios of *I. galbana* and *R. lamellosa* were relatively high, i.e., 1.5–9.2 and 5.5–15.0, respectively (Marlowe et al., 1984; Conte et al., 1998). $C_{37:4}$ was detected from *I.*

galbana and *R. lamellosa* regardless of growing temperature, but not from *G. oceanica* and *E. huxleyi* cultured at a water temperature of 15 °C or higher. Conversely, C_{38Me} was detected only from *G. oceanica* and *E. huxleyi* and not from *I. galbana* and *R. lamellosa* (Marlowe et al., 1984; Conte et al., 1998). The C_{37}/C_{38} ratio in core MD06-3040 ranged from 0.07 to 1.60 with a mean value of 0.65 (Fig. IIA-3b), most of which corresponded to that of *G. oceanica* and *E. huxleyi*. C_{38Me} was found in all analyzed samples of the core with C_{38Me}/C_{38Et} values of 0.06–0.59 (average: 0.27) (Fig. IIA-3c) and $C_{37:4}$ was not detected at all. Moreover, I observed sediments under a microscope and detected abundant *G. oceanica* and *E. huxleyi* from the core. Their relative abundance in the observed samples showed little variety (Fig. IIA-3g). Thus, I can determine that our $U_{37}^{K'}$ results were unaffected by haptophyte species change.

II-A-6.1.3. Effects of salinity

Some previous studies pointed out that $U_{37}^{K'}$ is not a good proxy for SST under low–salinity environments at high latitudes, such as the Nordic Sea, North Atlantic, and Baltic Sea (Rosell-Melé, 1998; Blanz et al., 2005). Reasons for the disturbed $U_{37}^{K'}$ –SST relationships in low-salinity areas have been offered that they reflect the contributions of a different type of alkenone produced by family Isochrysidaceae haptophytes, as I mentioned in the previous chapter, or that they reflect changes in the alkenone biosynthesis due to low-salinity stress (Schulz et al., 2000). Whatever the cause, the abundance of $C_{37:4}$ could be used to identify situations in which $U_{37}^{K'}$ is not a reliable paleothermometer (Rosell-Melé, 1998). Here, I could not detect any $C_{37:4}$ alkenones from all parts of the core, which indicated that the influence of low

salinity is limited for the $U_{37}^{K'}$-SST of core MD06-3040. It also suggests only a small effect from salinity variations on $U_{37}^{K'}$-SST in southern YS, where salinity changes between 28.0–34.0 psu (Tao et al., 2012). Moreover, the salinity around the core site, mainly controlled by the Yangtze River discharge, seemed not to decrease in Period II (e.g., Kubota et al., 2015). Therefore, our $U_{37}^{K'}$ drops in Period II could not reflect the low-salinity effects on alkenone production.

II-A-6.1.4. Effects of re-deposition

Affected by both the large rivers and the Pacific Ocean, the surface sediments in the ECS, which were mainly deposited after the deglaciation, exhibit successively different values of mean grain size, TOC content, and C/N ratio from the coast to the Okinawa Trough (Zhu et al., 2011; Bao et al., 2016). In addition to the continuous change in the ^{14}C age of shells, the absence of significant changes in these values in Period II suggests that continuous marine biological production and deposition occurred at the core site (Figs. IIA-2, IIA-3d–f).

Strengthening of the cold ECSCC could have transported alkenone produced in the cold YS to the core site, which might have resulted in the $U_{37}^{K'}$ drop. However, several other studies on sedimentation rate, grain size, and clay mineral analysis of sedimentary cores, collected from the inner shelf mud belt, have indicated that the ECSCC weakened at around 2000 BCE (Chen et al., 2017), which is opposite the trend in our SST record. Moreover, the sediment provenance analysis based on the clay mineral assemblage of core MD06-3040 revealed that most of the terrigenous sediment originated from the Yangtze River, and there were no significant changes in the sediment provenance in Period II (Fang et al., 2018). Therefore, our $U_{37}^{K'}$ drops in

Period II could not reflect re-suspension or re-transportation of sediments from the old, glacial materials deposited near the Okinawa Trough or sediments from the relatively cold YS.

II-A-6.2. SST fluctuation

The surface sediments of core MD06-3040 produced a $U^{K'}_{37}$-SST of 22.1°C, comparable with the observed modern annual mean SST (21.1°C) near the core site (27°52’30”N, 121°22’30”E). Therefore, this conversion formula proposed by Tao et al. (2012) was considered suitable to allow us to estimate reliable paleotemperatures.

II-A-6.2.1. Little Ice Age

The short-term SST drop (0.6–1.0 °C) during 1700–1850 BCE, could correspond to the Little Ice Age (LIA). The LIA, which corresponds with Bond Event 0, was a 1–2 °C cold event in the Northern Hemisphere caused by several volcanic eruptions and a lowering of solar activity (IPCC Assessment Report, 2014). The LIA has been recorded in several proxies such as tree rings, ice cores, and lake sediments, in East Asia (Yang et al., 2002; Mann et al., 2009; Cook et al., 2013). Evidence of this event has been confirmed by general climatic information extracted from Chinese historical documents that reported the occurrence of several severe cold and dry periods during this time (Wang et al., 1992). The characteristic of our SST records from 1000 BCE to the present day resembles previous AT reconstructions (Wang et al., 1992; Yang et al., 2002; Mann et al., 2009; Cook et al., 2013), which validates the reliability of our record as a temperature proxy.

II-A-6.2.2. Extraordinary cold episodes during the mid-Holocene

Several large drops of SST during Period II (by 3–4 °C) were the most prominent feature evident in our results. The similar $U_{37}^{K'}$-SST decrease could also be found from core MD06-3039 (Zhou et al., in prep.). Our $U_{37}^{K'}$-SST fluctuations are quite unique compared to other SST records reconstructed from the ECS. However their timing and magnitude is not consistent to our $U_{37}^{K'}$-SST records, SST drops during the same period (around 2000 BCE) have been noted previously from shallow marine proxies by alkenone SSTs and the pollen assemblage in Mutsu Bay, northern Japan (Kawahata et al., 2009), alkenone SSTs in cores B3 and ZY2 in the southern YS (Wang et al., 2011; Zhao et al., 2014), and the Sr/Ca ratio in fossil corals from Kikai Island in the eastern ECS (Kajita et al., 2017). In contrast, several cores recovered from the central part of the ECS, where SSTs were strongly controlled by the YSWC and the KC, never recorded the cooling event during the same period (e.g., Yuan et al., 2018). This suggests that our $U_{37}^{K'}$-SST records were strongly affected by terrestrial climate or coastal upwelling because of its coastal location, while other SST records from the open sea could reflect regional ocean currents.

In spite of some uncertainties in age estimations, the frequent and abrupt SST drops should have occurred around 2600 –1900 BCE, which could be associated with the global climatic episode called the 4.2 ka event. This event has been reported in several regions in China. In southeast China, both the Subtropical High over the northwestern Pacific Ocean and the East Asian monsoon play important roles in the modern regional climate. Several terrestrial monsoon records obtained in southern–central China, such as speleothems, lake levels, and sediment cores, have indicated a weakened EASM and abrupt drying and cooling shifts in southeast China during the

same period (An et al., 2000; Chen et al., 2005; Wang et al., 2005; Ma et al., 2009; Innes et al., 2014) (Fig. IIA-4b). In addition, various climatic proxies from arid and semiarid areas of northern and western China are sensitively influenced by variations in the EASM. A southward shift of the summer position of Intertropical Convergence Zone (ITCZ) around 2200 BCE was reported, which resulted in an abrupt transition of the climate from wet to dry (Wu et al., 2004; Xiao et al., 2004; Ji et al., 2005; Wen et al., 2010) (Fig. IIA-4c). The EASM is controlled by the path of the westerly jet (WJ) over eastern Asia (e.g., Tada et al., 2017). Nagashima et al. (2013) suggested that the limit of the seasonal northward progression of the WJ was shifted southward at around 2200 BCE because the contribution of dust from the Mongolian Gobi Desert relative to that from the Taklimakan Desert in the Japan Sea sediments, which can be used as a proxy for millennial-scale changes of the WJ path, show broad maxima at around 2200 BCE. (Fig. IIA-4d). This suggests that the southward shift of the WJ position could have resulted in the decrease in EASM moisture and heat energy transportation from the tropical Pacific Ocean to southeast China.

In addition to the modulation of EASM, the KC is also known to have varied around 24000–2000 BCE (the so-called *Pulleniatina* Minimum Event) (Ujiié et al., 2003). KC accounts for considerable heat flux from the Western Pacific Warm Pool to East Asia and exerts a significant impact on the climate of East Asia and its marginal seas (Tada and Murray, 2016). The abundance of the planktonic foraminifera *Pulleniatina obliquiloculata*, which is typically found in the KC area, has been reported to have decreased abruptly in collected sediment cores from the Okinawa Trough around 2200 BCE, indicating that the surface transport of the KC was reduced (Ujiié et al., 2003; Xiang et al., 2007) (Fig. IIA-4e).

As discussed by Hu and Wang (2016), coastal upwelling, with relatively low SST is commonly observed in East Asian marginal seas. Enhanced upwelling increases primary productivity and consequently the supply of organic materials to seafloor (Wei et al., 2008; Yang et al., 2013). The interannual variation of coastal upwelling along the Zhejiang coast is controlled by the variation in the wind stress and the coastal currents (Hu and Wang, 2016). Enhanced coastal upwelling in the core site, which could be caused by the modulation in monsoonal wind and KC might possibly accelerate the decline of SSTs during Period II. However, I have no evidence to suggest they are important because the amount of TOC and TN in the sediment were not change at all during the period (Fig. IIA-3d, e). There is no change in major/trace elements concentrations such as Mn, V, Co, Ni, Cu, Zn, Ba and U, which are related to ocean circulation and biogeochemical cycling (Shen, 2012MS; Yang et al., 2015; Bi et al., 2017).

Recent studies have suggested that the 4.2 ka event might also have been related to one of the widespread cold episodes forced by variations in solar output, called “Bond Events,” during which the subpolar and subtropical surface waters of the Atlantic Ocean were cooled (Fig. IIA-4f) (Bond et al., 2001). During the Holocene, China experienced millennial-scale climatic events, some of which could have been temporally correlated with Bond Events (e.g., Hong et al., 2005). Therefore, the 4.2 ka event, which corresponds with Bond Event 3, could possibly have been controlled by a similar forcing agent. However, the forcing mechanisms that markedly expanded the 4.2 ka event remain controversial; a weakened East Asian monsoon and a modulation of the KC might have amplified the decrease of temperature in the core site.

II-A-6.3. Holocene environmental change in the Yangtze delta and generalized features of its influence on human civilization

Many studies of sediment cores collected from the Yangtze delta have recorded high occurrence of phytoliths from the family Gramineae, which indicated that paddy rice cultivation was flourishing widely since around 5500 BCE (Yasuda et al., 2004; Chen et al., 2005; Itzstein-Davey et al., 2007b). The moderate EASM precipitation and relatively warm climate in the Yangtze delta region prior to 2200 BCE (Ji et al., 2005) would have been suitable for the development of rice cultivation. As described in Section 2.3, "Oceanographic setting", ATs in the coastal region are highly correlated with present-day SSTs at the core site. I believe this relationship has been satisfied after the HHS, because neither the sea level nor the distance between the core site and the coast have changed. Our finding of frequent and abrupt cold episodes around 2600–1900 BCE could reflect a large cold event experienced in the Yangtze delta region that was at least more severe than the LIA. The frequent and abrupt changes to a cold climate during Period II could have been responsible for the decline of rice cultivation because AT is a parameter that is critical for rice yield (Sugihara et al., 1991). In modern society, catastrophic damage to rice cultivation due to cold weather is not uncommon despite improvements both to the varieties of rice grown and the irrigation systems used. For example, the Mount Pinatubo eruption in 1991, the largest such event during the 20th century, released 20 million tons of sulfur dioxide into the stratosphere, which caused global ATs to drop temporarily in 1992–1993 by about 0.4 °C (Self et al., 1993). In Japan, the poorest rice crop obtained during 1950–2000 AD occurred in 1993. In northern Japan, paddy rice production was reduced to 56% of the average because of the cool

summer AT anomaly of ~3.5 °C (Japan Meteorological Agency Publictions). The $U_{37}^{K'}$ records in this study showed multiple abrupt drops of SST of 2–3 °C (concurrent AT drop could be estimated as 3–5 °C), during Period II, which could have been sufficient to have considerable negative impact on rice cultivation.

The relationship between the cultural interruption and climate change has been discussed in many studies, e.g., based on pollen records of terrestrial borehole cores or lake sediment cores from the Yangtze delta region (e.g. Stanley et al., 1999; Yu et al., 2000; Chen et al., 2005; Zhang et al., 2005; Tao et al., 2006; Davey et al., 2007b; Zong et al., 2011; Innes et al., 2014; Wang et al., 2017; Wang et al., 2018). However, there is no consensus on this topic because it is very difficult to reconstruct short-term abrupt climate changes using terrestrial borehole cores with possibly discontinuous deposition. Some studies have indicated that the climate became dry and cold in the lower reaches of the Yangtze River from 2200 to 1600 BCE (Yasuda et al., 2004; Chen et al., 2005; Tao et al., 2006; Innes et al., 2014), consistent with our alkenone records. However, Stanley et al. (1999) indicated the climate became warmer and wetter during this period, based on the relatively high proportions of evergreen tree pollen contained within the cores. Yu et al. (2000) speculated that a flood-induced expansion of Lake Taihu was partly responsible for the cultural interruption. Zhang et al. (2005) and Wang et al. (2018) insisted that coastal flooding due to sea-level rise and typhoon events were major causes of vulnerability of the Yangtze delta. However, Itzstein-Davey et al. (2007b) and Zong et al. (2011) reported that there were no severe floods or abrupt climate changes during this period and social causes might be more important than environmental changes. The well-dated, continuous, and high-resolution quantitative SST (or AT) records of this study

suggest the frequent and abrupt cold episodes could explain the changes in regional vegetation, decline of rice cultivation, and eventual collapse of the Yangtze Neolithic civilizations. Although I cannot provide a precise and quantitative mechanism regarding the linkage between environmental change and the fate of the Yangtze Neolithic civilizations, our research does provide important information for elucidating the relationship between climate change and the outcome of rice cultivating cultures.

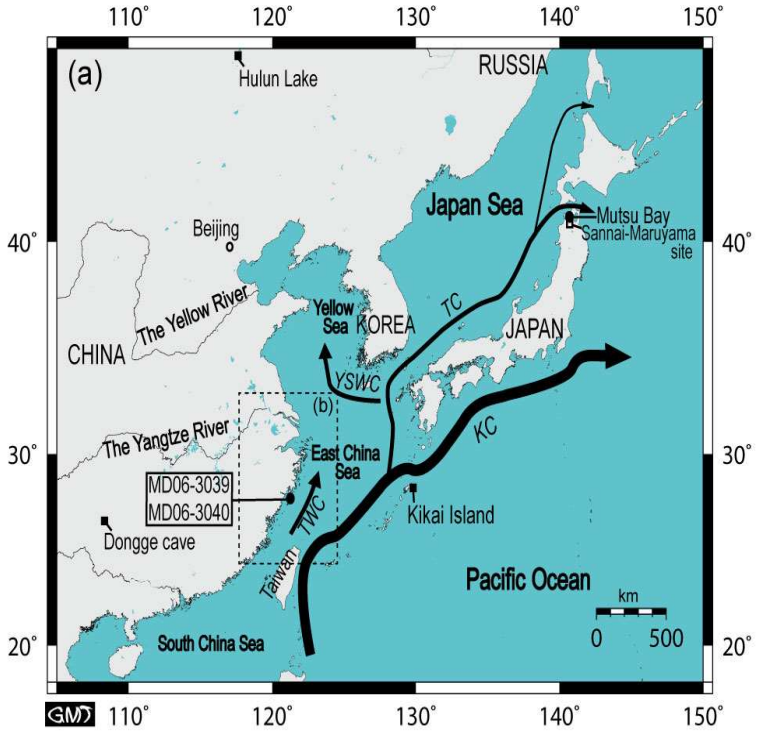
(a)
Hulun Lake
RUSSIA
Japan Sea
Mutsu Bay
Sannai-Maruyama site
Beijing
Yellow Sea
KOREA
TC
JAPAN
CHINA
The Yellow River
YSWC
(b)
The Yangtze River
East China Sea
KC
MD06-3039
MD06-3040
TWC
Kikai Island
Dongge cave
Taiwan
Pacific Ocean
km
0
500
South China Sea
110°
120°
130°
140°
150°
40°
30°
20°

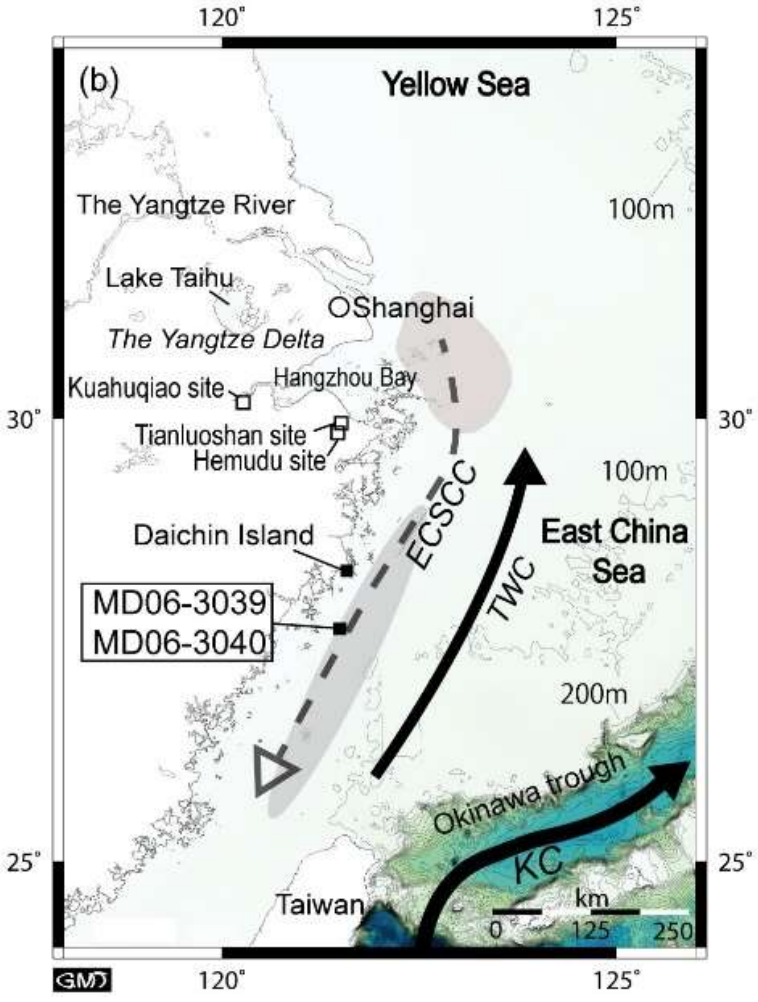
(b)
Yellow Sea
The Yangtze River
100m
Lake Taihu
Shanghai
The Yangtze Delta
Kuahuqiao site
Hangzhou Bay
Tianluoshan site
Hemudu site
ECSCC
100m
Daichin Island
East China Sea
TWC
MD06-3039
MD06-3040
200m
Okinawa trough
KC
Taiwan
km
0
125
250
120°
125°
30°
25°

Fig. IIA-1

(a) Map of the Yangtze delta region and surrounding areas, including the western North Pacific Ocean, East China Sea, Yellow Sea, South China Sea, and Japan Sea. Some locations of the sites of the geological records described in the other figures are shown. The arrows represent the paths of the Kuroshio Current (KC), the Tsushima Current (TC), the Taiwan Warm Current (TWC), and the Yellow Sea Warm Current (YSWC).

(b) Locations of the site of cores MD06-3040 and MD06-3039 and some of the major Yangtze delta archaeological sites (open squares). The dotted arrow and the gray shaded area represent the East China Sea Coastal Current (ECSCC) and the approximate location of the inner shelf mud belt, respectively. Bathymetric isolines are at 100-m depth intervals. The figures were generated using Generic Mapping Tools (Wessel and Smith, 1998).

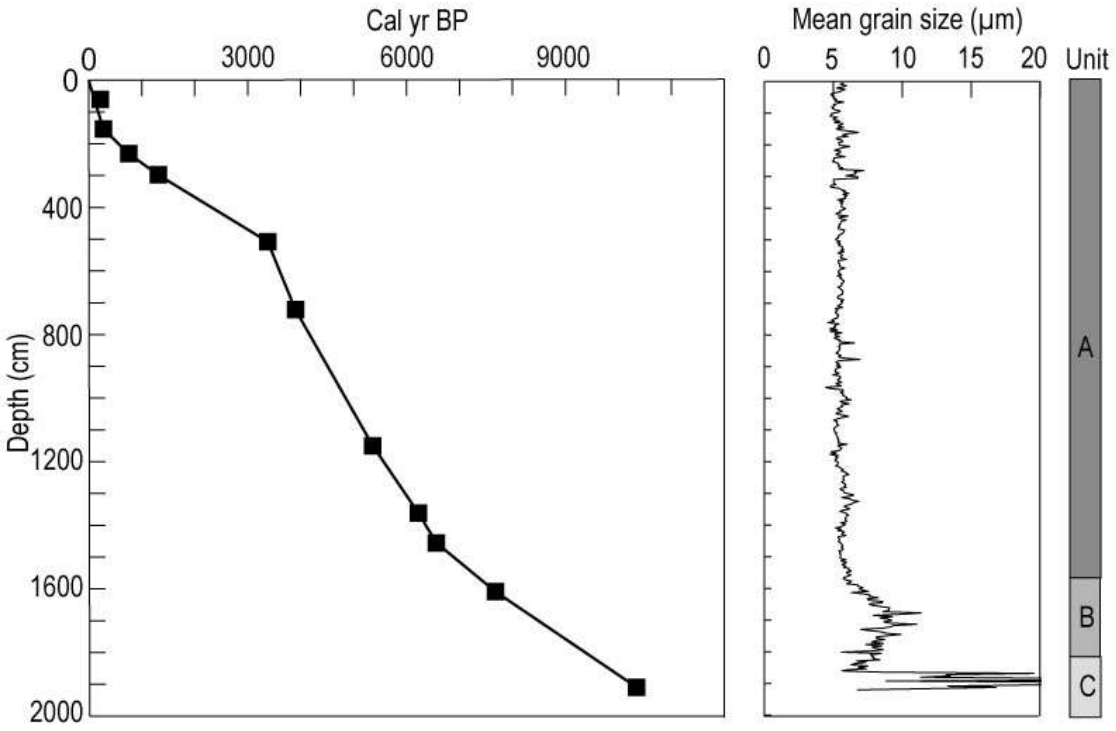

Fig. IIA-2

Core depth versus radiocarbon ages (Cal. yr BP) of shells and mean grain size (Wang et al., 2014) of core MS06-3040.

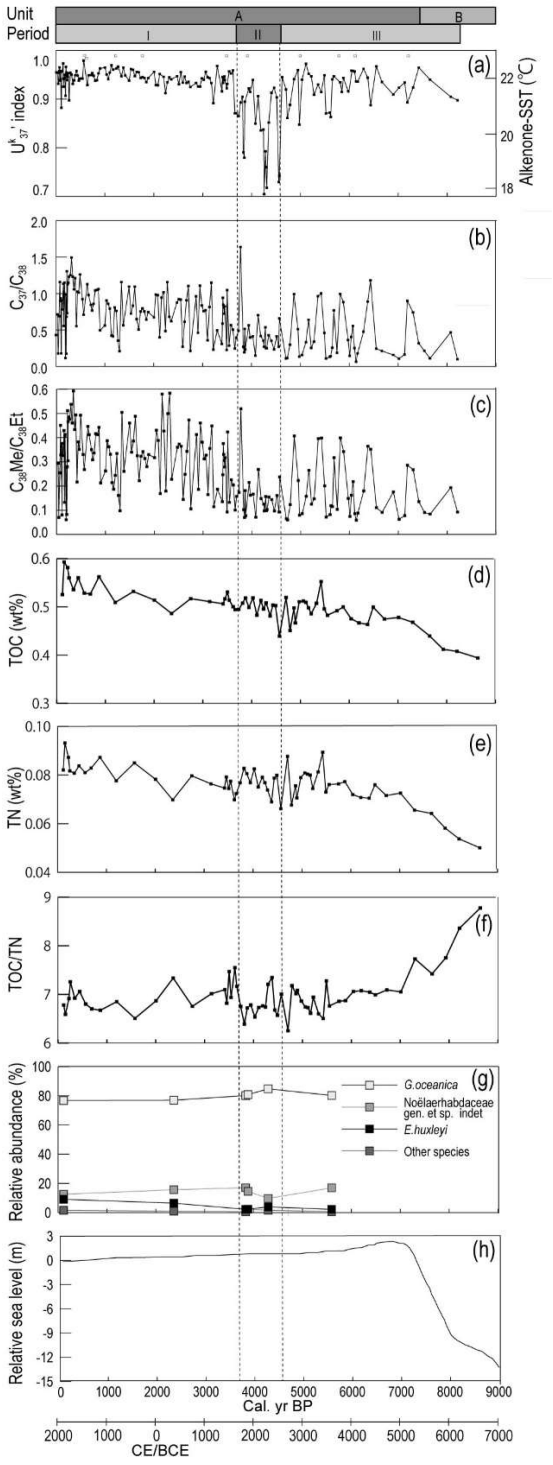

Fig. IIA-3

Time series records of (a) $U^{K'}_{37}$ index and alkenone temperature (black squares) and age control points (open squares), (b) C_{37}/C_{38} alkenone ratio, (c) C_{38Me}/C_{38Et} alkenone ratio, (d) TOC content, (e) TN content, (f) C/N ratio and (g) relative abundance of coccoliths. The sea level curve of the ECS (Liu et al., 2004) are also shown (h).

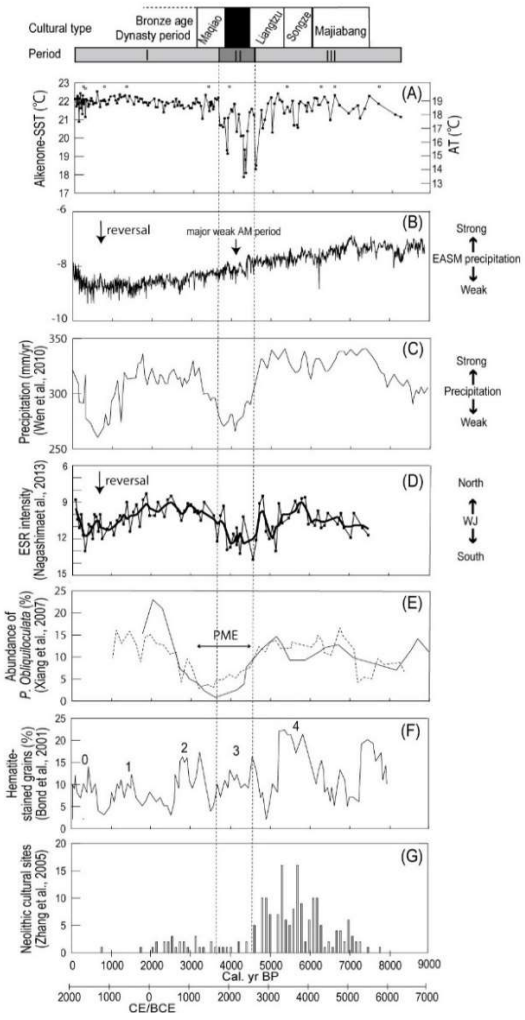

Fig. IIA-4

Time series records of (a) $U^{K'}_{37}$-SSTs in core MD06-3040 and estimated ATs with age control points shown in open squares, (b) $\delta^{18}O$ records of Dongge cave in China (Wang et al., 2005), (c) The amount of precipitation reconstructed from the pollen assemblage data recovered from lake Hulun (Wen et al., 2010). (d) ESR signal intensity of fine silt-sized quartz particles of D-GC-6 collected from the Japan Sea used as a proxy for the WJ path (Nagashima et al., 2013), (e) The timing of the PME observed in core E07 (solid line) and core A7 (dotted line), drilled from the Okinawa Trough (Xiang et al., 2007), (f) hematite-stained grains ratio of core VM29-191 collected from North Atlantic indicating drift ice event (Bond et al., 2001), and (g) number of cultural sites found in the Yangtze River delta region (Zhang et al., 2005). The change in the culture type flourished in the Yangtze delta is also shown in the upper column.

Table IIA-1

Depths and results of radiocarbon dating of cores MD06-3040 and MD06-3039.

Depth in MD06-3039 (cm)	Depth in MD06-3040 (cm)	Conventional 14C age (yr BP)	Calibrated age (Marine13) (Cal yr BP)	
			Intercept	Range
	61-62	580±20	220	148-271
140-141	(154-155)	627±21	275	255-293
210-211	(231-232)	1217±22	752	716-783
	298-299	1765±30	1309	1277-1338
	509-510	3490±25	3375	3339-3410
	723-724	3917±25	3896	3850-3940
	1151-1152	4992±34	5351	5294-5396
	1363-1364	5788±41	6211	6179-6262
	1457-1458	6120±23	6551	6505-6600
	1611-1612	7205±36	7666	7616-7704
	1912-1913	9479±33	10324	10251-10369

Table IIA-2

Summary of alkenone data from core MD06-3040.

Depth (cm)	Age (Cal. yr BP)	$U_{37}^{K'}$
5	9.0	0.955
17	30.4	0.954
25	44.8	0.931
37	66.2	0.958
41	73.4	0.965
45	80.6	0.938
49	87.7	0.955
53	94.9	0.941
61	109.2	0.882
65	116.4	0.958
73	130.7	0.957
81	145.0	0.974
85	152.2	0.925
89	159.3	0.942
93	166.5	0.943
97	173.6	0.950
109	195.1	0.907
113	202.3	0.966
117	209.4	0.954
121	216.6	0.947
125	223.8	0.939
129	230.9	0.950
133	238.1	0.946
141	252.4	0.954
149	266.7	0.898
157	293.6	0.954
161	318.4	0.950
165	343.1	0.931
169	367.9	0.939
173	392.7	0.949
177	417.5	0.958
181	442.3	0.949
185	467.0	0.938
189	491.8	0.942
197	541.4	0.942
201	566.2	0.979
213	640.5	0.929
217	665.3	0.949
225	714.8	0.949
229	739.6	0.953
233	768.6	0.948
237	801.9	0.938
241	835.1	0.939
245	868.4	0.953

249	901.6	0.963
261	1001.4	0.965
265	1034.7	0.951
269	1067.9	0.941
273	1101.2	0.955
277	1134.4	0.969
281	1167.7	0.961
289	1234.2	0.963
293	1267.4	0.967
301	1338.4	0.947
305	1377.5	0.965
317	1495.0	0.938
321	1534.2	0.962
325	1573.4	0.960
329	1612.5	0.947
333	1651.7	0.956
337	1690.9	0.955
341	1730.0	0.943
345	1769.2	0.945
349	1808.4	0.943
353	1847.5	0.935
357	1886.7	0.943
369	2004.2	0.956
373	2043.4	0.929
377	2082.5	0.928
381	2121.7	0.952
389	2200.0	0.946
393	2239.2	0.912
397	2278.4	0.934
401	2317.5	0.945
405	2356.7	0.941
417	2474.2	0.947
421	2513.4	0.930
425	2552.5	0.955
429	2591.7	0.934
433	2630.9	0.946
437	2670.0	0.933
441	2709.2	0.935
445	2748.4	0.925
457	2865.8	0.933
461	2905.0	0.926
465	2944.2	0.926
469	2983.3	0.943
473	3022.5	0.940
477	3061.7	0.956
481	3100.8	0.945
485	3140.0	0.943
489	3179.2	0.933
493	3218.3	0.892

501	3296.7	0.968
517	3394.5	0.916
521	3404.2	0.945
525	3414.0	0.933
529	3423.7	0.939
533	3433.4	0.943
537	3443.2	0.947
541	3452.9	0.939
557	3491.9	0.922
561	3501.6	0.931
577	3540.6	0.957
593	3579.5	0.953
609	3618.5	0.959
625	3657.4	0.871
637	3686.6	0.871
657	3735.3	0.865
673	3774.3	0.893
697	3832.7	0.791
705	3852.2	0.780
709	3861.9	0.895
737	3943.6	0.922
745	3970.8	0.915
761	4025.2	0.940
777	4079.6	0.850
793	4134.0	0.906
809	4188.4	0.836
825	4242.7	0.837
829	4256.3	0.705
837	4283.5	0.793
841	4297.1	0.760
845	4310.7	0.718
857	4351.5	0.852
873	4405.9	0.913
889	4460.3	0.923
905	4514.7	0.904
917	4555.5	0.730
921	4569.1	0.742
961	4705.1	0.920
969	4732.3	0.861
985	4786.7	0.888
1009	4868.3	0.941
1033	4949.8	0.960
1041	4977.0	0.848
1057	5031.4	0.940
1081	5113.0	0.973
1097	5167.4	0.952
1113	5221.8	0.947
1129	5276.2	0.909
1153	5359.1	0.930

1169	5424.0	0.915
1185	5488.9	0.949
1193	5521.4	0.871
1213	5602.5	0.872
1217	5618.7	0.863
1225	5651.2	0.941
1233	5683.6	0.947
1265	5813.5	0.935
1273	5845.9	0.915
1281	5878.4	0.944
1305	5975.7	0.916
1321	6040.6	0.959
1329	6073.1	0.958
1337	6105.5	0.957
1345	6138.0	0.936
1353	6170.4	0.936
1385	6290.6	0.962
1409	6377.4	0.944
1425	6435.3	0.888
1457	6551.0	0.967
1473	6666.8	0.935
1505	6898.5	0.909
1521	7014.4	0.923
1537	7130.2	0.934
1545	7188.1	0.893
1561	7304.0	0.924
1577	7419.8	0.965
1609	7651.5	0.940
1657	8072.4	0.905
1673	8213.7	0.898

Table IIA-3

Summary of organic carbon and nitrogen data from core MD06-3040.

Depth (cm)	Age (cal. yr BP)	TN (wt. %)	TOC (wt. %)	C/N
65	116.4	0.082	0.525	6.40
85	152.2	0.093	0.593	6.37
125	223.8	0.087	0.582	6.67
141	252.4	0.082	0.560	6.85
165	343.1	0.081	0.536	6.63
181	442.3	0.084	0.560	6.68
201	566.2	0.081	0.529	6.53
221	690.1	0.083	0.527	6.35
245	868.4	0.087	0.563	6.45
285	1200.9	0.078	0.509	6.55
325	1573.4	0.085	0.532	6.26
369	2004.2	0.078	0.514	6.56
405	2356.7	0.070	0.486	6.97
445	2748.4	0.080	0.517	6.49
485	3140.0	0.076	0.511	6.69
525	3414.0	0.075	0.506	6.78
541	3452.9	0.079	0.517	6.52
561	3501.6	0.074	0.531	7.13
577	3540.6	0.078	0.514	6.63
609	3618.5	0.070	0.500	7.17
625	3657.4	0.072	0.494	6.82
657	3735.3	0.077	0.495	6.45
689	3813.2	0.083	0.508	6.13
713	3871.7	0.081	0.519	6.44
737	3943.6	0.077	0.499	6.48
761	4025.2	0.083	0.519	6.28
785	4106.8	0.075	0.483	6.43
809	4188.4	0.079	0.513	6.49
825	4242.7	0.077	0.496	6.45
841	4297.1	0.074	0.508	6.88
865	4378.7	0.069	0.481	6.97
881	4433.1	0.079	0.504	6.39
897	4487.5	0.080	0.503	6.29
921	4569.1	0.066	0.439	6.64
961	4705.1	0.088	0.520	5.93
985	4786.7	0.068	0.451	6.66
1009	4868.3	0.076	0.498	6.58
1017	4895.5	0.071	0.467	6.61
1041	4977.0	0.079	0.511	6.47

1065	5058.6	0.081	0.512	6.33
1081	5113.0	0.080	0.509	6.34
1097	5167.4	0.080	0.498	6.22
1113	5221.8	0.075	0.486	6.52
1145	5330.6	0.081	0.507	6.24
1169	5424.0	0.089	0.553	6.18
1185	5488.9	0.073	0.496	6.80
1201	5553.8	0.076	0.483	6.34
1249	5748.5	0.076	0.492	6.44
1281	5878.4	0.077	0.500	6.46
1321	6040.6	0.072	0.475	6.60
1361	6202.9	0.071	0.467	6.59
1409	6377.4	0.071	0.464	6.57
1441	6493.1	0.076	0.500	6.57
1481	6724.8	0.072	0.475	6.63
1521	7014.4	0.073	0.478	6.59
1561	7304.0	0.066	0.468	7.14
1609	7651.5	0.064	0.440	6.84
1641	7931.0	0.058	0.412	7.08
1673	8213.7	0.054	0.408	7.58
1721	8637.7	0.050	0.394	7.87

Chapter II-B

High time-resolution alkenone paleotemperature variations in Tokyo Bay during the Meghalayan: implications for cold climates and social unrest in Japan

II-B-1. Introduction

The early Holocene is generally characterized by a warm climate in the Northern Hemisphere due to the higher summer insolation as compared with that at present (Wanner et al., 2015). However, previous studies have revealed that numerous cold periods existed during the Holocene, which may have been induced by the modulation of solar forcing, volcanic activity, and land-ocean-atmosphere thermal interactions (Mayewski et al., 2004; Wanner et al., 2008). In particular, a distinct change in the climate, known as the "4.2 ka BP event," marking the boundary between the Northgrippian and Meghalayan, has attracted attention as one of the semi-global scale climatic events during the Holocene (Walker et al., 2018). However, the magnitude and range of this event's influence remain controversial because its signature rarely occurs in ice cores and deep-sea sediment records. This event's controlling mechanisms are also unclear because there appears to have been no changes in the factors known to control the global climate system ca. 4.2 ka BP, such as solar activity, volcanic activity, and the concentration of greenhouse gases (Wanner et al., 2015).

I must increase our understanding of modern climatic variability and its socioeconomic impacts as a function of increasing greenhouse gas concentrations. An improved understanding of the paleoclimate during the Meghalayan is particularly important to distinguish the effects of anthropogenic climate change and natural climate variability, which is necessary to facilitate accurate predictions of future climate change. Numerous efforts have been made to collect proxy data to reconstruct the paleoclimate during the Meghalayan at both global and regional

scales. Studies have shown that, even after the 4.2 ka BP event, there were variations in the Meghalayan climate in the Northern Hemisphere, producing climate epochs, such as the Roman Warm Period (RWP), Dark Ages Cold Period (DACP), Medieval Warm Period (MWP), and Little Ice Age (LIA) (Ji et al., 2005; Mann et al., 2009; Cook et al., 2013; Helama et al., 2017). Most of these periods, however, have been identified with proxy records recovered from Europe. Thus, the spatial extent, magnitude, and length of these events are not uniform throughout the globe (IPCC AR5). Many processes are involved in both the external drivers and internal variability within the climate and carbon cycles, rendering the Holocene climate spatially diverse (Wanner et al., 2008).

Previous studies have also focused on the links between the paleoclimate and human civilizations during the Holocene. Recent studies, as well as Chapter II-A of this doctorate dissertation, have suggested that 4.2 ka BP climate change has influenced the vicissitudes of ancient human civilizations, flourished in Egypt, India, Mesopotamia, and China (Carolin et al., 2019; Ran and Chen, 2019; Sun et al., 2019; Watanabe et al., 2019). Even in the relatively sophisticated societies of medieval to early-modern times, statistical analyses suggest that changes in the temperature affected human settlements via social factors, such as decreased agricultural production, economic downturn, and ongoing wars (Zhang et al., 2010; Zhang et al., 2011; Yin et al., 2016). These studies have pointed out that abrupt changes in the climate, particularly extended cold events, had a significant influence on human civilizations. Therefore, high time-resolution quantitative regional paleoclimate records with reliable dating are important when discussing the cause(s) of the rise and fall of human civilizations in the past.

This study focused on changes in the paleotemperature of Tokyo Bay, located at the center of the Kanto area in central Japan. A better understanding of the paleoclimate of the Kanto area is fundamental to our understanding of the East Asian climate system because it is controlled by internal climate systems, such as the Kuroshio current, East Asian monsoon, and El-Niño Southern Oscillation (ENSO). The Kanto area is also important for Japanese history because it was the most populated area in Japan during the mid-Jomon to early-Yayoi era (i.e., ca. 3000–500 BCE), during which people survived by hunting, fishing, gathering, and primitive agriculture (Kito, 2000; Habu, 2004; Crema et al., 2016). As systems of centralized governance developed, Kanto area became a key area because several governments, controlled by warlords (*Samurai*) were established and/or prospered there (for further details, see section II-B-2.3.).

In previous studies, the paleotemperature in the Kanto area was reconstructed based on fossil evidence, such as shells and corals distributed along the coast of Tokyo Bay (Matsushima, 1979). A number of shell mounds are distributed along the coast, which have provided important information on the culture, lifestyle, and environment of earlier civilizations. However, these records only provide discontinuous and qualitative data. Sakaguchi (1983) analyzed long-term climatic fluctuations in the Ozegahara peatland in the northern part of the Kanto area using pollen analyses of peat borehole cores. Although this study provided a significant leap forward to our understanding, the study points out certain limitations related to continuity and proxy interpretation compared to studies using marine sediment cores. In recent years, marine sediment cores collected from shallow bays have attracted attention as paleotemperature archives for the coastal area because they offer

deposits more continuously than terrestrial borehole cores and coastal climate is, to a large extent, driven by coastal sea surface temperature (e.g., Cho and Lee, 2012; Salacup et al., 2019). In this study, I used a well-dated marine sediment core recovered from the central part of Tokyo Bay, which provide continuous and quantitative alkenone paleotemperature data, to elucidate decadal to centennial-scale temperature changes in the Kanto area, their controlling mechanisms, and their possible influences on historical transitions in Japan.

II-B -2. Study area and materials

II-B-2.1. Tokyo Bay

Tokyo Bay is a shallow bay (average depth of 38 m) with an area of 1380 km^2 and a water volume of 621 m^3, located in the central part of Japan (T. IIB-1a). Its seafloor is relatively flat and the inner part of the bay is composed of silty mud (Matsumoto, 1982). The water depth at the mouth of Tokyo Bay is shallow (approximately 50 m), limiting seawater exchange with the Pacific Ocean and creating a calm depositional basin (Fig. IIB-1b). Based on sea surface temperature (SST) data available at 35°22'30"N, 139°52'30"E from the Advanced Very High Resolution Radiometer (Reynolds et al., 2007), the annual mean SST from 2008 CE to 2012 CE was 19.2 °C, with maximum and minimum SSTs of 25.9 °C (July or August) and 12.6 °C (January or February), respectively. The mean annual air temperature recorded in Tokyo from 2008 CE to 2012 CE was 16.6 °C, with maximum and minimum values of 27.7 °C (August) and 6.1 °C (January), respectively (Japan Meteorological Agency: https://www.data.jma.go.jp/obd/stats/etrn/index.php). There is a good correlation between the monthly air temperatures and SSTs ($r^2 = 0.81$, $p < 0.001$) because Tokyo Bay is shallow and semi-closed; hence, it experiences little intrusion from the main flow of the Kuroshio Current (Japan Agency for Marine-Earth Science and Technology: http://www.jamstec.go.jp/aplinfo/kowatch/?cat=40). A stronger correlation between the air and sea surface temperatures was observed during the summer. Mean monthly sea surface salinity has a minimum value of 29 in the

summer and a maximum value of 33 in the winter (Japan Coast Guard: https://www1.kaiho.mlit.go.jp/KAN3/kaikyo.htm).

II-B-2.2. Core KT12-06-2B

Piston core KT12-06-2B (8.99 m in length) was recovered from the central part of Tokyo Bay (35°30'N, 139°53'E) at a water depth of 24 m during the TANSEI-MARU KT12-06 cruise (Fig. IIB-1b). Core KT12-06-2B primarily consists of gray homogeneous muddy sediments with sporadic scoria or pumice layers. An especially thick scoria layer was observed between depths of 22 and 28 cm from the core surface. Based on observations of the continuous section of the core using X-ray computed tomography (CT), there was no distinguishable substantial change in the sedimentary facies, except for the interbedded the thick scoria layer. Sub-samples of the core were taken at 2 cm intervals and preserved in dark conditions below 4 °C prior to geochemical analysis.

II-B-2.3. The history of the Kanto area, Japan

A summary of the history of the Kanto area surrounding Tokyo Bay is presented below. The native Japanese, known as the Jomon people, flourished after the last glacial period. The Jomon era (before ca. 10000−500 BCE) corresponded to the Mesolithic to Neolithic phases. The economy of this period was generally based on hunting and gathering (Matsui and Kanehara, 2006). The Jomon people lived in pit dwellings and used pottery (Habu, 2004). From 1000 BCE to 500 BCE, immigrants moved from eastern China to western Japan, introducing the paddy rice cultivation method (Hall, 1993). This period, characterized by paddy rice cultivation,

settlement, and improvements to pottery and copperware, is known as the Yayoi era. The total population increased to approximately 590,000 ca. 250 CE supported by highly productive farming (Kito, 2000). From the start of the Yayoi era, small city-states were developed and war became common.

Near 300 CE, several small city-states competed for power with each other. They gradually became integrated and a small nation, known as "*Yamato*," was established. Following this, a centralized imperial court developed, which governed the entirety of Japan throughout the Asuka (592–710 CE), Nara (710–794 CE), and Heian (794–1185 CE) eras (Hall, 1993). In the middle of the Heian period, the imperial court became unstable, resulting in a coup executed by the regional warlords (*Samurai*). The first *Samurai* administration was established in Kamakura in the Kanto area (known as the Kamakura shogunate governed by the Minamoto and Hojo families; 1185–1333 CE), replaced by the Ashikaga shogunate (1336–1573 CE) governed by the Ashikaga family. Conflicts among many of the *Samurai* families continued until the beginning of the Edo era (1603 CE) when Japan began to be governed by the Tokugawa family. At this time, Tokyo was established as the modern capital city of Japan (Hall, 1993).

II-B -3. Methods

II-B-3.1. Age determination

Twenty-two molluscan shells, identified as *Acila divaricata* and *Nassarius variegata, which live on the muddy bottom surface of shallow seas (T. Sasaki, personal comm.),* were extracted from the sediment core. After the shells were washed to remove sediment residues, they were dated via radiocarbon accelerator mass spectroscopy (AMS) at the Atmosphere and Ocean Research Institute and the Micro Analysis Laboratory of the University of Tokyo (Yokoyama et al., 2019). The shell samples were placed in vacuum test tubes, which were evacuated using a needle valve attached to a vacuum line system. The tubes were then placed in a heat block (80 °C) and phosphoric acid was introduced through an airtight cylinder. When the samples had completely dissolved, the tubes were removed from the heat block. The product CO_2 was passed through a vacuum line and cryogenically transferred into a graphitization reactor via a series of cryogenic traps used to purify the gas. Graphite was formed on iron powder in a hydrogen atmosphere heated to 630 °C. The graphite was pressed into target holders and analyzed via AMS.

All ^{14}C age results were calibrated to calendar years using the OxCal ver. 4.2.4 software (Ramsey and Lee, 2013) with the Marine 13 dataset (Reimer et al., 2013). A regional specific reservoir correction (ΔR) of 60 ± 31 years was used, as reported by Komori et al. (2017).

The relatively thick scoria layer observed between depths of 22 and 28 cm in the core was observed via CT imaging (Fig. IIB-2a). Widely distributed, thick scoria layers in cores collected near the surface throughout Tokyo Bay have been identified

as volcanic products of the Hoei eruption in 1707 (Matsumoto, 1983; Sano et al., 2011). Therefore, I interpret this scoria layer to have originated from the Hoei eruption.

II-B-3.2. Alkenone analysis

The sediment samples were dried and crushed into a fine powder for organic matter analysis. The lipid content of each powdered sediment sample (approximately 2.5 g) was extracted by sonication using a mixed solvent of dichloromethane/methanol (70:30, v/v) and then saponified with 0.5 mol L^{-1} of KOH in MeOH. The saponified samples were then extracted with n-hexane to obtain the neutral components (Ohkouchi et al., 2005). The neutral lipids were separated into four subfractions via silica gel column chromatography. The N-1 fraction (hydrocarbons) was extracted using n-hexane/dichloromethane (95:5, v/v). The N-2 fraction (ketones, esters, and aldehydes) was collected using n-hexane/dichloromethane (4:6, v/v). Subsequently, the N-2 fraction was introduced into a gas chromatograph with a flame ionization detector (GC-FID) equipped with a HP-5ms fused silica capillary column (60 m/0.25 mm internal diameter, Agilent) at the Japan Agency for Marine-Earth Science and Technology. The oven temperature was programmed as follows: maintained at 60 °C for 1 min, raised to 200 °C at 20 °C/min, raised to 310 °C at 15 °C/min, and maintained at 310 °C for 40 min (Harada et al., 2003). The retention times of the alkenones were confirmed by analyzing the alkenones extracted from the cultured strain of *Gephyrocapsa oceanica*, and suspended particle matter in Lake Ichinomegata, where Group I type alkenones with di-, tri-, and tetra- unsaturated C_{37} and C_{38} alkenones were previously

detected (Longo et al., 2018). Several procedural blanks, which were analyzed parallel to the sample analysis, showed no C_{37} alkenone contamination.

II-B-4. Results

II-B-4.1. Radiocarbon dating

Core KT12-06-2B provided continuous environmental records for the previous 4400 years, as represented by the calendar age-depth profiles (Fig. IIB-2b, Table IIB-1). A strong positive correlation was obtained when the radiocarbon ages of the molluscan shells were plotted against depth ($r^2 = 0.98$), which suggests that stable sedimentation occurred consistently at the core site. The average sedimentation rate was 1.95 m kyr^{-1}, which was remarkably higher than that of the cores retrieved from the open ocean off the coast of the Kanto area (Oba and Maruyama, 2004). I constructed the age model for the core using a *P* sequence deposition model (Ramsey, 2008), which was implemented in the computer program OxCal. Assuming that the age of the surface sediment is 2012 CE, when the core was recovered, the bottom of the Hoei scoria layer was deposited in 1703 CE, which is similar to the correct age of 1707 CE. This confirms that the age model is reasonably accurate.

II-B-4.2. Alkenone SST

The alkenone unsaturation index $U^{K'}_{37}$, defined as $[C_{37:2}]/([C_{37:2}] + [C_{37:3}])$, where $[C_{37:2}]$ and $[C_{37:3}]$ indicates the relative abundance of di-unsaturated C_{37} alkenone and tri-unsaturated C_{37} alkenone, respectively, can be recovered from marine sediments. This index has been confirmed to be highly correlated with the SST (Brassell et al., 1986; Müller et al., 1998; Prahl et al., 1988). A global core top calibration between the $U^{K'}_{37}$ and SST has been widely used for temperature calculations in the open oceans (Müller et al., 1998). This relationship, however, can

slightly vary in certain marginal seas (e.g., Tao et al., 2012); the variation may be caused by multiple factors, including genotypic diversities in alkenones that produce haptophytes (Yamamoto et al., 2000) and nutrient conditions of the seas (Herbert, 2001). Based on the polarizing microscope and scanning electron microscope (SEM) observations, most coccoliths collected from core KT12-06-2B belong to the family Noëlaerhabdaceae. Several coccoliths could not be identified at the species level because of diagenesis. Of those that could be identified, *G. oceanica* was the most abundant. Unfortunately, an in-situ calibration in Tokyo Bay has not been established yet; therefore, the following relationship was applied to this core based on culture experiments of *G. oceanica* GO1 isolated from Mutsu Bay, which is near Tokyo Bay and has a similar marine environment (Sawada et al., 1996):

$SST\ (°C) = (U^{K'}_{37} + 0.204)/0.044$

($r^2 = 0.951$, n=11, Standard deviation of residues = 0.62 °C)

The analytical error for $U^{K'}_{37}$-SST was 0.05 °C (± 1σ) based on 11 replicated analyses.

I analyzed down core variability of $U^{K'}_{37}$ to generate a decadal to centennial-scale $U^{K'}_{37}$-SST records covering the last 4400 years (Figs. IIB-3a and IIB-4a; Table IIB-2). The $U^{K'}_{37}$-SST in the core top sediment (approximately upper 2 cm) was 21.3 °C, which is similar enough to the current observed mean annual SST of 19.2 °C. The time series record of $U^{K'}_{37}$-SST showed high temperatures of 22–25 °C in the early Meghalayan, which then gradually decreased to the present with several decadal to centennial-scale extensive cold periods at ca. 1050 (±80) CE (20.5 °C), 50 (±108) CE (20.3 °C), 440 (±84) BCE (20.0 °C), and 2300 (±66) BCE (19.5 °C).

II-B -5. Discussion

II-B-5.1. Assessment of alkenone SST time series records

Before discussing the temperature variation results, I must establish the reliability of the $U^{K'}_{37}$-SST reconstruction. Alkenones produced in the ocean mainly derive from *G. oceanica* and *Emiliania huxleyi* (Group III haptophytes), which are genetically related to each other (Bendif et al., 2014, 2015). However, haptophytes of different genera living in fresh or brackish lacustrine environments, such as certain Group II haptophytes (e.g., *Isochrysis galbana* and *Ruttnera lamellosa*), and uncultured Group I haptophytes also produce alkenones with significantly lower $U^{K'}_{37}$ values than those of *G. oceanica* and *E. huxleyi* (Nakamura et al., 2014; Longo et al., 2016; Araie et al., 2018). The relative contributions to alkenones produced by these three haptophyte types can be roughly evaluated based on the alkenone fingerprints, i.e., the absence or presence of $C_{37:4}$ and C_{38}Me, as well as the C_{37}/C_{38} ratio (Marlowe et al., 1984; Chu et al., 2005; Kaiser et al., 2019; Salacup et al., 2019). According to the culture experiments, substantial amounts of $C_{37:4}$ have been detected from *I. galbana, R. lamellosa,* and Group I haptophytes regardless of growing temperature. This signature, however, is absent in *G. oceanica* and *E. huxleyi* cultured at water temperatures above 15 °C (Prahl et al., 1988). In contrast, C_{38}Me has only been detected in *G. oceanica* and *E. huxleyi,* but never for *I. galbana* and *R. lamellosa* (Marlowe et al., 1984). The C_{37}/C_{38} ratios recorded in the brackish lacustrine environment are typically over 1.8, whereas those in marine settings are approximately 1.0 (Salacup et al., 2019 and references therein). Group I and Group II haptophytes have been considered to be minor contributors to $U^{K'}_{37}$ values in ocean

settings except for extremely low salinity (<7) environments such as the inner Baltic Sea (Bendle et al., 2005; Kaiser et al., 2019). As observed in the case of Chesapeake and Narragansett bays which have lower salinities than Tokyo Bay, the alkenone fingerprints recorded in the sediment are similar to those produced by Group III haptophytes and the contributions of Group I and Group II haptophytes are considered to be small. In those bays salinity ranges 10–30, and $U^{K'}_{37}$ values well reflect local SST fluctuations (Mercer et al., 2005; Salacup et al., 2019).

In this study, the C_{37}/C_{38} ratio ranges between 0.45 and 1.47, which is nearly comparable with the ratios for the cultured strains of Group III haptophytes (Fig. IIB-3b) (Conte et al., 1998). I carefully verified that the C_{38}Me occurs in all analyzed samples and that $C_{37:4}$ was never detected, which suggests that Group I and II haptophytes contributed little to total alkenone production throughout the 4400 years (Fig. IIB-3c). Therefore, *G. oceanica* abundantly observed in the sediment (Fig. IIB-3d) was the predominant producer of alkenones in the core, and changes in this alkenone producer did not significantly influence $U^{K'}_{37}$. Although the weak negative correlation between C_{37}/C_{38} ratio and $U^{K'}_{37}$ (r^2=0.43) suggests that physiological conditions of haptophytes may be altered as temperature fluctuates, it does not deny the reliability of $U^{K'}_{37}$ as temperature proxy (Conte et al., 1998; Ono et al., 2009).

The $U^{K'}_{37}$-SST values in the open ocean can sometimes be disturbed by changes in the alkenone production depth (Ohkouchi et al., 1999). However, changes in the alkenone production depth are likely small in our study because the water depth surrounding the coring site was only 24 m, with vertical water temperature differences of 2 °C or less, except for June and July when weak stratification occurs (Hattori, 1983). At present, the mouth of Tokyo Bay between the Miura and Boso

peninsulas is narrow (10 km in width) and shallow (50 m in depth), which indicates that the inner part of the bay maintains a semi-closed condition (Fig. IIB-1b). The depth of the core site changed little during the Meghalayan because changes in the global sea level that were related to the ice volume were negligible (Lambeck et al., 2014) and the vertical crustal movement caused by recent earthquakes was small (<1 m) in the inner part of the bay (Shishikura et al., 2007). Only 1–3 m of vertical changes in the coastline were suggested by the terrestrial borehole cores and the locations of shell mounds along the coast of the inner Tokyo Bay (Tanabe, 2019) (Fig. IIB-2c).

The coast of Japan has often been damaged by large tsunamis about 5–15 m high (e.g., the Genroku (1703 CE), Hoei (1707 CE), Ansei Tokai (1854 CE), Taisho Kanto (1923 CE) and Tohoku (2011 CE) earthquakes), but only tidal level changes of approximately 1–2 m have been observed inside Tokyo Bay, which is protected by Boso and Miura peninsulas (e.g., Hatori, 1984, 2006; Sasaki et al., 2012; Muragishi et al., 2015). The immunity to large tsunami damage in the inner areas of Tokyo Bay is also supported by model studies (Shibayama et al., 2013) and reflected in the Japanese official government hazard map. Despite the frequent occurrence of large-scale earthquake tsunamis in the last few hundred years, the tephra layer deposited by the Hoei eruption (1703 CE) is well-preserved in the core (Fig. IIB-2a) as well as the other short cores recovered in Tokyo Bay (Matsumoto, 1983). Therefore, stratigraphic disturbances are expected to have been small, which guarantees the accuracy of the $U^{K'}_{37}$-SST time-series records.

II-B -5.2. General trend of temperature change

The climate of the coastal area of the Pacific side of Japan is affected by the warm Kuroshio and cold Oyashio currents (Fig. IIB-1a). These currents meet each other off the northeast coast of the Kanto area to form the subarctic front with the most pronounced latitudinal gradients of SST in the North Pacific (Kida et al., 2016). The temperature in this area is susceptible to global changes in atmospheric and oceanic circulations (e.g., Suganuma et al., 2018; Haneda et al., 2019) because the latitudinal position of the subarctic front is controlled by the changes in the distribution of atmospheric pressure systems, including the behavior of the ENSO, the monsoon intensity, and the position of westerly jets, which are associated with the insolation variability in the Northern Hemisphere (Yamamoto et al., 2004; Oba et al., 2006; Isono et al., 2009). The reconstructed temperatures in Tokyo bay were generally higher than those in the present, exhibiting a declining trend over the long term, which roughly matches the changes in the orbital-forcing summer insolation throughout the northern hemisphere (Fig. IIB-4a and 4b) (Laskar et al., 2004). This trend is also consistent with the millennial scale 2–3 °C temperature decrease during the mid- to late-Holocene recorded in the core from the Boso peninsula, thus indicating the southern displacement of the subarctic front between the Kuroshio and Oyashio currents in the western Pacific (Yamamoto et al., 2004; Oba et al., 2006). Our decadal to centennial-scale temperature records provide new evidence of several interruptions of the warm condition, which have been labeled as C1–C9 during the last 4400 years (Fig. IIB-4a). Here, C1, C3, C4, and C6 were particularly extended cold periods. The timings of these cold periods were generally coincident with

minimums in solar activity (Fig. IIB-4c) and/or large volcanic eruptions, except for the coldest event, C1 (Fig. IIB-4d) (Solanki et al., 2004; Sigl et al., 2015).

As described in numerous previous studies, one single process did not cause the Holocene cooling events (Wanner et al., 2008). Among the many external and internal drivers of Holocene climate variability, total solar irradiance (TSI) has been identified as one of the ultimate controlling factors (Bond et al., 2001). TSI variability during the Holocene, generally linked to the evolution of dark and bright magnetic features on the solar surface (sunspot number), has been quantitatively reconstructed from natural variations in cosmogenic isotope concentrations with the use of physics-based models (Solanki et al., 2004; Usoskin et al., 2007; Steinhilber et al., 2009; Vieira et al., 2011). The 11-year TSI variations between the sunspot maximum and minimum is 0.17–0.20 (W m^{-2}), which can induce less than 0.1 K variations in the Earth's surface temperature based on the simple heat capacity calculation (Lean et al., 2005; Fröhlich, 2006). However, as many regional paleotemperature records, including our study, have indicated, climate variation during the Holocene was significantly larger than that predicted from this calculation, as well as being different in each region (Gray et al., 2010). Although the detailed mechanism has not been completely elucidated, recent studies have suggested that particularly large variations in ultraviolet irradiance play an important role in amplifying the surface temperature changes via mechanisms in thermal changes of the stratosphere (Meehl et al., 2009; Ineson et al., 2011, 2015).

Volcanic eruptions can also cause regional-to-global scale cold events due to surface aerosol injections into the stratosphere that shield the Earth's surface from incoming solar radiation (Robock, 2000). The timing of large volcanic eruptions

during the Holocene can be estimated based on the amount of sulfate aerosol contained in ice cores (Wanner et al., 2008; Sigl et al., 2015). The climate impact potential of each volcanic eruption is not directly related to its magnitude. Without well-defined models that include detailed information on a given past eruption, I cannot quantitatively define the magnitude of temperature reduction that may have occurred due to a specific eruption (Gao et al., 2008). Nevertheless, previous studies have proposed that the general effects of volcanic eruptions can endure for more than a decade via ocean-atmosphere interactions, such as the ENSO and/or monsoon systems (Emile-Geay et al., 2008; Anchukaitis et al., 2010).

Although it is difficult to attribute precise and detailed mechanisms to episodes of climate variability, I present the possible causes of the observed temperature variations in Tokyo Bay. This study provides information that can help us understand climate change throughout East Asia and the northeastern Pacific Ocean, and its possible influence on the vicissitudes of human civilizations in the Kanto area, central Japan.

II-B-5.3. Climate in the late Jomon era

Temperatures from ca. 2400 BCE to 900 BCE were generally 1–2 °C higher than those at present, except for the large cold period ca. 2350–2250 BCE (C1). The relatively warm climate during the mid- to late-Holocene is consistent with the results of previous paleoclimate studies based on paleofaunal characteristics of coastal areas near Tokyo bay. In shell mounds dated to between 2000 and 3000 BCE, species that inhabit relatively warm seas, such as *Anomalocardia squamosa*, *Meropesta nicobarica*, *Cerithium coralium*, *Nassarius bellulus*, and *Guamanian*

nerite, have been identified, indicating that the SST at this time was warmer than the present by 1–2 °C (Matsushima, 1979; 2006). Fossil corals dated to between 2000 and 4500 BCE, recovered from raised terraces in Tateyama, also suggest that the SST was approximately 2 °C higher during this period (Nakata et al., 1980). Pollen data from the Oze Plateau have also revealed generally warm conditions (Sakaguchi, 1983).

The notable cold minimum period (C1) may correspond to the 4.2 ka BP event. Numerous proxies from areas throughout the globe indicate cooler or drier changes in the climate during this period, which might have an influence on the collapse of ancient civilizations that flourished in the world (Walker et al., 2012). In Japan, the largest Jomon archeological site flourished along the coast of Mutsu Bay also collapsed around that period under the cold climate (Kawahata et al., 2009; Kawahata, 2019). Previous studies have suggested that the Indian and Asian summer monsoons weakened around this period due to dominantly dry conditions, which are recorded in a number of lakes located in northwestern China, near the limit of the monsoon front (Mehrotra et al., 2019). This interpretation is also supported by high-resolution stalagmite $\delta^{18}O$ records from Eurasia, which are a reliable proxy for the summer monsoon (Wang et al., 2005; Berkelhammer et al., 2012) (Fig. IIB-4e). The retreat of the summer monsoon, which transports heat energy from the equatorial Pacific to the continents, should have played an important role in climate cooling throughout East Asia, including Tokyo Bay.

Although a few cases of rapid SST decrease have been reported from deep-sea sediments in East Asia, several paleo-SST datasets from coastal shallow sea areas record decreases in the temperature (Yellow Sea (Wang et al., 2011); East China Sea

(Chapter II-A of this doctorate dissertation). These studies were based on the alkenone temperature proxy, which quantitatively reflects the changes in the paleotemperature of the surface layer of the sea. Our study provides the first direct evidence of a sharp temperature drop that is likely connected to the 4.2 ka BP event in Japan, which may lead to an improved understanding of this event in East Asia.

II-B-5.4 Climate in the Yayoi era

Temperatures from ca. 900 BCE to 300 CE fluctuated centennially, including substantial drops in the temperature ca. 800 BCE (C2), 440 BCE (C3), and 100 CE (C4). The C2 and C3 events can be attributed to the long term weakening of solar activity ca. 800 and 450 BCE, i.e., periods that are sometimes referred to as the Greek and Homeric minimums, respectively (Solanki et al., 2004; van Geel et al., 2004; Usoskin et al., 2007; Steinhilber et al., 2012). These cold periods did not occur regionally, but rather over a wide area in the mid to high latitudes (Mayewski et al., 2004). Martin-Puertas et al. (2012) proposed that atmospheric circulation patterns shifted during the solar minimum, which may have amplified climate cooling in the mid-latitudes. A large volcanic eruption that occurred ca. 426 BCE may also have accelerated the C3 event (Sigl et al., 2015). In East Asia, a relatively cold climate caused by a weakening of the summer monsoon or intensification of the winter monsoon has been widely reported using multiple proxies (Yamamoto, 1980; Wang et al., 2011). Therefore, I conclude that the cold periods observed in our data from Tokyo Bay were caused by similar mechanisms.

Despite the C4 cold period not corresponding to a solar minimum, previous studies from Japan based on pollen data and historical documents have suggested

that low temperatures prevailed during this period (Yamamoto, 1980; Sakaguchi, 1983; Yoshino, 2007). Although the cause of this cold climate is still controversial, several large volcanic eruptions, such as Mt. Taupo in the 2nd century CE, may be strong candidates (Wilson et al., 1985; Nogami et al., 2014; Sigl et al., 2015). This cold period can also be observed in China, which has profound significance in that it aligns with an important social crisis in Japan. The large period of civil unrest, known as "Wakoku-Tairan," occurred at the end of the Yayoi era, which led to the establishment of the centralization era. The "Book of Later Han," a Chinese historical document, recorded that the Japanese people suffered from abnormal climate and famines in the 2nd century CE (Kobashi, 2017). Our temperature records indicate that the C4 cold period is comparable to this description. The "History of the Three Kingdoms," a Chinese historical document, recorded a cold climate in China during the same period (Yamamoto et al.,1980), as well as based on compiled pollen data recovered from central to northern China (Li et al., 2017). Chinese society also experienced unrest during the cold climate, with large-scale famines and peasant uprisings that resulted in a decrease in population and the decline of the Later Han dynasty (Zhang et al., 2010; Yin et al., 2016).

The temperature after C4 was relatively high compared to that at present, which may have been caused by a relatively high solar activity and the absence of major volcanic eruptions during this period (Wanner et al., 2015). The moderate climate, known as the RWP, occurred during this period in the northern hemisphere (Desprat et al., 2003; Patterson et al., 2010; Wang et al., 2012).

II-B-5.5. Climate in the Centralization era

A particularly high time-resolution analysis (conducted approximately every 18 years on average) was performed after ca. 300 CE to compare the temperature variability in Tokyo Bay with other high time-resolution paleoclimate and Japanese historical records. The $U^{K'}_{37}$-SSTs recorded in the sediment core derived from Hiroshima Bay (western Japan) show similar fluctuations during this period, which suggests that these temperature changes were common in Japan (Kawahata et al., 2017) (Fig IIB-5). After the RWP, the temperature suddenly dropped (C5). The timing of C5 matches that of a global cooling event known as the DACP (Helama et al., 2017), which may be linked to the North Atlantic ice rafting event that occurred at ca. 600 CE (Bond et al., 2001). Recently, a collection of quantitatively reconstructed temperature records from tree-ring widths measured in the mountainous areas of Russia and European Alps illustrated a particularly large cold period dated to between 536 and 660 CE, known as the "Late Antique Little Ice Age (LALIA)" (Büntgen et al., 2016) (Fig. IIB-4f). Other studies have compiled multiple types of global proxy data to propose that the northern hemisphere became cold around the C5 event (Ljungqvist, 2010; Marcott et al., 2013), initiating the so-called "migration period," during which widespread invasions occurred from the north to the south of Europe (Wanner et al., 2015). This cold climate is also recorded in pollen data from the Oze Plateau, which supports our records (Sakaguchi, 1983). Global cooling at this time may have been caused by large volcanic eruptions in 536, 540, and 547 CE (Sigl et al., 2015), which were likely sustained by the ocean and sea-ice feedback (Büntgen et al., 2016; Helama et al., 2017). The timing of the C5 event corresponds to the Kohun and Asuka era in Japan, during which numerous

wars among locals occurred, leading to the establishment of a centralized system (Hall et al., 1993).

Four small cold periods were observed between 1000 and 1700 CE (C6–C9). Although it is difficult to distinguish one event from the other due to error in the ^{14}C age model, these cold periods may reflect periods of low solar activity, i.e., the Oort (1010–1080 CE), Wolf (1280–1340 CE), Spörer (1420–1550 CE), and Maunder (1645–1715 CE) minimums (Bard and Raisbeck, 2000; Solanki et al., 2004; Usoskin et al., 2007; Steinhilber et al., 2012) (Fig. IIB-4c). These relatively cold periods, referred to as the LIA, have also been reported by several previous studies in East Asia (Raymond and Phillip, 1993; Esper et al., 2002; Kawakubo et al., 2017), which suggests that solar activity played an important role in climate change in East Asia, including Tokyo Bay. Several local volcanic eruptions, such as Fuji (1707 CE; Hoei eruption) and Asama (1783 CE), may also have contributed to the amplification of the cold climate.

The lowest temperature during the centralization period occurred around ca. 1050 CE. This cold period can be verified based on Japanese historical documents (cherry blossom phenological data) from in and around the ancient capital city of Kyoto, which suggests that spring temperatures in the 11th century CE were lower by 2ºC than spring temperatures in the relatively warm 10th century CE (Aono and Saito, 2010). Therefore, this cooling shift appears to have commonly occurred throughout Japan. Temperatures in the northern hemisphere are generally considered to have recovered after LALIA during the MWP (ca. 950–1100 CE). However, according to the IPCC AR5, the MWP was not synchronous throughout the globe with an undefined period. Therefore, I assumed that the MWP in Japan did not

correspond to that in other areas. Although it is difficult to specify the exact causes, the possible mechanism of the cooling in Japan may have been a more active El-Niño mode, which has been reported by several proxy-based reconstructions (Yan et al., 2011) (Fig. IIB-4g). Under modern conditions, during an El-Niño episode, the westerly jet stream shifts to the south, the Pacific High weakens, and the Okhotsk High is enhanced, which generally results in a cold and cloudy/rainy summer in Japan (Kobayashi et al., 2015). The initial stages of the imperial court period (the Nara to early Heian era) likely experienced a warm climate. However, after the climate cooled in the middle of the Heian era (C6), famines and revolts began to occur frequently. This unrest resulted in the expansion of the role of *Samurai* families in Japan, finally leading to a transition from an aristocratic society to a feudalistic *Samurai* society (the Kamakura era and following periods) (Hall, 1993).

Although I cannot provide a precise and quantitative mechanism explaining the link(s) between climate change and Japanese history, certain cold periods identified in our $U^{K'}_{37}$-SST data appear to correspond well with periods of social turbulence. In modern society, the negative impacts of abnormal weather are becoming an increasingly urgent topic of debate. Our study provides important information that improves our awareness of the potential social impacts of a future climate crisis.

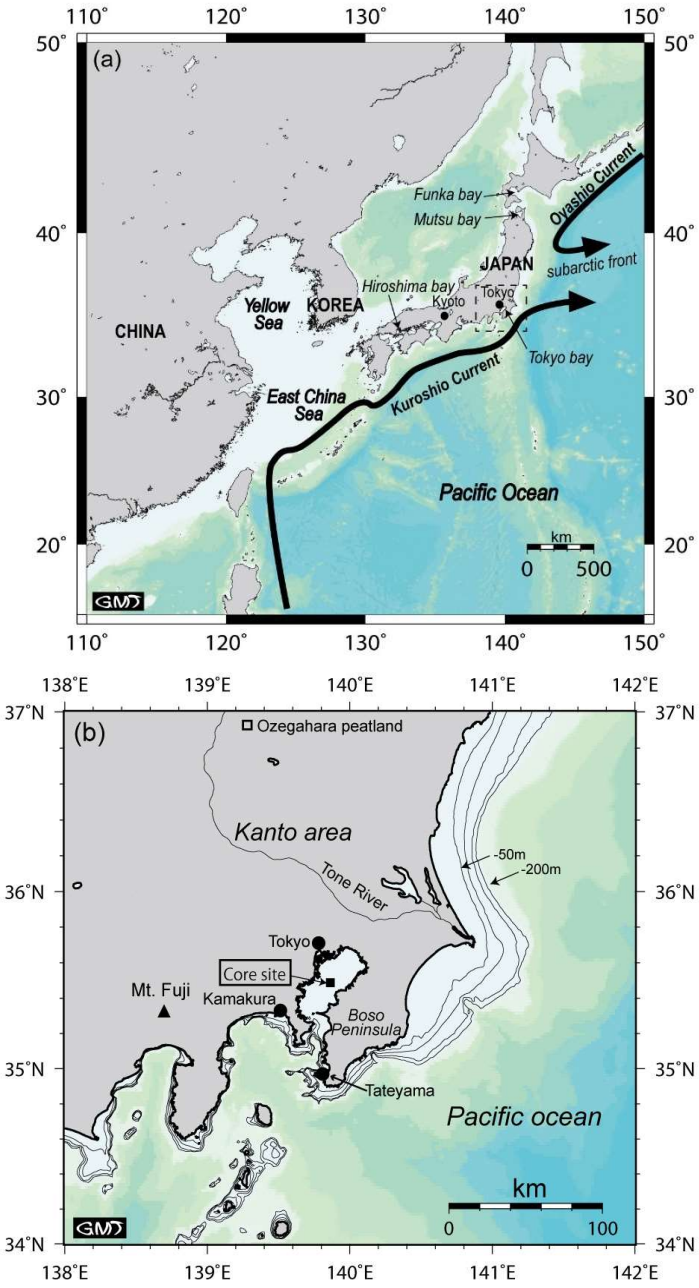

Fig. IIB-1

(a) Map of the western North Pacific, including the Kanto area (dashed square) of Japan. The bold arrows represent the paths of the Kuroshio and Oyashio currents. (b) Map of the Kanto area, central Japan (dashed square in Fig. IIB-1a). The sampling location of core KT12-06-2B (35°30'N, 139°53'E) is shown by the solid square. Current water depths are defined by the thin lines. Sites mentioned in the text are also shown. These figures were generated using the Generic Mapping Tools software (Wessel and Smith, 1998).

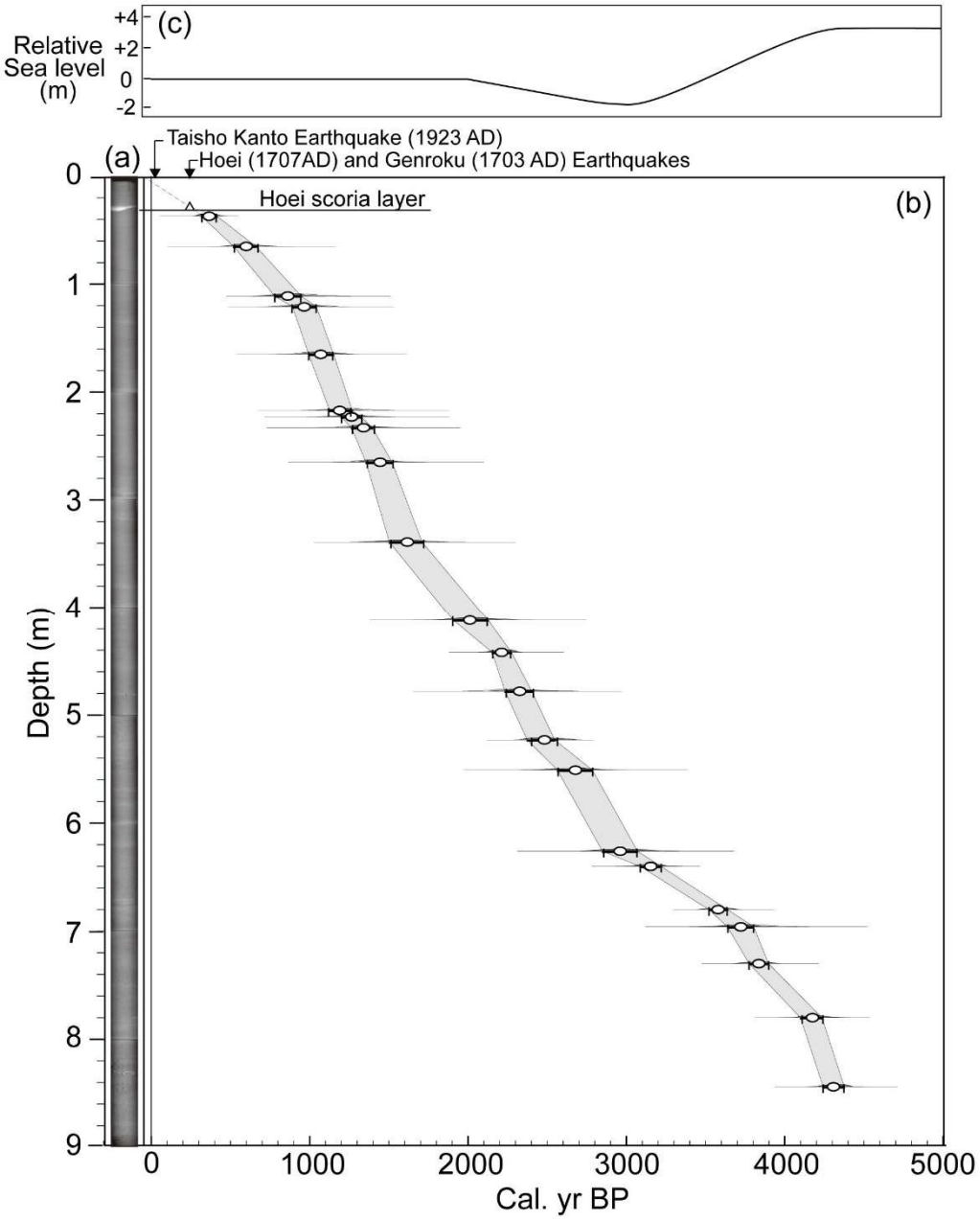

Fig. IIB-2

(a) CT image and (b) depth versus radiocarbon age (calibrated in years before present) of core KT12-06-2B. The gray colored area represents 1σ errors. The open triangle represents the 6-cm-thick scoria layer produced by the Hoei eruption. (c) The local relative change in sea level observed along the coast of the inner Tokyo Bay (Tanabe et al., 2019).

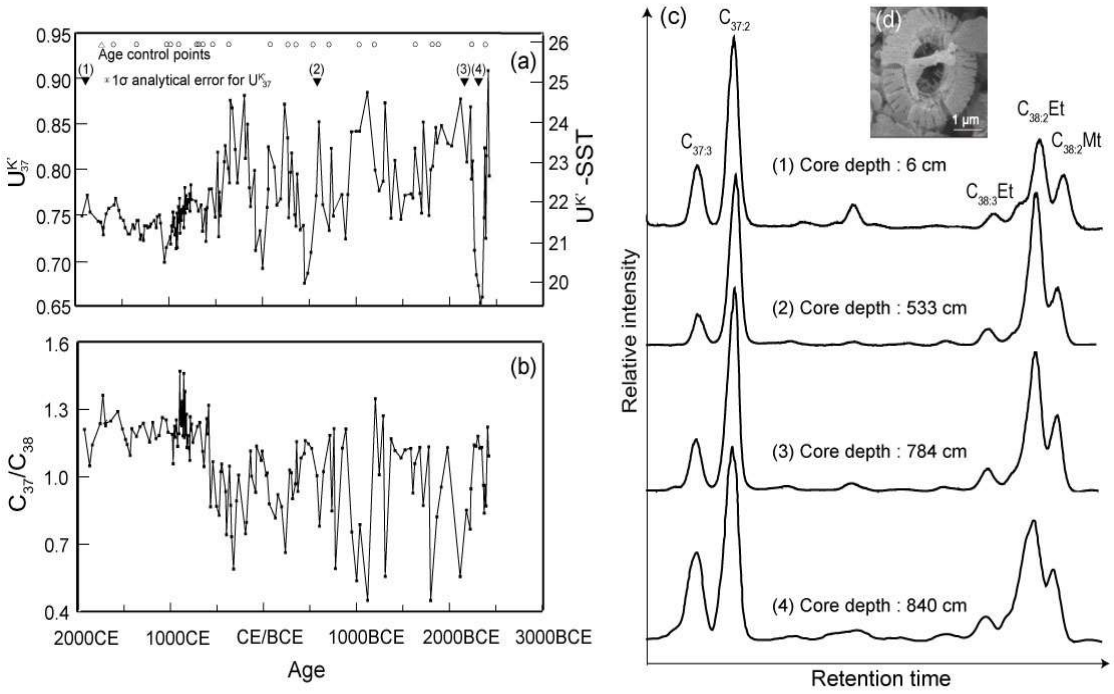

Fig. IIB-3

Time series records of (a) $U^{K'}_{37}$ and (b) C_{37}/C_{38} ratios. The ^{14}C age controlling points and timing of the Hoei eruption are denoted by open circles and triangles, respectively. The typical alkenone chromatogram at the numbered analytical points (solid triangles) and SEM picture of *G. oceanica* contained in the sediment are shown in (c) and (d), respectively.

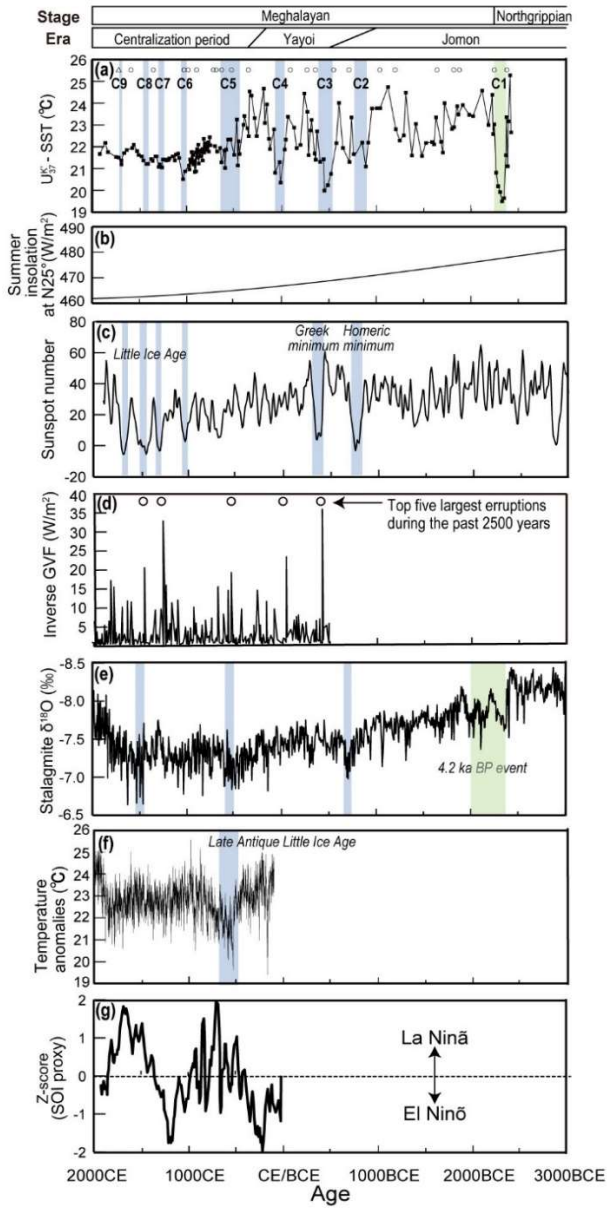

Fig. IIB-4

Time series records of (a) $U^{K'}_{37}$-SST, (b) summer insolation at 25°N (Laskar et al., 2004), (c) sunspot numbers estimated from atmospheric radiocarbon levels (Solanki et al., 2004), (d) global volcanic forcing (GVF) depicted by sulfate concentrations in ice cores from Greenland and Antarctica (Sigl et al., 2015), (e) $\delta^{18}O$ records of Dongge cave as a proxy for the summer monsoon (Wang et al., 2005), (f) Eurasian summer temperature variability reconstructed from tree ring width chronologies (Büntgen et al., 2016), and (g) SOI proxy from sedimentary cores sampled from the tropical Pacific (Yan et al., 2011). The green and gray colored bars represent the relatively cold periods.

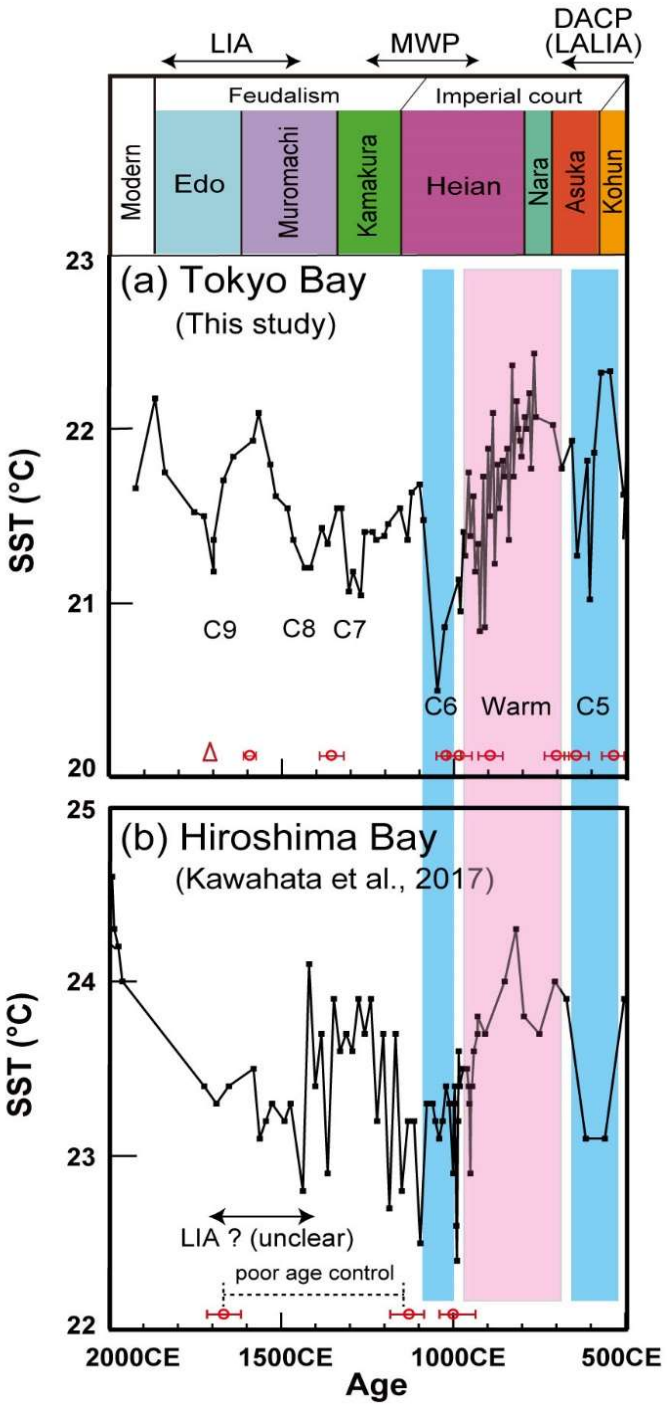

Fig. IIB-5

Time series of $U^{K'}_{37}$-SST during the last 1,500 years in (a) Tokyo and (b) Hiroshima bays. The upper row shows each historical period and the broad categories of social systems at that time in Japan. The relatively cold periods (C5–C9) in Tokyo Bay are also shown. The age controlling points are represented with an open triangle (the Hoei scoria layer) and circles (^{14}C age of shells) with 1σ error.

Table IIB-1. Depth and radiocarbon-derived dates of the molluscan shells retrieved from core KT12-06-2B. The range of calendar ages defines a 68.2% confidence interval.

Sample name	Lab. no.	Depth	AMS ^{14}C age	Calibrated age (Marine13)	
				Range	Mean
		(cm)	(yr BP)	(Cal. yr BP)	(Cal. yr BP)
KT12St2B-36	YAUT-042602	36	774 ± 25	307–406	361
KT12St2B-2-64	MTC-16496	64	1079 ± 95	519–776	603
KT12St2B-3-14	MTC-16497	111	1440 ± 93	814–1040	930
KT12St2B-3-24	MTC-16498	121	1473 ± 93	854–1080	967
KT12St2B-3-68	MTC-16500	165	1559 ± 93	951–1161	1056
KT12St2B-4-20	MTC-16502	217	1752 ± 97	1141–1351	1242
KT12St2B-4-26	MTC-16503	223	1776 ± 93	1170–1369	1269
KT12St2B-4-36	MTC-16504	233	1815 ± 98	1200–1411	1315
KT12St2B-4-68	MTC-16505	265	1917 ± 99	1302–1513	1420
KT12St2B-5-42	MTC-16506	339	2080 ± 95	1467–1715	1591
KT12St2B-6-14	MTC-16507	412	2454 ± 96	1891–2147	2036
KT12St2B-6-44	YAUT-042603	442	2610 ± 29	2170–2290	2219
KT12St2B-6-80	MTC-16508	478	2674 ± 96	2145–2425	2307
KT12St2B-7-24	YAUT-042604	523	2819 ± 33	2380–2572	2493
KT12St2B-7-52	MTC-16509	551	2976 ± 99	2518–2791	2658
KT12St2B-8-21	MTC-16510	626	3235 ± 96	2843–3107	2985
KT12St2B-8-40	YAUT-042606	640	3371 ± 31	3077–3219	3152
KT12St2B-8-80	YAUT-042609	680	3738 ± 30	3534–3661	3588
KT12St2B-8-96	MTC-16511	696	3873 ± 94	3626–3888	3766
KT12St2B-9-30	YAUT-042611	730	3926 ± 31	3757–3899	3826
KT12St2B-9-80	YAUT-042612	780	4186 ± 31	4104–4255	4188
KT12St2B-10-44	YAUT-042613	844	4286 ± 32	4263–4398	4320

Table IIB-2

Summary of alkenone data from core KT12-06-2B.

Depth (cm)	Cal. yr BP	$U_{37}^{K'}$
7	23	0.749
11	80	0.772
13	109	0.753
19	194	0.743
21	223	0.742
25	251	0.728
27	251	0.736
31	280	0.751
33	308	0.757
37	365	0.761
39	382	0.768
43	416	0.755
45	432	0.747
49	466	0.744
51	483	0.736
55	516	0.729
57	533	0.729
61	566	0.739
63	583	0.735
67	611	0.744
69	623	0.744
73	645	0.723
75	657	0.728
79	680	0.722
81	691	0.738
85	714	0.738
87	725	0.736
91	748	0.737
93	759	0.740
99	794	0.744
103	816	0.736
105	828	0.748
109	851	0.750

111	862	0.741
115	903	0.698
117	924	0.714
121	965	0.726
123	970	0.718
127	979	0.738
129	984	0.732
133	994	0.753
135	999	0.737
139	1008	0.747
141	1013	0.728
145	1022	0.735
147	1027	0.713
151	1037	0.752
153	1041	0.714
157	1051	0.759
159	1056	0.742
163	1065	0.768
165	1070	0.730
169	1079	0.755
171	1084	0.744
175	1093	0.756
177	1098	0.752
181	1107	0.759
183	1111	0.736
187	1121	0.780
189	1125	0.752
193	1134	0.771
195	1139	0.764
197	1144	0.761
199	1148	0.757
203	1158	0.767
205	1162	0.764
209	1171	0.773
211	1176	0.754
215	1185	0.783
217	1190	0.767

221	1240	0.765
223	1265	0.754
227	1295	0.761
229	1310	0.732
233	1340	0.756
235	1347	0.721
239	1360	0.758
245	1380	0.778
253	1406	0.778
265	1445	0.747
277	1473	0.819
281	1482	0.726
285	1491	0.775
289	1501	0.749
307	1543	0.808
311	1552	0.826
325	1584	0.801
331	1598	0.785
335	1607	0.876
341	1628	0.867
347	1660	0.822
351	1682	0.785
365	1757	0.881
367	1768	0.812
371	1790	0.850
375	1811	0.780
377	1822	0.759
385	1866	0.799
387	1876	0.711
396	1925	0.733
398	1936	0.691
406	1979	0.758
408	1990	0.778
412	2012	0.825
422	2078	0.802
426	2105	0.761
432	2145	0.768

438	2186	0.872
444	2219	0.834
448	2231	0.747
454	2250	0.797
458	2263	0.818
468	2295	0.750
472	2307	0.738
476	2320	0.795
486	2354	0.733
496	2389	0.739
499	2399	0.675
509	2434	0.686
519	2469	0.709
529	2525	0.771
533	2553	0.852
539	2595	0.761
549	2664	0.733
553	2686	0.823
559	2709	0.749
563	2724	0.874
583	2799	0.772
593	2837	0.724
600	2863	0.772
610	2901	0.841
624	2953	0.842
628	2988	0.842
634	3071	0.885
640	3154	0.799
644	3196	0.776
648	3239	0.787
650	3260	0.873
656	3324	0.746
660	3366	0.810
666	3430	0.745
670	3473	0.771
676	3536	0.773
678	3558	0.769

680	3579	0.823
686	3633	0.774
688	3651	0.752
690	3669	0.852
698	3729	0.749
704	3749	0.800
710	3769	0.803
720	3803	0.846
724	3816	0.829
734	3863	0.848
744	3931	0.828
750	3972	0.826
764	4067	0.877
774	4134	0.808
780	4175	0.869
784	4183	0.789
790	4196	0.809
800	4216	0.711
810	4237	0.684
820	4258	0.672
830	4278	0.653
840	4299	0.660
850	4318	0.747
854	4326	0.823
860	4337	0.724
864	4344	0.815
874	4363	0.908
880	4374	0.793

Chapter III

Development of alkenone paleothermometer: applications to the outcrop and lacustrine sediment

Chapter III-A

Biomarkers in the rock outcrop of the Kazusa Group reveal paleoenvironments of the Kuroshio region

第Ⅲ-A 章については、5 年以内に
雑誌等で刊行予定のため、非公開

Chapter III-B

Genomic and geochemical identification of the long-chain alkenone producers in the estuarine Lake Takahoko, Japan: implications for paleotemperature reconstructions

第Ⅲ-B 章については、5 年以内に
雑誌等で刊行予定のため、非公開

Chapter IV

Summary

IV-1. Conclusion of Chapter II-A

In the Yangtze delta area, using the sedimentary cores MD06-3040 and MD06-3039 collected from the coastal area of East China Sea, I obtained quantitative and high-time resolution paleotemperature records. According to ^{14}C ages of molluscan shells extracted from the sediment cores, the cores recovered continuously the time period from ca. 6000 BCE to the present.

1) Considering that the values of TOC contents, TOC/TN ratios, coccolith assemblages and mean grain size are stable for the last 8.0 ka, I assume changes in infer SST fluctuations. AT were estimated from SST because of the positive correlation between both variables near the core site.

2) Despite potential chronological errors in our used depths-age model, the $U^{K'}_{37}$ records suggested that frequent and abrupt cold episodes (3-4℃ SST drop) occurring between 2600 and 1900 BCE can be related to a global climatic transition called 4.2 ka event, during which East Asian monsoon regime and the KC mode was altered.

3) The Yangtze Neolithic civilization was one of the earliest rice cultivating civilizations in the world and may have been vulnerable to AT change. Indeed, the extraordinary cold climate in the Yangtze delta could be one of the possible reasons for the collapse of the Yangtze Neolithic civilization around 4.2 ka.

IV-2. Conclusion of Chapter II-B

Sedimentary core KT12-06-2B was recovered from Tokyo Bay to reconstruct the paleoenvironment of the Kanto area, central Japan. The chronology of the core was determined using ^{14}C ages of 22 molluscan shells extracted from the sediment core, showed that the sediment core recovered continuously over the time period from ca. 2400 BCE to the present. Regional paleotemperatures were quantitatively estimated with the use of the $U^{K'}_{37}$ thermometer. Our results suggest the following:

1) The temperature during the Meghalayan was generally warmer than present exhibiting a declining trend, which roughly corresponds to changes in the summer insolation and to the millennial-scale latitudinal shift of the subarctic front. The largest cold episode, interrupting the relatively warm period of the late-Jomon era,

occurred ca. 2300 BCE, which may be related to the global climatic transition known as the 4.2 ka event caused by a shift in the monsoonal regime.
2) The temperature during the Yayoi era recorded centennial-scale fluctuations. Specifically, cold periods occurred ca. 440 BCE and 100 CE, which may have been caused by solar activity minimums and/or volcanic eruptions. Severe climate during the Wakoku-Tairan period of civil unrest in the 2nd century CE, recorded in Chinese historical documents, was detected using a climate proxy.
3) After the establishment of the centralization system of government, historical archives indicated that warm conditions prevailed until ca. 300 CE, followed by cold periods at ca. 500 CE. These warm and cold periods may correspond to the RWP and LALIA (overlaps with the DACP), respectively. A temperature drop at 1050 CE has been recorded by multiple climate proxies throughout Japan, and may have been caused by a strong El Niño. These cold periods appear to coincide with the timing of social unrest and major shifts in the governmental system of Japan.

IV-3. Conclusion of Chapter III-A

It could be the first to report that LCAs and *n*-alkanes were well preserved in the rock samples from outcrop of the Kazusa Group and it is likely that paleoenvironmental information were well- preserved as well. I investigated rock samples from the Otadai Formation, which is exposed along the Yoro River, and spans the time interval corresponding to the MIS 33 to 29 (ca. 1.1−1.0 Ma) . The variations in $U^{K'}_{37}$ and ACL of *n*-alkanes fit well and are synchronous with those of the global sea-level variations; therefore my data probably reflect the changes in SST and terrestrial environments forced by glacial-interglacial cycles, respectively. CPI of *n*-alkanes, which weakly correlated with C/N ratio, might be also influenced by the freshness of organic matter, whereas no correlations were observed between $U^{K'}_{37}$, ACL and C/N ratio. $U^{K'}_{37}$, ACL, and CPI values in the Shoryuji section which is about 10 km far from the Yoro River section showed similar values, which suggested that those values seemed not to be influenced by the sedimentary process in the Kazusa forearc basin. Based on the modern calibration, during MIS 33 to 29, $U^{K'}_{37}$-SSTs fluctuated from 22.8 ℃ to 26.6 ℃. Although these temperatures were significantly

higher than the $U^{K'}_{37}$-SSTs recorded in the modern sediments around the Boso Peninsula, Mg/Ca paleotemperatures of *Globigerina bulloides*, which also indicated the high SSTs, vouched the validity of $U^{K'}_{37}$-SSTs in the Otadai formation. High temperatures obtained in my study, might be related to the direct influence of the warm Kuroshio current in the Kazusa forearc during the MIS 33 to 29. This research demonstrated the classical biomarker-based paleoenvironmental information can be extracted from the subaerially exposed geological samples, if preservation conditions of biomarkers are respected.

IV-4. Conclusion of Chapter III-B

I am the first to report the presence of LCAs produced by Group II haptophytes in a Japanese lake, which were identified using a combination of genomic and organic geochemical analysis. Two distinct clades of haptophyte species (Tak-A and Tak-B) are probably responsible for the production of LCAs in Lake Takahoko. Tak-A is a close relative of Hap-A originating from Lake George, and Tak-B is genetically identified as *Isochrysis galbana*. According to the findings of previous culture experiments for these haptophyte species, similar $U^{K'}_{37}$ calibrations can be applied to Tak-A and Tak-B, which can remove the species effect and allow the down-core paleotemperature reconstructions. The $U^{K'}_{37}$-SST recorded in the surface sediment corresponds to the lake temperature in summer. Although it is necessary to carefully consider changes in haptophyte species and bloom timing of the past, brackish lakes having multiple Group II haptophytes may be suitable for lake paleotemperature reconstructions. This research shows that $U^{K'}_{37}$ paleothermometer has the potential to become a strong tool for reconstructing lake water temperatures.

IV-5. General conclusion and future perspectives

In this doctorate dissertation, I presented both application studies and proxy development studies about alkenone paleothermometry. LCAs-based proxy has been one of the most established and sophisticated proxies for SST in open ocean settings.

I focused on that LCAs are contained not only in deep-sea sediments but also coastal shallow-sea sediments and some restricted lacustrine sediments, where other quantitative paleotemperature proxies are mostly unavailable. I applied alkenone paleothermometry to the coastal sediment cores and reconstructed Holocene paleoclimate changes in coastal East Asia. I also discovered that alkenone paleothermometer is also applicable to on-land geologic stratum and lacustrine sediments, which shows the large potential of my method.

In Chapter II, I provided the high-time resolution and quantitative paleotemperature records from off the Yangtze delta and Tokyo Bay and suggested that climate changes had a large impact on Chinese and Japanese societies of the past. The largest cold events during the mid- to late-Holocene were detected in both sites at around 2200 BCE. Although the Global Boundary Stratotype Section and Point (GSSP) of 4.2 ka event was set in the speleothem collected from a cave in northern India (Berkelhammer et al., 2012; Walker et al., 2018), my results validates that East Asia was also under the direct influence of 4.2 ka event as was suggested by previous studies (Ran and Chen, 2019). The results of Chapter II-A had large impacts on the ongoing debates about the reasons for the collapse of the Yangtze Neolithic civilizations at around 2200 BCE (Sun et al., 2019; Griffiths et al., 2020). The clear evidence of the 4.2 ka event in Japan was shown by Chapter II-B, which validates the previous data of Sakaguchi (1983). It also detected the other decadal- to centennial-scale climatic changes around Tokyo Bay during the Meghalayan, and confirmed some important climatic events, which was previously assumed by the historical studies.

Sediment cores recovered from continental shelves and inner bays usually have high sedimentation rates; therefore, these studies can provide high-time resolution, quantitative, and continuous paleotemperature records in coastal areas where humans have been settled during the Holocene. Recent studies statistically proposed that the temperature change is the primary controlling factor that determined the fate of human society via social factors such as decreased agricultural production, economic downturn, and war (e.g., Zhang et al., 2010; Zhang et al., 2011). Therefore, accurate paleotemperature records in the coastal area are necessary

to precisely understand human history, which brings us important lessons for our fate in the climate change era.

My studies also confirmed that alkenone paleotemperature fluctuations from off the coast of Yangtze delta and Tokyo Bay did not match except for the 4.2 ka event. For example, the Medieval Warm Period detected off the Yangtze delta area was not completely consistent with the paleotemperature trend in Tokyo Bay. On the other hand, several cold periods, including Late Antique Little Ice Age (considered to be the same event as Dark Ages Cold Period in this study), detected from the Tokyo Bay were not seen in off the Yangtze delta area. Holocene climate changes in the monsoonal area, which was controlled by multiple factors including solar activity, and volcanic eruptions, varied greatly from region to region (Wanner et al., 2008). Therefore, enriching local paleoclimatic records with high-time resolution is necessary to reach an overall elucidation of past climate changes with their controlling mechanisms. Although I could not conduct specific verification in this study, it is better to evaluate the seasonal variation of LCAs production using sediment traps and other methods to accurately interpret the $U^{K'}_{37}$-SSTs recorded in the sediments collected from inner bays where environments are often homogenous. In my future research, I will provide more and more quantitative paleotemperature records using coastal sediment cores with particular attention to climatology and historically important areas. These studies will accelerate the interdisciplinary interpretations of earth science and social science.

In Chapter III, I discovered LCAs in the Kazusa Group (Chapter III-A) and Lake Takahoko (Chapter III-B), each met the optimum conditions for alkenone preservations allowing paleotemperature reconstructions. The stratigraphic studies in the Kazusa Group have a long history over the past 50 years, providing detailed chronologies based on magnetic, microfossils, and oxygen isotope stratigraphy covering almost the entire Pleistocene. I detected that LCAs and *n*-alkanes are contained and well-preserved in the rock outcrops of the Otadai Formation in the Kazusa group, which can potentially reveal long, continuous, and high-time resolution SST and its related terrestrial climate changes in the Kazusa forearc basin. The environments of the Kazusa forearc basin should be deeply related to the

evolution of the KC and EAM, biomarker records in the Kazusa Group can clarify mechanisms causing the global climatic changes that occurred during the Pleistocene, such as the mid-Pleistocene Transition and the geomagnetic reversal-induced climate changes (Kitaba et al., 2013; McClymont et al., 2013).

Applications of alkenone paleothermometry to lacustrine settings have not been well established compared to those in the open ocean because of the genetic diversity and omnipresence of LCAs producers. My study in Lake Takahoko and other surrounding lakes showed that the environmental-DNA analysis is useful to identify lakes in which LCAs are present containing the information about LCAs-producing haptophyte species, which is necessary to detect the applicable calibrations. This method should be also applicable to the other settings; therefore, the results of Chapter III-B can contribute to improving alkenone paleothermometry as a rare paleotemperature proxy applicable to the lacustrine environments. In my future research, I will take long sediment cores from Lake Takahoko that reaches the Jomon era and reconstruct lake water temperature changes in the past. It can be direct evidence of the terrestrial paleoclimate in Aomori Prefecture, where the particularly prosperous Jomon cultures were flourished (Kawahata, 2019).

In more than 30 years of research history, LCAs is considered to be a very robust paleothermometer. My doctorate dissertation showed the further potential of this proxy. In recent years, more and more paleotemperature proxies have been proposed and applied to paleoenvironmental studies. However, some of which are subject to insufficient constraints in modern calibration, prevailing unreliable knowledge. Paleoclimatologists should use the reliable proxy, whose origin is strongly constrained and the environmental response is strictly confirmed by the modern settings and/or ideal laboratory experimental environments. From this point of view, LCAs have been and will continue to be one of the best proxies to reveal the history of the Earth.

Acknowledgement

I am deeply grateful to all the people who supported and advised me in completing my PhD research. I would like to express my appreciation to Professor HODAKA KAWAHATA who has taught me the essence of science and provided me the opportunity and the freedom to explore the vast frontiers of Earth science. He always encouraged me to start new research. Professor YUSUKE YOKOYAMA kindly collaborated with my research and always showed me his attractive science. Associate Professor JUNICHIRO KURODA gave me considerable advice, deep discussions and financial supports. Assistant Professor KENJI MARC RAYMOND MATSUZAKI proofread and improved the quality of my doctorate dissertation.

Dr. MASAYUKI UTSUNOMIYA invited me to the world of field geology, which significantly expanded my research field. Dr. HIDETO NAKMURA gave me cutting-edge knowledge in organic geochemistry. Dr. KE WANG and Mr. BANG ZHENG kindly helped me to promote intimate communication with Chinese scientists. The international collaboration works with Prof. HONGBO ZHENG, Prof. SHOUYE YANG, and Prof. BIN ZHOU were meaningful for my career development as a scientist. Dr. TOSHIHIRO YOSHIMURA and Dr. AYUMI MAEDA greatly helped me in a geochemical analysis of planktic foraminifer. Dr. YOSUKE MIYAIRI and Dr. CHIKAKO SAWADA instructed me ^{14}C analysis using the AMS. Dr. MIYAKO SATO and Dr. HIDAMI SUGA supported me on GC analysis. I greatly appreciate those scientists who kindly collaborated with my research in their special fields.

I would like to express my deep gratitude to Dr. NAOHIKO OHKOUCHI, Dr. NAOMI HARADA and Dr. ATSUSHI SUZUKI for their great supports in my experiments and constructive advice to improve my science. Researchers and technicians in Geological Survey of Japan, AIST and Biogeochemistry program, JAMSTEC always kindly helped my laboratory work. I appreciate the professors in the Department of Earth and Planetary Science, the University of Tokyo, who conducted the geological excursions in Kiyoshumi, Boso Peninsula, and Yunnan Province, China. Many of my research ideas were born on these occasions.

Dr. SHINJI UEDA, Mr. SHUN TOKIOKA, and Mr. SHUHEI SAWAMURA supported my fieldwork in many lakes. Dr. TAKAHIRO TSUJI gave me information

about the TR-3 core, which is necessary for my studies on the Kazusa Group. Dr. AKIRA MIZUYAMA, Dr. MIYUKI NISHIJIMA, Dr. AKIRA IGUCHI, and Dr. SHINYA KAJITA gave me advice on molecular biological analysis.

I appreciate the members of KAWAHATA-laboratory, especially Dr. YUTA ISAJI and Dr. YUKI OTA for teaching me many the geochemical analysis and giving advices on my research life. Mrs. YOKO NISHIKURA and Mrs. RICA UCHIDA kindly supported my daily experiments and office works. Friendly, constructive, and severe discussions with OFGS and ACES members were always the driving force of my research. I would like to thank Dr. EIICHI TAJIKA, Dr. HODAKA KAWAHATA, Dr. JUNICHIRO KURODA, Dr. AKIHIRO KANO, Dr. HAJIME KAYANE, and Dr. AYAKO ABE, who reviewed my doctoral dissertation, for their valuable suggestions. Finally, I would like to express my greatest gratitude to my family for their support in my daily life.

References

Chapter I

Anderson, N.J. and Leng, M.J., 2004. Increased aridity during the early Holocene in West Greenland inferred from stable isotopes in laminated-lake sediments. Quaternary Science Reviews 23, 841–849.

Araie, H. et al., 2018. Novel alkenone-producing strains of genus Isochrysis (Haptophyta) isolated from Canadian saline lakes show temperature sensitivity of alkenones and alkenoates. Organic Geochemistry 121, 89–103.

Asami, R. et al., 2020. High-Resolution Evidence for Middle Holocene East Asian Winter and Summer Monsoon Variations: Snapshots of Fossil Coral Records. Geophysical Research Letters 47(16), e2020GL088509.

Anand, P., Elderfield, H., Conte, M. H., 2003. Calibration of Mg/Ca thermometry in planktonic foraminifera from a sediment trap time series. Paleoceanography 18(2).

Barker, S., Greaves, M., Elderfield, H., 2003. A study of cleaning procedures used for foraminiferal Mg/Ca paleothermometry. Geochemistry, Geophysics, Geosystems 4(9).

Beck, J. W. et al., 1992. Sea-surface temperature from coral skeletal strontium/calcium ratios. Science 257, 644-647.

Bendif, E.M., Probert, I., Schroeder, D.C. and de Vargas, C., 2013. On the description of Tisochrysis lutea gen. nov. sp. nov. and Isochrysis nuda sp. nov. in the Isochrysidales, and the transfer of Dicrateria to the Prymnesiales (Haptophyta). Journal of Phycology 25, 1763–1776.

Bendif, E.M. et al., 2014. Genetic delineation between and within the widespread coccolithophore morpho-species Emiliania huxleyi and Gephyrocapsa oceanica (Haptophyta). Journal of Phycology 50, 140–148.

Blaga, C. I., Reichart, G. J., Heiri, O., Damsté, J. S. S., 2009. Tetraether membrane lipid distributions in water-column particulate matter and sediments: a study of 47 European lakes along a north–south transect. Journal of Paleolimnology 41(3), 523-540.

Blanz, T., Emeis, K.C. and Siegel, H., 2005. Controls on alkenone unsaturation ratios along the salinity gradient between the open ocean and the Baltic Sea. Geochimica et Cosmochimica Acta 69, 3589–3600.

Branson, O., 2013. The coordination of Mg in foraminiferal calcite. Earth and Planetary Science Letters, 383, 134-141.

Brassell, S. C., Eglinton, G., Maxwell, J. R., 1983. The geochemistry of terpenoids and steroids. Biochemical Society Transactions, 11(5), 575-586.

Brassell, S.C., Eglinton, G., Marlowe, I., Pflaumann, U.P. and Sarnthein, M., 1986. Molecular stratigraphy: a new tool for climatic assessment. Nature, 320, 129–133.

Brassell, S.C., 1993. Applications of Biomarkers for Delineating Marine Paleoclimatic Fluctuations during the Pleistocene. Organic Geochemistry, Chapter 34, 699–738.

Brassell, S. C., Dumitrescu, M., 2004. Recognition of alkenones in a lower Aptian porcellanite from the west-central Pacific. Organic Geochemistry, 35(2), 181-188.

Brassell, S. C., 2014. Climatic influences on the Paleogene evolution of alkenones. Paleoceanography, 29(3), 255-272.
Broecker, W., 2013. How to think about the evolution of the ratio of Mg to Ca in seawater. American Journal of Science, 313(8), 776-789.
Castañeda, I. S., Schouten, S., 2011. A review of molecular organic proxies for examining modern and ancient lacustrine environments. Quaternary Science Reviews 30(21-22), 2851-2891.
Chu, G. et al., 2005. Long-chain alkenone distributions and temperature dependence in lacustrine surface sediments from China. Geochimica et Cosmochimica Acta 69, 4985–5003.
CLIMAP Project Members., 1976. The surface of the ice-age earth. Science, New Series 191 1131-1137.
Conte, M.H., Thompson, A., Eglinton, G. and Green, J.C., 1995. Lipid Biomarker Diversity in the Coccolithophorid Related Species Gephyrocapsa Oceanica. Journal of Phycology 31, 2, 272-282.
Conte, M.H. et al., 2006. Global temperature calibration of the alkenone unsaturation index (U^{k}_{37}) in surface waters and comparison with surface sediments. Geochemistry, Geophysics, Geosystems 7 (2).
Cranwell, P.A., 1985. Long-chain unsaturated ketones in recent lacustrine sediments. Geochimica et Cosmochimica Acta 49, 1545–1551.
D'Andrea, W.J., Theroux, S., Bradley, R.S. and Huang, X., 2016. Does phylogeny control U^{K}_{37}-temperature sensitivity Implications for lacustrine alkenone paleothermometry. Geochimica et Cosmochimica Acta 175, 168–180.
DeLong, K. L., 2014. A reconstruction of sea surface temperature variability in the southeastern Gulf of Mexico from 1734 to 2008 CE using cross-dated Sr/Ca records from the coral Siderastrea siderea. Paleoceanography 29(5), 403-422.
Elderfield, H., Ganssen, G., 2000. Past temperature and δ 18 O of surface ocean waters inferred from foraminiferal Mg/Ca ratios. Nature 405(6785), 442-445.
Farrimond, P., Eglinton, G., Brassell, S. C., 1986. Alkenones in Cretaceous black shales, Blake-Bahama Basin, western North Atlantic. Organic Geochemistry 10(4-6), 897-903.
Felis, T. et al., 2014. Intensification of the meridional temperature gradient in the Great Barrier Reef following the Last Glacial Maximum. Nature Communications 5(1), 1-8.
Fujine, K., Yamamoto, M., Tada, R. and Kido, Y., 2006. A salinity-related occurrence of a novel alkenone and alkenoate in Late Pleistocene sediments from the Japan Sea. Organic Geochemistry 37, 1074–1084.
Grove, M., 2015. Climatic variability, plasticity, and dispersal: A case study from Lake Tana, Ethiopia. Journal of human evolution 87, 32-47.
Hatfield, J. L. et al., 2011. Climate impacts on agriculture: implications for crop production. Agronomy journal 103(2), 351-370.
Herbert, T. D., 2006. Alkenone Paleotemperature. The oceans and marine geochemistry 6, 391.
Hayashi, E. et al., 2013. Growth-rate influences on coral climate proxies tested by a multiple colony culture experiment. Earth and Planetary Science Letters, 362, 198-206.
Hoefs, M. J., Versteegh, G. J., Rijpstra, W. I. C., de Leeuw, J. W., Damsté, J. S. S., 1998. Postdepositional oxic degradation of alkenones: Implications for the

measurement of palaeo sea surface temperatures. Paleoceanography 13(1), 42-49.
Imbrie, J.and Kipp, N.G., 1971. A new micropaleontological method for quantitative paleoclimatology: application to a late Pleistocene Caribbean core. The late Cenozoic glacial ages 71-181.
Inoue, M., Suzuki, A., Nohara, M., Hibino, K., Kawahata, H., 2007. Empirical assessment of coral Sr/Ca and Mg/Ca ratios as climate proxies using colonies grown at different temperatures. Geophysical Research Letters 34(12).
Inoue, M., Suwa, R., Suzuki, A., Sakai, K., Kawahata, H., 2011. Effects of seawater pH on growth and skeletal U/Ca ratios of Acropora digitifera coral polyps. Geophysical Research Letters 38(12).
IPCC Fifth Assessment Report, 2014. Cambridge: Cambridge University Press.
Kirilenko, A. P., Sedjo, R. A., 2007. Climate change impacts on forestry. Proceedings of the National Academy of Sciences 104(50), 19697-19702.
Kaiser, J. et al., 2019. Changes in long chain alkenone distributions and Isochrysidales groups along the Baltic Sea salinity gradient. Organic Geochemistry 127, 92–103.
Kajita, H.et al., 2017. Holocene sea surface temperature variations recorded in corals from Kikai Island, Japan. Geochemical Journal 51(4), e9-e14.
Kajita, H. et al., 2018. Extraordinary cold episodes during the mid-Holocene in the Yangtze delta: Interruption of the earliest rice cultivating civilization. Quaternary Science Reviews 201, 418–428.
Kajita, H. et al., 2020a. Genomic and geochemical identification of the long-chain alkenone producers in the estuarine Lake Takahoko, Japan: Implications for temperature reconstructions. Organic Geochemistry, 103980.
Kajita, H. et al., 2020b. High time-resolution alkenone paleotemperature variations in Tokyo Bay during the Meghalayan: Implications for cold climates and social unrest in Japan. Quaternary Science Reviews 230, 106160.
Kajita, H., and Nakamura, H., 2020. Diversity of long-chain alkenone producers - Developments of temperature proxy in inland waters-. Geochemistry (Chikyuukagaku) 54(2), 79-96.
Kawakubo, Y., Alibert, C., Yokoyama, Y., 2017. A reconstruction of subtropical western North Pacific SST variability back to 1578, based on a Porites Coral Sr/Ca record from the northern Ryukyus, Japan. Paleoceanography 32(12), 1352-1370.
Kelley, C. P., Mohtadi, S., Cane, M. A., Seager, R., Kushnir, Y., 2015. Climate change in the Fertile Crescent and implications of the recent Syrian drought. Proceedings of the national Academy of Sciences 112(11), 3241-3246.
Kim, J. H. et al., 2010. New indices and calibrations derived from the distribution of crenarchaeal isoprenoid tetraether lipids: Implications for past sea surface temperature reconstructions. Geochimica et Cosmochimica Acta 74(16), 4639-4654.
Lee, K.E., Bahk, J.J. and Choi, J., 2008. Alkenone temperature estimates for the East Sea during the last 190,000 years. Organic Geochemistry 39, 741–753.
Li, J., Philp, R.P., Fan, P.U. and Allen, J., 1996. Long-chain alkenones in Qinghai Lake sediments. Geochimica et Cosmochimica Acta 60, 235–241.

Liu, Z., 2018. Transient temperature asymmetry between hemispheres in the Palaeogene Atlantic Ocean. Nature Geoscience 11, 656–660.
Longo, W.M., 2016. Temperature calibration and phylogenetically distinct distributions for freshwater alkenones: Evidence from northern Alaskan lakes. Geochimica et Cosmochimica Acta 180, 177–196.
Lea, D. W., Mashiotta, T. A., Spero, H. J., 1999. Controls on magnesium and strontium uptake in planktonic foraminifera determined by live culturing. Geochimica et Cosmochimica Acta 63(16), 2369-2379.
Leipe, C., Kito, N., Sakaguchi, Y., Tarasov, P. E., 2013. Vegetation and climate history of northern Japan inferred from the 5500-year pollen record from the Oshima Peninsula, SW Hokkaido. Quaternary International 290, 151-163.
Lobell, D. B., Burke, M. B., 2008. Why are agricultural impacts of climate change so uncertain? The importance of temperature relative to precipitation. Environmental Research Letters 3(3), 034007.
Matsuzaki, K. M., Itaki, T., 2017. New northwest Pacific radiolarian data as a tool to estimate past sea surface and intermediate water temperatures. Paleoceanography 32(3), 218-245.
Matsuzaki, K. M., Itaki, T., Tada, R., 2019. Paleoceanographic changes in the Northern East China Sea during the last 400 kyr as inferred from radiolarian assemblages (IODP Site U1429). Progress in Earth and Planetary Science 6(1), 22.
Matsuzaki, K. M., Suzuki, N., Tada, R., 2020. An intensified East Asian winter monsoon in the Japan Sea between 7.9 and 6.6 Ma. Geology 48, 919-923.
Mayewski, P. A. et al., 2004. Holocene climate variability. Quaternary research 62(3), 243-255.
McConnell, J. R. et al., 2020. Extreme climate after massive eruption of Alaska's Okmok volcano in 43 BCE and effects on the late Roman Republic and Ptolemaic Kingdom. Proceedings of the National Academy of Sciences 117(27), 15443-15449.
McClymont, E. L., Rosell-Melé, A., Giraudeau, J., Pierre, C. Lloyd, J. M., 2005. Alkenone and coccolith records of the mid-Pleistocene in the south-east Atlantic: Implications for the $U^{K'}_{37}$ index and South African climate. Quaternary Science. Reviews 24, 1559-1572.
McGregor, H.V., Dima, M., Fischer, H.W. and Mulitza, S., 2018. Rapid 20th-centuryincrease in coastal upwelling off northwest Africa revealed by high-resolution marine sediment cores. Science 315, 637–639.
Min, G. R.,1995. Annual cycles of UCa in coral skeletons and U/Ca thermometry. Geochimica et Cosmochimica Acta 59(10), 2025-2042.
Müller, P. J., Čepek, M., Ruhland, G. Schneider, R. R., 1997. Alkenone and coccolithophorid species changes in late Quaternary sediments from the Walvis Ridge: Implications for the alkenone paleotemperature method. Palaeogeography. Palaeoclimatology. Palaeoecology 135, 71-96.
Müller, P.J., Kirst, G., Ruhland, G., von Storch, I. and Rosell-Melé, A., 1988. Calibration of the alkenone paleotemperature index $U^{K'}_{37}$ based on core-tops from the eastern South Atlantic and the global ocean (60°N–60°S). Geochimica et Cosmochimica Acta 62, 10, 1757–1772.
Nakagawa, T., Tarasov, P. E., Nishida, K., Gotanda, K., Yasuda, Y., 2002. Quantitative pollen-based climate reconstruction in central Japan: application

to surface and Late Quaternary spectra. Quaternary Science Reviews 21(18-19), 2099-2113.
Nakagawa, T., 2005. Pollen/event stratigraphy of the varved sediment of Lake Suigetsu, central Japan from 15,701 to 10,217 SG vyr BP (Suigetsu varve years before present): description, interpretation, and correlation with other regions. Quaternary Science Reviews 24(14-15), 1691-1701.
Nakagawa, T. et al., 2008. Regulation of the monsoon climate by two different orbital rhythms and forcing mechanisms. Geology 36(6), 491-494.
Nakamura, H., Sawada, K., Araie, H., Suzuki, I. and Shiraiwa, Y., 2014. Long chain alkenes, alkenones and alkenoates produced by the haptophyte alga Chrysotila lamellosa CCMP1307 isolated from a salt marsh. Organic Geochemistry 66, 90–97.
Nakamura, H., 2016. Composition of long chain alkenones and alkenoates as a function of growth temperature in marine haptophyte Tisochrysis lutea. Organic Geochemistry 99, 78–89.
Nigrini, C., 1970. Radiolarian assemblages in the North Pacific and their application to a study of Quaternary sediments in core V20-130. In Geological Investigations of the North Pacific (Vol. 126, pp. 139-183). Geological Society of America New York.
Nürnberg, D., Bijma, J., Hemleben, C., 1996. Assessing the reliability of magnesium in foraminiferal calcite as a proxy for water mass temperatures. Geochimica et Cosmochimica Acta 60(5), 803-814.
Prahl, F.G., Muehlhausen, L.A. and Zahnle, D.L., 1988. Further evaluation of long-chain alkenones as indicators of paleoceanographic conditions. Geochimica et Cosmochimica Acta 2303–2310.
Prahl, F.G. and Wakeham, S.G., 1987. Calibration of unsaturation patterns in long-chain ketone compositions for palaeotemperature assessment. Nature 330, 367–369.
Prahl, F.G., de Lange, G.J., Lyle, M. and Sparrow, M.A., 1989. Post-depositional stability of long-chain alkenones under constracting redox conditions. Nature 341, 434–437.
Prahl, F. G., Sparrow, M. A., Wolfe, G. V., 2003. Physiological impacts on alkenone paleothermometry. Paleoceanography 18(2).
Powers, L., 2010. Applicability and calibration of the TEX86 paleothermometer in lakes. Organic Geochemistry 41(4), 404-413.
Rabinowitz, H. S., Polissar, P. J., Savage, H. M., 2017. Reaction kinetics of alkenone and n-alkane thermal alteration at seismic timescales. Geochemistry, Geophysics, Geosystems 18(1), 204-219.
Rechka, J. A., Maxwell, J. R., 1988. Characterisation of alkenone temperature indicators in sediments and organisms. Organic Geochemistry 13(4-6), 727-734.
Rosenthal, Y., Boyle, E. A., Slowey, N., 1997. Temperature control on the incorporation of magnesium, strontium, fluorine, and cadmium into benthic foraminiferal shells from Little Bahama Bank: Prospects for thermocline paleoceanography. Geochimica et Cosmochimica Acta 61(17), 3633-3643.
Salacup, J. M., Farmer, J. R., Herbert, T. D., Prell, W. L., 2019. Alkenone paleothermometry in coastal settings: Evaluating the potential for highly

resolved time series of sea surface temperature. Paleoceanography and Paleoclimatology 34(2), 164-181.
Sampei, Y., Inaba, T., Suzuki, N., 2003. Abnormally abundant alkenone-derived C37 and C38 n-alkanes in Miocene Onnagawa siliceous mudstones, northeast Japan. Organic geochemistry 34(9), 1247-1258.
Sawada, K., Handa, N., Shiraiwa, Y., Danbara, A. and Montani, S., 1996. Long-chain alkenones and alkyl alkenoates in the coastal and pelagic sediments of the northwest north Pacific, with special reference to the reconstruction of Emiliania huxleyi and Gephyrocapsa oceanica ratios. Organic Geochemistry 24, 751–764.
Schiebel, R., Hemleben, C., 2017. Planktic foraminifers in the modern ocean (pp. 1-358). Berlin: Springer.
Schouten, S., Hopmans, E. C., Schefuß, E., Damste, J. S. S., 2002. Distributional variations in marine crenarchaeotal membrane lipids: a new tool for reconstructing ancient sea water temperatures?. Earth and Planetary Science Letters 204(1-2), 265-274.
Schouten, S., Hopmans, E. C., Damsté, J. S. S., 2013. The organic geochemistry of glycerol dialkyl glycerol tetraether lipids: a review. Organic geochemistry 54, 19-61.
Seki, O., Kawamura, K., Ikehara, M., Nakatsuka, T., Oba, T., 2004. Variation of alkenone sea surface temperature in the Sea of Okhotsk over the last 85 kyrs. Organic Geochemistry 35(3), 347-354.
Simoneit, B. R., Prahl, F., Leif, R. N., Mao, S. Z., 1994. Alkenones in sediments of Middle Valley, Leg 139: application as thermal sensors.
Stocker et al., 2013, Climate Change 2013: The Physical Science Basis (Cambridge Univ. Press).
Sumaila, U. R., Cheung, W. W., Lam, V. W., Pauly, D., Herrick, S., 2011. Climate change impacts on the biophysics and economics of world fisheries. Nature climate change 1(9), 449-456.
Tarasov, P. E. et al., 2011. Progress in the reconstruction of Quaternary climate dynamics in the Northwest Pacific: A new modern analogue reference dataset and
its application to the 430-kyr pollen record from Lake Biwa. Earth-Science Reviews 108(1-2), 64-79.
Theroux, S., D'Andrea, W.J., Toney, J., Amaral-Zettler, L. and Huang, Y., 2010. Phylogenetic diversity and evolutionary relatedness of alkenone-producing haptophyte algae in lakes: Implications for continental paleotemperature reconstructions. Earth and Planetary Science Letters 300, 311–320.
Theroux, S., Toney, J., Amaral-Zettler, L. and Huang, Y., 2013. Production and temperature sensitivity of long chain alkenones in the cultured haptophyte pseudoisochrysis paradoxa. Organic Geochemistry 62, 68–73.
Thiel, V., Jenisch, A., Landmann, G., Reimer, A. and Michaelis, W., 1997. Unusual distributions of long-chain alkenones and tetrahymanol from the highly alkaline Lake Van, Turkey. Geochimica et Cosmochimica Acta 61, 2053–2064.
Tierney, J. E., Malevich, S. B., Gray, W., Vetter, L., Thirumalai, K., 2019. Bayesian calibration of the Mg/Ca paleothermometer in planktic foraminifera. Paleoceanography and Paleoclimatology 34(12), 2005-2030.

Wanner, H. et al., 2008. Mid-to Late Holocene climate change: an overview. Quaternary Science Reviews 27(19-20), 1791-1828.
Marlowe, I T, Brassell, S.C., Eglinton, G. and Green, J.C., 1984a. Long chain unsaturated ketons and esters in living algae and marine sediments. Organic Geochemistry 6, 135–141.
Marlowe, I. T., 1984b. Long chain (n-C_{37}-C_{39}) alkenones in the prymnesiophyceae. distribution of alkenones and other lipids and their taxonomic significance. British Phycological Journal 19, 203–216.
Watanabe, T., Minagawa, M., Oba, T., Winter, A., 2001. Pretreatment of coral aragonite for Mg and Sr analysis: Implications for coral thermometers. Geochemical journal 35(4), 265-269.
Watanabe, T. et al., 2011. Permanent El Niño during the Pliocene warm period not supported by coral evidence. Nature 471(7337), 209-211.
Watanabe, T. K., Watanabe, T., Yamazaki, A., Pfeiffer, M., Claereboudt, M. R., 2019. Oman coral δ 18 O seawater record suggests that Western Indian Ocean upwelling uncouples from the Indian Ocean Dipole during the global-warming hiatus. Scientific reports 9(1), 1-9.
Volkman, J.K., Eglinton, G., Corner, E.D.S. and Forsberg, T.E.V., 1980a. Long-chain alkenes and alkenones in the marine coccolithophorid. Phytochemistry 19, 1–4.
Volkman, J. K., Eglinton, G., Corner, E.D.S. and Sargent, J.R., 1980b. Novel unsaturated straight-chain C37-C39 methyl and ethyl ketones in marine sediments and a coccolithophore Emiliania huxleyi. Physics and Chemistry of the Earth 12, 219–227.
Volkman, J.K., barrett, S.M., Blackburn, S.I. and Sikes, E.L., 1995. Alkenones in Gephyrocapsa oceanica: Implications for studies of paleoclimate. Geochimica et Cosmochimica Acta 59(3), 513-520.
Volkman, J.K., Burton, H.R., Everitt, D.A. and Allen, D.I., 1988. Pigment and lipid compositions of algal and bacterial communities in Ace Lake, Vestfold Hills, Antarctica. Hydrobiologia 165, 41–57.
Wang, R. and Zheng, M., 1998. Occurrence and environmental significance of long-chain alkenones in Tibetan Zabuye Salt Lake, SW China. International Journal of Salt Lake Research 6, 281–302.
Weijers, J. W., Schouten, S., Spaargaren, O. C., Damsté, J. S. S., 2006. Occurrence and distribution of tetraether membrane lipids in soils: Implications for the use of the TEX86 proxy and the BIT index. Organic Geochemistry 37(12), 1680-1693.
Zheng, Y., Huang, Y., Andersen, R.A. and Amaral-Zettler, L.A. 2016. Excluding the di-unsaturated alkenone in the UK37 index strengthens temperature correlation for the common lacustrine and brackish-water haptophytes. Geochimica et Cosmochimica Acta 175, 36–46.
Zink, K.G., Leythaeuser, D., Melkonian, M. and Schwark, L., 2001. Temperature dependency of long-chain alkenone distributions in Recent to fossil limnic sediments and in lake waters. Geochimica et Cosmochimica Acta 65, 253–265.

Chapter II-A

An, C.B., Tang, L., Barton, L., Chen, F.H., 2005. Climate change and cultural response around 4000 cal. yr B.P. in the western part of Chinese Loess Plateau. Quaternary Research 63, 347-352.

An, Z., 2000. Asynchronous Holocene optimum of the East Asian monsoon. Quaternary Science Reviews 19, 743–762.

Andersen, R.A., Kim, J.I., Tittley, I., Yoon, H.S., 2014. A re-investigation of Chrysotia (Prymnesiophyceae) using material collected from the type locality. Phycologia 53, 463-473.

Araie, H., 2018. Novel alkenone-producing strains of genus Isochrysis (Haptophyta) isolated from Canadian saline lakes show temperature sensitivity of alkenones and alkenoates. Organic Geochemistry 121, 89-103.

Atahan, P., Grice, K., Dodson, J., 2007. Agriculture and environmental change at Qingpu, Yangtze delta region, China: a biomarker, stable isotope and palynological approach. The Holocene 17,4, 507-515.

Bao, R., 2016. Widespread dispersal and aging of organic carbon in shallow marginal seas. Geology 44(10), 791-794.

Berkelhammer, M., 2012. An Abrupt Shift in the Indian Monsoon 4000 Years Ago. Geophysical Monograph Series 198, 75-87.

Bi, L. et al., 2017. Provenance study of the Holocene sediments in the Changjiang (Yangtze River) estuary and inner shelf of the East China sea. Quaternary International 441, 147-161.

Blanz, T., Emeis, K.C., Siegel, B., 2005. Controls on alkenone unsaturation ratios along the salinity gradient between the open ocean and the Baltic Sea. Geochimica et Cosmochimica Acta 69, 3589-3600.

Bollman, J., Baumann, K., Thierstein, H.R., 1998. Global dominance of gephyrocapsa coccoliths in the late Pleistocene: Selective dissolution, evolution, or global environmental change? Paleoceanography 13, 517-529.

Bond, G. et al., 2001. Persist Solar Influence on North Atlantic Climate During the Holocene. Science 294, 2130-2136.

Brassell, S.C., Eglinton, G., Marlowe, I.T., Pflaumann, U., Sarnthein, M., 1986. Molecular stratigraphy: a new tool for climatic assessment. Nature 320, 129-133.

Conte, M. H., 2006. Global temperature calibration of the alkenone unsaturation index (U^{K}_{37}') in surface waters and comparison with surface sediments. Geochemistry Geophysics Geosystems 7(2).

Conte, M.H., Thompson, A., Lesley, D., Harris, R.P., 1998. Genetic and physiological influences on the alkenone/alkenoate versus growth temperature relationship in Emiliania huxleyi and Gephyrocapsa oceanica. Geochimica et Cosmohimica Acta 62, 51-68.

Cook, E. R. et al., 2013. Tree-ring reconstructed summer temperature anomalies for temperate East Asia since 800 C.E. Climate Dynamics 41, 2957-2972.

Chang, K.C. The archaeology of ancient China (fourth edition), 1986. Yale University Press, 192-255.

Chapman, M.R., Shackleton, N.J., Zhao, M., Eglinton, G., 1996. Faunal and alkenone reconstructions of subtropical North Atlantic surface hydrography and paleotemperature over the last 28 kyr. Paleoceanography 11, 343-357.

Chen, F.H., Shi, Q., Wang, J.M., 1999. Environmental changes documented by sedimentation of Lake Yiema in arid China since the Late Glaciation. Journal of Paleolimnology 22, 159-169.
Chen, Z., Wang, Z., Schneiderman, J., Tao, J., Cai, Y., 2005. Holocene climate fluctuations in the Yangtze delta of eastern China and the Neolithic response. The Holocene 15, 915-924.
Chen, J. et al., 2017. Provenance discrimination of the clay sediment in the western Taiwan Strait and its implication for coastal current variability during the late-Holocene. The Holocene 27, 110-121.
Chu, G. et al., 2005. Long-chain alkenone distributions and temperature dependence in lacustrine surface sediments from China. Geochimica et Cosmohimica Acta 69, 4985-5003.
Clift, P.D., 2017. Cenozoic sedimentary records of climate-tectonic coupling in the Western Himalaya. Progress in Earth and Planetary Science 4, 39.
Cullen, H.M., 2000. Climate change and the collapse of the Akkadian empire: Evidence from the deep sea. Geology 28(4), 379-382.
deMenocal, P.B., 2005. Cultural Responses to Climate Change During the Late Holocene. Science 292, 667-673.
Drysdale, R., 2006. Late Holocene drought responsible for the collapse of Old World civilizations is recorded in an Italian cave flowstone. Geology 34(2), 101-104.
Fang, J., Liu, Z., Zhao, Y., 2018. High-resolution clay mineral assemblages in the inner shelf mud wedge of the East China Sea during the Holocene: Implications for the East Asian Monsoon evolution. Science China Earth Sciences 61(9), 1316-1329.
Fuller, D.Q., 2009. The Domestication Process and Domestication Rate in Rice: Spikelet Bases from the Lower Yangtze. Science 323, 1607-1610.
Haug, G.H. et al., 2003. Climate and the Collapse of Maya Civilization. Science 299, 1731-1735.
Hecht, H. and Oguchi, T., 2017. Global evaluation of erosion rates in relation to tectonics. Progress in Earth and Planetary Science 4(1), 40.
Herbert, T.D., 2001. Review of alkenone calibrations (culture, water column, and sediments). Geochemistry, Geophysics, Geosystems 2, 2000GC000055.
Hori, K., Saito, Y., Zhao, Q., Wang, P., 2002. Architecture and evolution of the tide-dominated Changjiang (Yangtze) river delta, China. Sedimentary Geology 146, 249-264.
Hong, Y. T., Hong, B., Shibata, Y., Hirota, M., Zhu, Y.X., Leng, X.T., Wang, Y., Wang, H., Yi, L., 2005. Inverse phase oscillations between the East Asian and Indian Ocean summer monsoons during the last 12000 years and paleo-El Ninõ. Earth and Planetary Science letters 231, 337-346.
Hu, J. and Wang, H., 2016. Progress on upwelling studies in the China seas. Review of Geophysics 54, 653-673.
Innes, J.B., Zong, Y., Wang, Z., Chen, Z., 2014. Climatic and palaeoecological changes during the mid- to Late Holocene transition in eastern China: high-resolution pollen and non-pollen palynomorph analysis at Pingwang, Yangtze coastal lowlands. Quaternary Science Reviews 99, 164-175.
IPCC Fifth Assessment Report, 2014. Cambridge: Cambridge University Press.

Itzstein-Davey, F., Athan, P., Dodson, J., Taylor, D., Zheng, H., 2007a. Environmental and cultural changes during the terminal Neolithic: Qingpu, Yangtze delta, eastern China. The Holocene 17, 7, 875-887.
Itzstein-Davey, F., Athan, P., Dodson, J., Taylor, D., Zheng, H., 2007b. A sediment-based record of Lateglacial and Holocene environmental changes from Guangfulin, Yangtze delta, eastern China. The Holocene 17, 8, 1221-1231.
Japan Meterological Agency publications. Available at: http://www.data.jma.go.jp/obd/stats/data/bosai/report/kanman/1993/1993.html (Accessed: October 2018)
Ji, J., Shen, J., Balsam, W., Chen, J., Liu, L., Liu, X., 2005. Asian monsoon oscillations in the northeastern Qinghai–Tibet Plateau since the late glacial as interpreted from visible reflectance of Qinghai Lake sediments. Earth and Planetary Science letters 233, 61-70.
Kajita, H. et al., 2017. Holocene sea surface temperature variations recorded in corals from Kikai Island, Japan. Geochemical Journal 51, e9-e14.
Kawahata, H., 2009. Changes of environments and human activity at the Sannai-Maruyama ruins in Japan during the mid-Holocene Hypsithermal climatic interval. Quaternary Science Reviews 28, 964-974.
Kawahata, H., 2017a. Climatic change and its influence on human society in western Japan during the Holocene. Quaternary International 440, 102-117.
Kawahata, H., Ishizaki, Y., Kuroyanagi, A., Suzuki, A., Ohkushi, K., 2017b. Quantitative reconstruction of temperature at a Jōmon site in the Incipient Jōmon Period in northern Japan and its implications for the production of early pottery and stone arrowheads. Quaternary Science Reviews 157, 66-79.
Kim, A.H., Lee, K.E., Bae, S.W., 2015. Sea surface temperature proxies (alkenones, foraminiferal Mg/Ca, and planktonic foraminiferal assemblage) and their implications in the Okinawa Trough. Progress in Earth and Planetary Science 2, 43.
Kubota, Y., Tada, R., Kimoto, K., 2015. Changes in East Asian summer monsoon precipitation during the Holocene deduced from a freshwater flux reconstruction of the Changjiang (Yangtze River) based on the oxygen isotope mass balance in the northern East China Sea. Climate of the Past 11, 265-281.
Lambeck, K., Rouby, H., Purcell, A., Sun, Y., Sambridge, M., 2014. Sea level and global ice volumes from the Last Glacial Maximum to the Holocene. Proceedings of the National Academy of Sciences 111, 15296-15303.
Li, Y. et al., 2010. Palaeoecological records of environmental change and cultural development from the Liangzhu and Qujialing archaeological sites in the middle and lower reaches of the Yangtze River. Quaternary International 277, 29-37.
Liu, B., 2017. Earliest hydraulic enterprise in China, 5,100 years ago, Proceedings of the National Academy of Sciences 144 (52), 13637-13642.
Liu, J.P., Milliman, J.D., Gao, S., Cheng, P., 2004. Holocene development of the Yellow River's subaqueous delta, North Yellow Sea. Marine Geology 209, 45-67.
Liu, J.P. et al., 2007. Flux and fate of Yangtze River sediment delivered to the East China Sea. Geomorphology 85, 208-224.
Liu, K.B., Sun, S., Jiang, X., 1992. Environmental Change in the Yangtze River Delta since 12,000 Years B.P. Quaternary Research 38, 32-45.

Liu, Y. et al., 2016. Pollen evidence to interpret the history of rice farming at the Hemudu site on the Ningshao coast, eastern China. Quaternary international 426, 195-203.
Locarnini, R. A. et al., 2013. *World Ocean Atlas 2013, Volume 1: Temperature.* S. Levitus, Ed., A. Mishonov Technical Ed.; NOAA Atlas NESDIS 73, 40 pp.
Ma, C., Zhu, C., Zheng, C., Qian, Y., Zhao, Z., 2009. Climate changes in East China since the Late-glacial inferred from high-resolution mountain peat humification records. Science in China Series D-Earth Science 52, 118-131.
Maeda, L., Kawahata, H., Nohara, M., 2002. Fluctuation of biogenic and abiogenic sedimentation on the Shatsky Rise in the western North Pacific during the late Quaternary. Marine Geology 189, 197-214.
Mann, M.E. et al., 2009. Global Signatures and Dynamical Origins of the Little Ice Age and Medieval Climate Anomaly. Science 326, 1256-1260.
Marlowe, I.T., et al., 1984. Long chain (n-C37–C39) alkenones in the Prymnesiophyceae. Distribution of alkenones and other lipids and their taxonomic significance. Organic Geochemistry 6, 135-141.
Mayewski, P.A. et al., 2004. Holocene climate variability. Quaternary Research 62, 243-255.
Meyers, P.A., 1994. Preservation of elemental and isotopic source identification of sedimentary organic matter. Chemical Geology 114, 289-302.
Milliman, J.D., Huang-ting, S., Sheng, Y.Z., Meade, R.H., 1985. Transport and deposition of river sediment in the Changjiang estuary and adjacent continental shelf. Continental Shelf Research 4, 37-45.
Muller, P. J., kirst, G., Ruhland, G., Storch, I. V., Rosell-Melé, A., 1998. Calibration of the alkenone paleotemperature index U^{k}_{37}' based on core-tops from the eastern South Atlantic and the global ocean (60°N-60°S). Geochimica et Cosmohimica Acta 62, 1757-1772.
Nakamura, A., 2016. Weak monsoon event at 4.2 ka recorded in sediment from Lake Rara, Himalayas. Quaternary International 397, 349-359.
Nakamura, H., Sawada, K., Araie, H., Suzuki, I., Shiraiwa, Y., 2014. Long chain alkenes, alkenones and alkenoates produced by the haptophyte alga Chrysotila lamellosa CCMP1307 isolated from a salt marsh. Organic Geochemistry 66, 90-97.
Nagashima, K., Tada, R., Toyoda, S., 2013. Westerly jet-East Asian summer monsoon connection during the Holocene. Geochemistry, Geophysics, Geosystems 14.
Ohkouchi, N., Kawamura, K., Kawahata, H., Okada, H., 1999. Depth ranges of alkenone production in the central Pacific Ocean. Global Biochemical Cycles 13, 695-704.
Ohkouchi, N., Xu, L., Reddy, C. M., Montlucon, D., Eglinton, T. I., 2005. Radiocarbon dating of alkenones from marine sediments: I. Isolation protocol. Radiocarbon 47, 401-412.
Prahl, F.G., Muehlhausen, L.A., Zahnle, D.L., 1988. Further evaluation of long-chain alkenones as indicators of paleoceanographic conditions. Geochimica et Cosmochimica Acta 52, 2303-2310.
Ramsey, C.B. and Lee, S., 2013. Recent and planned developments of the program Oxcal, 2013. Radiocarbon 55, 720-730.

Reimer, P.J. et al., 2013. INTCAL13 AND MARINE13 RADIOCARBON AGE CALIBRATION CURVES 0–50,000 YEARS CAL BP. Radiocarbon 55, 1869-1887.
Reymonds, R. W. et al., 2007. Daily high-resolution-blended analysis for sea surface temperature. Journal of Climate 20, 5473-5496. (Available at: http://iridl.ldeo.columbia.edu/)
Rosell-Melé, A., 1998. Interhemispheric appraisal of the value of alkenone indices as temperature and salinity proxies in high-latitude locations. Paleoceanography 13, 694-703.
Saito, K. et al., 2017. ESR signal intensity of quartz in the fine-silt fraction of riverbed sediments from the Yangtze River: a provenance tracer for suspended particulate matter. Progress in Earth and Planetary Science 4:4 Doi.org/10.1186/s40645-017-0118-9.
Schulz, H.M., Schöner, A., Emeis, K.C., 2000. Long-chain alkenone patterns in the Baltic Sea – an ocean – freshwater transition. Geochimica et Cosmochimica Acta 64, 469-477.
Self, S., Zhao, J., Holasek, R. E., Torres, R. C., King, A. J., 2013. The Atmospheric Impact of the 1991 Mount Pinatubo. NASA/CR-93-207274, NAS 1.26:207274, SOEST-Contrib-3563, 1089-1115.
Shao, J. Q., 2012. Sedimentological Records of the Changjiang Sediment and its paleoenvironment Response in the East China Sea During the Holocene. MSc thesis, Tongji University, Shanghai, China. (in Chinese with English abstract)
Stanley, D.J., Chen, Z., Song, J., 1999. Inundation, Sea-Level Rise and Transition from Neolithic to Bronze Age Cultures, Yangtze Delta, China. Geoarchaeology 14, 15-26.
Stanley, D.J., Krom, M.D., Cliff, B.A., Woodward, J.C., 2003. Short Contribution: Nile Flow Failure at the End of the Old Kingdom, Egypt: Strontium Isotopic and Petrologic Evidence. Geoarchaeology 18(3), 395-402.
Staubwasser, M., Sirocko, F., Grootes, P.M., Segl, M., 2003. Climate change at the 4.2 ka BP termination of the Indus valley civilization and Holocene south Asian monsoon variability. Geophysical research letters 30(8), 1425, doi:10.1029/2002GL016822.
Sun, Q., Chu, G., Liu, G., Li, S., Wang, X., 2007. Calibration of alkenone unsaturation index with growth temperature for a lacustrine species, Chrysotila lamellose (Haptophyceae). Organic Geochemistry 38, 1226-1234.
Sugihara, Y., 1991. The Influence of Climatic Variation on the Climatic Productivity of Paddy Rice. Journal of Geology 100(6), 851-868.
Tada and Murray, 2016. Preface for the article collection “Land-Ocean Linkages under the Influence of the Asian Monsoon”. Progress in Earth and Planetary Science 3, 24.
Tada, R., Zheng, H., Clift, Peter D., 2016. Evolution and variability of the Asian monsoon and its potential linkage with uplift of the Himalaya and Tibetan Plateau. Progress in Earth and Planetary Science 3, 4.
Tanaka, Y., 2003. Coccolith fluxes and species assemblages at the shelf edge and in the Okinawa Trough of the East China Sea. Deep-Sea Research II 50, 503-511.

Tao, J., Chen, M., Xu, S., 2006. A Holocene environmental record from the southern Yangtze River delta, eastern China. Palaeogeography, Palaeoclimatology, Palaeoecology 230, 204-229.
Tao, S. et al., 2012. Alkenone distribution in surface sediments of the southern Yellow Sea and implications for the U^{K}_{37}' thermometer. Geo-Marine Letters 32, 61-71.
Ujiié, Y., Ujiié, H., Taira, A., Nakamura, T., Oguri, K., 2003. Spatial and temporal variability of surface water in the Kuroshio source region, Pacific Ocean, over the past 21,000 years: evidence from planktonic foraminifera. Marine Micropaleontology 49, 335-364.
Versteegh, G.J.M., Riegman, R., de Leeuw, J.W., Jensen, J.H.F., 2001. U^{K}_{37}' values for Isochrysis galbana as a function of culture temperature, light intensity and nutrient concentrations. Organic Geochemistry 32, 785-794
Volkman, J.K., Eglinton, G., Corner, E.D., Sargent J.R., 1980. Novel unsaturated straight-chain C37-C39 methyl and ethyl ketones in marine sediments and a coccolithophore Emiliania huxleyi. Physics and Chemistry of the Earth 12, 219-227.
Walker, M.J.C. et al., 2012. Formal subdivision of the Holocene Series/Epoch: a Discussion Paper by a Working Group of INTIMATE (Integration of ice-core, marine and terrestrial records) and the Subcommission on Quaternary Stratigraphy (International Commission on Stratigraphy). Journal of Quaternary Science 27, 649-659.
Wang, K. et al., 2014. Millennial-scale East Asian Summer Monsoon variability recorded in grain size and provenance of mud belt sediments on the inner shelf of the East China Sea during mid-to late Holocene. Quaternary International 349, 79-89.
Wang, L. et al., 2011. Sea surface temperature records of core ZY2 from the central mud area in the South Yellow Sea during last 6200 years and related effect of the Yellow Sea Warm Current. Chinese science Bulletin 56, 1588-1595.
Wang, P. and Zheng, D. Recent Studies of the Reconstruction of East Asian Monsoon Climate in the Past using historical literature of China, 1992. Journal of the Meteorological Society of Japan 70, 423-446.
Wang, X. et al., 2017. Environmental changes and human activities at a fortified site of the Liangthu culture in eastern China: Evidence from pollen and charcoal records. Quaternary International 438, 189-197.
Wang, Y. et al., 2005. The Holocene Asian Monsoon: Links to Solar Changes and North Atlantic Climate. Science 308, 854-857.
Wang, Z. et al., 2018. Middle Holocene marine flooding and human response in the south Yangtze coastal plain, East China. Quaternary Science Reviews 187, 80-93.
Wei, G., Tang, D., Wang, S., 2013. Distribution of chlorophyll and harmful algal blooms (HABs): A review on space based studies in the coastal environments of Chinese marginal seas. Advances in Space Research 41, 12-19.
Wen, R., 2010. Holocene precipitation and temperature variations in the East Asian monsoonal margin from pollen data from Hulun Lake in northeastern Inner Mongolia, China. Boreas 32, 262-272.
Wessel, P. and Smith, W.H.F., 1998. New, improved version of Generic Mapping Tools released, EOS Transactions American Geophysical Union 79(47), 579.

Wu, W. and Liu, T., 2004. Possible role of the ‘‘Holocene Event 3’’ on the collapse of Neolithic Cultures around the Central Plain of China. Quaternary International 117, 153-166.
Xiang, R. et al., 2007. Paleoenvironmental change in the middle Okinawa Trough since the last deglaciation: Evidence from the sedimentation rate and planktonic foraminiferal record. Palaeogeography, Palaeoclimatorogy, Palaeoecology 243, 378-393.
Xiao, J., et al., 2004. Holocene vegetation variation in the Daihai Lake region of north-central China: a direct indication of the Asian monsoon climatic history. Quaternary Science Reviews 23, 1669-1679.
Xing, L., 2013. Holocene Temperature Records from the East China Sea Mud Area Southwest of the Cheju island Reconstructed by the U^{K}_{37}’ and TEX_{86} Paleothermometers. Journal of Ocean University of China 12(4), 599-604.
Wessel, P. and Smith, W.H.F., 1998. New, improved version of Generic Mapping Tools released, EOS Transactions American Geophysical Union 79(47), 579.
Yang, B., Braeuning, A., Johnson, K.R., Yafeng, S., 2002. General characteristics of temperature variation in China during the last two millennia. Geophysical Research letters 29, 1324.
Yang, D., Yin, B., Sun, J., Zhang, Y. Numerical study on the origins and the forcing mechanism of the phosphate in upwelling areas off the coast of Zhejiang province, China in summer. Journal of Marine Systems 123-124, 1-18.
Yang, S., Bi, L., Li, C., Wang, Z., Dou, Y., 2015. Major sinks of the Changjiang (Yangtze River)-derived sediments in the East China Sea during the late Quaternary. River-Dominated Shelf Sediments of East Asian Seas, Geological Society, London, Special publications, 429.
Yang, T.N., 2004. Summer and winter distribution and malformation of coccolithophores in the East China Sea. Micropaleontology 50, 157-170.
Yasuda, Y., 2004. Environmental archaeology at the Chengtoushan site, Hunan Province, China, and implications for environmental change and the rise and fall of the Yangtze River civilization. Quaternary International 123-125, 149-158.
Yu, S., Zhu, C., Song, J., Qu, W., 2000. Role of climate in the rise and fall of Neolithic cultures on the Yangtze delta. Boreas 29, 157-165.
Yuan, Z., 2018. Spatiotemporal temperature variations in the East China Sea shelf during the Holocene in response to surface circulation evolution. Quaternary International 482, 46-55.
Zhang, Q., Zhu, C., Liu, T., Jiang, T., 2005. Environmental change and its impacts on human settlement in the Yangtze Delta, P.R. China. Catena 60, 267-277.
Zhao, M., Ding, L., Xing, L., Qiao, S., Yang, Z., 2014. Major Mid-Late Holocene Cooling in the East China Sea Revealed by an Alkenone Sea Surface Temperature Record. Journal of Ocean University of China 13, 935-940.
Zheng, Y., Kissel, C., Zheng, H.B., Laj, C., Wang, K., 2010. Sedimentation on the inner shelf of the East China Sea: Magnetic properties, diagenesis and paleoclimate implications. Marine Geology 268, 34-42.
Zheng, Y. et al., 2009. Rice fields and modes of rice cultivation between 5000 and 2500 BC in east China. Journal of Archaeological Science 36, 2609-2616.
Zong, Y. et al., 2007. Fire and flood management of coastal swamp enabled first rice paddy cultivation in east China, Nature 449, 459-462.

Zong, Y., Innes, J.B., Wang, Z., Chen, Z., 2011. Mid-Holocene coastal hydrology and salinity changes in the east Taihu area of the lower Yangtze wetlands, China. Quaternary Research 76, 69-82.
Zhu, C. et al., 2011. Characterizing the depositional settings for sedimentary organic matter distributions in the Lower Yangtze River-East China Sea Shelf System. Estuarine, Coastal and Shelf Science 93, 182-191.
Zweng, M.M., et al., 2013. World Ocean Atlas 2013, Volume 2: Salinity. S. Levitus, Ed., A. Mishonov Technical Ed.; NOAA Atlas NESDIS 74, 39 pp.

Chapter II-B

Anchukaitis, K.J., Buckley, B.M., Cook, E.R., Cook, B.I., D'Arrigo, R.D., Ammann, C.M., 2010. Influence of volcanic eruptions on the climate of the Asian monsoon region. Geophysical Research Letteers 37, 1–5.
Aono, Y., Saito, S., 2010. Clarifying springtime temperature reconstructions of the medieval period by gap-filling the cherry blossom phenological data series at Kyoto, Japan. International Journal of Biometeorology 54, 211–219.
Araie, H., et al., 2018. Novel alkenone-producing strains of genus Isochrysis (Haptophyta) isolated from Canadian saline lakes show temperature sensitivity of alkenones and alkenoates. Organic Geochemistry 121, 89–103.
Bard, B.E., Raisbeck, G., 2000. Solar irradiance during the last 1200 years based on cosmogenic nuclides. Tellus 52B, 985–992.
Bendif, E.M., et al., 2014. Genetic delineation between and within the widespread coccolithophore morpho-species Emiliania huxleyi and Gephyrocapsa oceanica (Haptophyta). Journal of Phycology 50, 140–148.
Bendif, E.M., Probert, I., Young, J.R., von Dassow, P., 2015. Morphological and Phylogenetic Characterization of New Gephyrocapsa Isolates Suggests Introgressive Hybridization in the Emiliania/Gephyrocapsa Complex (Haptophyta). Protist 166, 323–336.
Bendle, J., Rossell-Melé, A., Ziveri, P., 2005. Variability of unusual distributions of alkenones in the surface waters of the Nordic seas. Paleoceanography 20, PA2001.
Berkelhammer, M., 2012. An abrupt shift in the Indian Monsoon 4 , 000 years ago. Climates, Landscapes, and Civilizations 75–87.
Bond, G., 2001. Persistent solar influence on North Atlantic climate during the Holocene. Science 294, 2130–2136.
Brassell, S., Eglinton, G., Marlowe, I., Pflaumann, U.P., Sarnthein, M., 1986. Molecular stratigraphy: a new tool for climatic assessment. Nature 320, 129–133.
Büntgen, U., et al., 2016. Cooling and societal change during the Late Antique Little Ice Age from 536 to around 660 AD. Nature Geoscience 9, 231–236.
Carolin, S.A. et al., 2019. Precise timing of abrupt increase in dust activity in the Middle East coincident with 4.2 ka social change. Proceedings of National Academy of Science 116, 67–72.
Cho, H. Y. and Lee, K. H., 2012. Development of an air-water temperature relationship model to predict climate-induced future water temperature in estuaries. Journal of Environmental Engineering, 138(3), 171–176.
Chu, G., et al., 2005. Long-chain alkenone distributions and temperature dependence

in lacustrine surface sediments from China. Geochimica et Cosmochimica Acta 69, 4985–5003.
Conte, M.H., Thompson, A., Lesley, D., Harris, R.P., 1998. Genetic and physiological influences on the alkenone/alkenoate versus growth temperature relationship in *Emiliania huxleyi* and *Gephyrocapsa oceanica.* Geochimica et Cosmochimica Acta 62, 51–68.
Cook, E.R. et al., PAGES Asia 2k Members, 2013. Tree-ring reconstructed summer temperature anomalies for temperate East Asia since 800 C.E. Climate Dynamics 41, 2957–2972.
Crema, E.R., Habu, J., Kobayashi, K., Madella, M., 2016. Summed Probability Distribution of ^{14}C Dates Suggests Regional Divergences in the Population Dynamics of the Jomon Period in Eastern Japan. PLoS One 11, 1–18.
Desprat, S., Sánchez Goni, M.F., Loutre, M.F., 2003. Revealing climatic variability of the last three millennia in northwestern Iberia using pollen influx data. Earth and Planetary Science Letters 213, 63–78.
Emile-Geay, J., Seager, R., Cane, M.A., Cook, E.R., Haug, G.H., 2008. Volcanoes and ENSO over the past millennium. Journal of Climate 21, 3134–3148.
Esper, J., Cook, E.R., Schweingruber, F.H., 2002. Low-Frequency Signals in long Tree-Ring Chronologies for Reconstructing Past Temperature Variability. Science 295, 2250-2253.
Fröhlich, C., 2006. Solar irradiance variability since 1978: Revision of the PMOD composite during solar cycle 21, Space Science Reviews 125, 53–65.
Gao, C., Robock, A., Ammann, C., 2008. Volcanic forcing of climate over the past 1500 years: An improved ice core-based index for climate models. Journal of Geophysical Research. Atmos. 113, 1–15.
Gray, L.J., et al., 2010. SOLAR INFLUENCES ON CLIMATE. Reviews of Geophysics 48, RG4008.
Habu, J., 2004. Ancient Jomon of Japan. Cambridge University Press, UK, pp. 1–332.
Hall, J.W., 1993. The Cambridge History of Japan. Cambridge University Press, Cambridge, 1–6.
Haneda, Y., Okada, M., Kubota, Y., Suganuma, Y., 2020. Millennial-scale hydrographic changes in the northwestern Pacific during marine isotope stage 19: Teleconnections with ice melt in the North Atlantic. Earth and Planetary Science Letters 534, 116107.
Harada, N., Shin, K.H., Murata, A., Uchida, M., Nakatani, T., 2003. Characteristics of alkenones synthesized by a bloom of emiliania huxleyi in the Bering Sea. Geochimica et Cosmochimica Acta 67, 1507–1519.
Hatori, 1984. Behavior of the Tokai Tsunamis of 1707 and 1854 in the Kanto and East Izu Districs. Bulletin of the Earthquake Research Institute 59, 501–518 (in Japanese with English abstract).
Hatori, T., 2006. Behaviors of the 1703 Genroku Kanto, the 1854 Ansei Tokai and Other Tsunamis along the Coast of the Tokyo Bay to Uraga Strait. Historical Earthquakes 21, 37–45 (in Japanese with English abstract).
Hattori, A., 1983. Oceanographic features of Tokyo Bay -Water circulation, hydrography, and nutrient supply: an overview-, Geochemistry 17, 16–26 (in Japanese).
Helama, S., Jones, P.D., Briffa, K.R., 2017. Dark Ages Cold Period: A literature

review and directions for future research. The Holocene 27, 1600–1606.
Herbert, T.D., 2001. Review of alkenone calibrations (culture, water column, and sediments). Geochemistry, Geophysics, Geosystems 2.
Ineson, S. et al., 2015. Regional climate impacts of a possible future grand solar minimum. Nature Communications 6, 1–8.
Ineson, S., Scaife, A.A., Knight, J.R., Manners, J.C., Dunstone, N.J., Gray, L.J., Haigh, J.D. Solar forcing of winter climate variability in the Northern Hemisphere. Nature Geoscience 4, 753–754.
IPCC Fifth Assessment Report (AR5), 2014. Cambridge: Cambridge University Press.
Isono, D., 2009. The 1500-year climate oscillation in the midlatitude North Pacific during the Holocene. Geology 37(7), 591–594.
Ji, J., Shen, J., Balsam, W., Chen, J., Liu, L., Liu, X., 2005. Asian monsoon oscillations in the northeastern Qinghai–Tibet Plateau since the late glacial as interpreted from visible reflectance of Qinghai Lake sediments. Earth and Planetary Science Letters 233, 61–70.
Kaiser, J., 2019. Changes in long chain alkenone distributions and Isochrysidales groups along the Baltic Sea salinity gradient. Organic Geochemistry 127, 92–103.
Kawahata, H., 2019. Climatic reconstruction at the Sannai-Maruyama site between Bond events 4 and 3 –implication for the collapse of the society at 4.2 ka event. Progress in Earth and Planetary Science 6, 63.
Kawahata, H. et al., 2017. Climatic change and its influence on human society in western Japan during the Holocene. Quatanary International 440, 102–117.
Kawahata, H. et al., 2009. Changes of environments and human activity at the Sannai-Maruyama ruins in Japan during the mid-Holocene Hypsithermal climatic interval. Quatanary Science Reviews 28, 964–974.
Kawakubo, Y., Alibert, C., Yokoyama, Y., 2017. A Reconstruction of Subtropical Western North Pacific SST Variability Back to 1578, Based on a *Porites* Coral Sr/Ca Record from the Northern Ryukyus, Japan. Paleoceanography 32, 1352–1370.
Kida, S. et al., 2016. Oceanic fronts and jets around Japan: a review. In: Nakamura, H., Isobe, A., Minibe, S., Mitsudera, H., Nonaka, M., Suga, T. (Eds.), “Hot Spots” in the Climate System. Springer Japan, 1–30.
Kito, H., 2000. Jinkou kara yomu Nihon no rekishi (History of Japan, Based on the Population). Koudansya Publishers, Tokyo, pp. 1–283 (in Japanese).
Kobashi, K., 2017. Climate variation, and famines proto-Japanese “Wajin” met. The Archaeological Journal 696, 19–23 (in Japanese).
Kobayashi, S., et al., 2015. The JRA-55 Reanalysis: General Specifications and Basic Characteristics. Journal of Meteorological Society of Japan. Ser. II 93, 5–48.
Komori, J., Shishikura, M., Ando, R., Yokoyama, Y., Miyairi, Y., 2017. History of the great Kanto earthquakes inferred from the ages of Holocene marine terraces revealed by a comprehensive drilling survey. Earth and Planetary Science Letters 471, 74-84.
Lambeck, K., Rouby, H., Purcell, A., Sun, Y., Sambridge, M., 2014. Sea level and global ice volumes from the Last Glacial Maximum to the Holocene. Proceedings of Natiional Acadademy of Science 111, 15294–15303.

Laskar, J., Robutel, P., Joutel, F., Gastineau, M., Correia, A.C.M., Levrard, B., 2004. A long-term numerical solution for the insolation quantities of the Earth. Astronomy and Astrophysics 428, 261–285.
Lean, J., Rottman, G., Harder, J., Kopp, G., 2005. Sorce contributions to new understanding of global change and solar variability. Solar Physics 230, 27–53.
Li, J., Dodson, J. et al., 2017. Quantifying climatic variability in monsoonal northern China over the last 2200 years and its role in driving Chinese dynastic changes. Quatanary Science Reviews 159, 35–46.
Ljungqvist, F.C., 2010. A new reconstruction of temperature variability in the extra-tropical northern hemisphere during the last two millennia. Geografiska Annaler Series A *Physical Geography* 92, 339–351.
Longo, W.M. et al., 2018. Widespread occurrence of distinct alkenones from Group I haptophytes in freshwater lakes: Implications for paleotemperature and paleoenvironmental reconstructions. Earth and Planetary Science Letters 492, 239–250.
Longo, W.M. et al., 2016. Temperature calibration and phylogenetically distinct distributions for freshwater alkenones: Evidence from northern Alaskan lakes. Geochimica et Cosmochimica Acta, 180, 177–196.
Mann, M.E. et al., 2009. Medieval Climate Anomaly. Science 326, 1256–1260.
Marcott, S.A., Shakun, J.D., Clark, P.U., Mix, A.C., 2013. A reconstruction of regional and global temperature for the past 11,300 years. Science 339, 1198–1201.
Marlowe, I.T., Green, J.C., Neal, A.C., Brassell, S.C., Eglinton, G., Course, P.A., 1984. Long chain (n-C_{37}-C_{39}) alkenones in the prymnesiophyceae. Distribution of alkenones and other lipids and their taxonomic significance. British Physiological Journal 19, 203–216.
Martin-Puertas, C. et al., 2012. Regional atmospheric circulation shifts induced by a grand solar minimum Nature 5, 397–401.
Matsui, A., Kanehara, M., 2006. The question of prehistoric plant husbandary during the Jomon Period in Japan. World Archaeology 38(2), 259–273.
Matsushima, Y., 1979. Littoral molluscan assemblages during the Post-glacial Jomon Transgression in the southern Kanto, Japan. The Quaternary Research 17, 243–265 (in Japanese with English abstract).
Matsushima, Y., 2006. Jomon transgression deduced from shell deposits. Yurindo Yokohama 1–216 (in Japanese).
Matsumoto, E., 1983. The sedimentary environment in the Tokyo Bay. Geochemistry 17, 27–32 (in Japanese with English abstract).
Mayewski, P.A. et al., 2004. Holocene climate variability. Quatanary Research 62, 243–255.
Meehl, G.A., Arblaster, J.M., Matthes, K., Sassi, F., van Loon, H.,2009. Amplifying the Pacific Climate System Response to a Small 11-Year Solar Cycle Forcing. Science 325, 1114–1118.
Mehrotra, N., Shah, S.K., Basavaiah, N., Laskar, A.H., Yadava, M.G., 2019. Resonance of the '4.2ka event' and terminations of global civilizations during the Holocene, in the palaeoclimate records around PT Tso Lake, Eastern Himalaya. Quatanary International 507, 206–216.
Mercer, J., Zhao, M., Colman, S.M., 2005. Seasonal variations of alkenones and U^{K}_{37} in the Chesapeake Bay water column. Estuarine, Coastal and Shelf Science 63,

675–682.
Müller, P.J., Kirst, G., Ruhland, G., Von Storch, I., Rosell-Melé, A., 1998. Calibration of the alkenone paleotemperature index U37K based on core-tops from the eastern South Atlantic and the global ocean (60°N-60°S). Geochimica et Cosmochimica Acta 62, 1757–1772.
Murasugi, J., Satake, K., Isobe, T., Harada, T., 2015. Re-examination of Tsunami Damage in Tokyo Bay from the 1703 Genroku Kanto Earthquake. Historical Earthquakes 30, 149–157 (in Japanese with English abstract).
Nakamura, H., Sawada, K., Araie, H., Suzuki, I., Shiraiwa, Y., 2014. Long chain alkenes, alkenones and alkenoates produced by the haptophyte alga Chrysotila lamellosa CCMP1307 isolated from a salt marsh. Organic Geochemistry 66, 90–97.
Nakata, T., Koba, M., Imaizumi, T., Jo, W.R., Matsumoto, H., Suganuma, T., 1980. Holocene marine terraces and seismic crustal movements in the southern part of Boso peninsula, Kanto, Japan. Geographical Review of Japan 53(1), 29–29 (in Japanese with English abstract).
Nogami, M., 2014. Taupo eruption and disorder of Wa country caused by famine at the end of 2nd century. Proceedings of the General Meeting of the Association of Japanese Geographers, 2014(0), 100009.
Oba, T., Irino, T., Yamamoto, M., Murayama, M., Takamura, A., Aoki, K., Paleoceanographic change off central Japan since the last 144,000 years based on high-resolution oxygen and carbon isotope records. Global Planetary Change 53, 5–20.
Oba, T., Murayama, M. Sea-surface temperature and salinity changes in the northwest Pacific since the Last Glacial Maximum. Journal of Quaternary Research 19(4), 335–346.
Ohkouchi, N., Kawamura, K., Kawahata, H., 1999. Distributions of three- to seven-ring polynuclear aromatic hydrocarbons on the deep sea floor in the central pacific. Environmental Science and Technology 33, 3086–3090.
Ohkouchi, N., Xu, L., Reddy, C.M., Montlucon, D., Eglinton, T.I., 2005. Radiocarbon dating of alkenones from marine sediments: I. Isolation protocol. Radiocarbon 47, 401–412.
Ono, M. Sawada, K., Kubota, M., Shiraiwa, Y., 2009. Change of the unsaturation degree of alkenone and alkenoate during acclimation to salinity change in Emiliania huxleyi and Gephyrocapsa oceanica with reference to palaeosalinity indicator. Res. Organic Geochemistry 25, 53–60.
Patterson, W.P., Dietrich, K.A., Holmden, C., Andrews, J.T., 2010. Two millennia of North Atlantic seasonality and implications for Norse colonies. Proceedings of National Academy of Science 107, 5306–5310.
Prahl, F.G., Muehlhausen, L.A., Zahnle, D.L., 1988. Further evaluation of long-chain alkenones as indicators of paleoceanographic conditions. Geochimica et Cosmochimica Acta 52, 2303–2310.
Ran, M., Chen, L., 2019. The 4.2 ka BP climatic event and its cultural responses. Quatanary International 521, 158–167.
Ramsey, C.B., 2008. Deposition models for chronological records. Quaternary Science Reviews 27, 42–60.
Ramsey, C.B., Lee, S., 2013. Recent and planned developments of the program Oxcal, 2013. Radiocarbon 55, 720-730.

Raymond, S.B., Philip, D.J., 1993. Little Ice Age summer temperature variations: their nature and relevance to recent global warming trends. The Holocene 3,4, 367-376.
Reimer, P.J. et al., 2013. INTCAL13 AND MARINE13 RADIOCARBON AGE CALIBRATION CURVES 0-50,000 YEARS CAL BP. Radiocarbon 55, 1869-1887.
Reynolds, R.W., Smith, T.M., Liu, C., Chelton, D.B., Casey, K.S., Schlax, M.G., 2007. Daily high-resolution-blended analysis for sea surface temperature. Journal of Climate 20, 5473–5496.
Robock, A., 2000. Volcanic eruptions and climate. Reviews of Geophysics 38, 191–219.
Sakaguchi Y., 1983. Warm and Cold Stages in the Past 7600 Years in Japan and their Global Correlation. Bulletin of the Department of Geography University of Tokyo 15, 1–31.
Salacup, J.M., Farmer, J.R., Herbert, T.D., Prell, W.L., 2019. Alkenone Paleothermometry in Coastal Settings: Evaluating the Potential for Highly Resolved Time Series of Sea Surface Temperature. Paleoceanography and Paleoclimatology 34, 164–181.
Sano, T., Fukuoka, T., Ishino, M., 2011. Petrological Constrains on Magma Evolution of the Fuji Volcano: A Case Study for the 1707 Hoei Eruption. Memoirs of the National *Science* Museum, Tokyo 47, 471–496.
Sasaki, J.et al., 2012. Behavior of the 2011 Tohoku earthquake tsunami and resultant damage in Tokyo Bay. Coastal Engineering Journal 54, 1250012.
Sawada, K., Handa, N., Shiraiwa, Y., Danbara, A., Montani, S., 1996. Long-chain alkenones and alkyl alkenoates in the coastal and pelagic sediments of the northwest north Pacific, with special reference to the reconstruction of Emiliania huxleyi and Gephyrocapsa oceanica ratios. Organic Geochemistry 24, 751–764.
Shibayama, T., Ohira, K., Takabatake, T., 2013. Present and future tsunami and storm surge protections in Tokyo and Sagami Bays. Proceedings of the 7th International Conference on Asian and Pacific Coasts, 24–26.
Shishikura, M., Echigo, T., Kaneda, H., 2007. Marine reservoir correction for the Pacific coast of central Japan using ^{14}C ages of marine mollusks uplifted during historical earthquakes. Quatanary Reserach. 67, 286–291.
Sigl, M. et al., 2015. Timing and climate forcing of volcanic eruptions for the past 2,500 years. Nature 523, 543–549.
Solanki, S.K., Usoskin, I.G., Kromer, B., Schüssler, M., Beer, J., 2004. Unusual activity of the Sun during recent decades compared to the previous 11 , 000 years. Nature 431, 1084–1087.
Steinhilber, F. et al., 2012. 9,400 years of cosmic radiation and solar activity from ice cores and tree rings. Proceedings of National Academy of Science 109, 5967–5971.
Steinhilber, F., Beer, J., Fro, C., 2009. Total solar irradiance during the Holocene Geophysical Research Letters 36, 1–5.
Suganuma, Y. et al., 2018. Paleo-climatic and paleoceanographic records of Marine Isotope Stage 19 at the Chiba composite section, central Japan: a reference for the Early-Middle Pleistocene boundary. Quatanary Science Reviews 191, 406–430.

Sun, Q. et al., 2019. Climate as a factor for Neolithic cultural collapses approximately 4000 years BP in China. Earth-Science Reviews 197, 102915.
Tanabe, S., 2019. Formation mechanisms of the post-LGM incised-valley fills beneath the Tokyo and Nakagawa lowlands, central Japan. The journal of the geological society of Japan 125, 55–72. https://doi.org/10.5575/geosoc.2018.0021 (in Japanese with English abstract).
Tao, S. et al., 2012. Alkenone distribution in surface sediments of the southern Yellow Sea and implications for the $U^{K'}_{37}$ thermometer. Geo-Marine Letters 32, 61–71.
Usoskin, I.G., Solanki, S.K., Kovaltsov, G.A., 2007. Grand minima and maxima of solar activity : new observational constraints. Astronomy and Astrophysics 309, 301–309.
van Geel, B. et al., 2004. Climate change and the expansion of the Scythian culture after 850 BC: A hypothesis. Journal of Archaeological Science 31, 1735–1742.
Vieira, L.E.A., Solanki, S.K., Krivova, N.A., Usoskin, I., 2011. Evolution of the solar irradiance during the Holocene. Astronomy and Astrophysics 6, 1–20.
Walker, M.J.C. et al., 2012. Formal subdivision of the Holocene Series/Epoch: A Discussion Paper by a Working Group of INTIMATE (Integration of ice-core, marine and terrestrial records) and the Subcommission on Quaternary Stratigraphy (International Commission on Stratigraphy). Journal of Quatanary Science 27, 649–659.
Walker, M.J.C. et al., 2018. Formal ratification of the subdivision of the Holocene Series/ Epoch (Quaternary System/Period): two new Global Boundary Stratotype Sections and Points (GSSPs) and three new stages/ subseries. Episodes 41, 213–223.
Wang, L.B. et al., 2011. Sea surface temperature records of core ZY2 from the central mud area in the South Yellow Sea during last 6200 years and related effect of the Yellow Sea Warm Current. Chinese Science Bulltein 56, 1588–1595.
Wang, T., Surge, D., Mithen, S., 2012. Seasonal temperature variability of the Neoglacial (3300-2500BP) and Roman Warm Period (2500-1600BP) reconstructed from oxygen isotope ratios of limpet shells (Patella vulgata), Northwest Scotland. Palaeogeography Palaeoclimatology Palaeoecology 317–318, 104–113.
Wang, Y. et al., 2005. The Holocene Asian monsoon: links to solar changes and North Atlantic climate. Science 308, 854–857.
Wanner, H. et al., 2008. Mid- to Late Holocene climate change: an overview. Quatanary Science Reviews 27, 1791–1828.
Wanner, H., Mercolli, L., Grosjean, M., Ritz, S.P., 2015. Holocene climate variability and change; a data-based review. Journal of Geological Society London. 172, 254–263.
Watanabe, T.K., Watanabe, T., Yamazaki, A., Pfeiffer, M., 2019. Oman corals suggest that a stronger winter shamal season caused the Akkadian Empire (Mesopotamia) collapse. Geology 47, 1141–1145.
Wessel, P., Smith, W.H.F., 1998. New, improved version of generic mapping Tools released. EOS Transactions American Geophysical Union 79(47), 579.
Wilson, C.J.N., Walker, G.P.L., 1985. The Taupo eruption, New Zealand I. General Aspects. Philosophical Transactions of the *Royal Society A* 314, 199-228.

Yamamoto, M., Shiraiwa, Y., Inouye, I., 2000. Physiological responses of lipids in Emiliania huxleyi and Gephyrocapsa oceanica (Haptophyceae) to growth status and their implications for alkenone paleothermometry. Organic Geochemistry 31, 799–811.
Yamamoto, M., Suemune, R., and Oba, T., 2005, Equatorward shift of the subarctic boundary in the northwestern Pacific during the last deglaciation. Geophysical Research Letters 32, L05609.
Yamamoto, T., 1980. Climatic fluctuation in prehistoric Japan and its influence on the change of burial styles. Bulletin of Institution Study Economy Tokuyama Univ. 2, 95-103.
Yan, H. et al., 2011. A record of the Southern Oscillation Index for the past 2,000 years from precipitation proxies. Nature Geoscience 4, 611–614.
Yin, J., Su, Y., Fang, X., 2016. Climate change and social vicissitudes in China over the past two millennia. Quaternary Research 86, 133–143.
Yokoyama, Y. et al., 2019. A single stage Accelerator Mass Spectrometry at the Atmosphere and Ocean Research Institute, The University of Tokyo. Nuclear Instruments and Methods in Physics Research Section B 455, 311–316.
Yoshino, M., 2007. Overview of the Studies on Climate Change during the Historical Period. Journal of Geography 116 (6), 836–850 (in Japanese with English abstract).
Zhang, D.D., 2011. The causality analysis of climate change and large-scale human crisis, Proceedings of National Academy of Science 108, 17296-17301.
Zhang, Z. et al., 2010. Periodic climate cooling enhanced natural disasters and wars in China during AD 10-1900. Proceedings of the Royal Society B: Biological Science 277, 3745–3753.

Chapter III-A

第Ⅲ-A 章については、5 年以内に
雑誌等で刊行予定のため、非公開

Chapter III-B

第Ⅲ-A 章については、5 年以内に
雑誌等で刊行予定のため、非公開

Chapter IV

Berkelhammer, M., 2012. An Abrupt Shift in the Indian Monsoon 4000 Years Ago. Geophysical Monograph Series 198, 75-87.

Kawahata, H., 2019. Climatic reconstruction at the Sannai-Maruyama site between Bond events 4 and 3 –implication for the collapse of the society at 4.2 ka event. Progress in Earth and Planetary Science 6, 1–18.

Kitaba, I., Hyodo, M., Katoh, S., Dettman, D. L., Sato, H., 2013. Midlatitude cooling caused by geomagnetic field minimum during polarity reversal. Proceedings of the National Academy of Science 110(4), 1215-1220.

Griffiths, M. L. et al., 2020. End of Green Sahara amplified mid-to late Holocene megadroughts in mainland Southeast Asia. Nature communications 11(1), 1-12.

McClymont, E. L., Sosdian, S. M., Rosell-Melé, A., Rosenthal, Y., 2013. Pleistocene sea-surface temperature evolution: Early cooling, delayed glacial intensification, and implications for the mid-Pleistocene climate transition. Earth-Science Reviews 123, 173-193.

Ran, M., Chen, L., 2019. The 4.2 ka BP climatic event and its cultural responses. Quatanary International 521, 158–167.

Sakaguchi Y., 1983. Warm and Cold Stages in the Past 7600 Years in Japan and their Global Correlation. Bulletin of the Department of Geography University of Tokyo 15, 1–31.

Sun, Q. et al., 2019. Climate as a factor for Neolithic cultural collapses approximately 4000 years BP in China. Earth-Science Reviews 197, 102915.

Walker, M. et al., 2018. Formal ratification of the subdivision of the Holocene Series/Epoch (Quaternary System/Period): two new Global Boundary Stratotype Sections and Points (GSSPs) and three new stages/subseries. Episodes 41(4), 213-223.

Wanner, H. et al., 2008. Mid- to Late Holocene climate change: an overview. Quatanary Science Reviews 27, 1791–1828.

Zhang, D. D. et al., 2011. The causality analysis of climate change and large-scale human crisis. Proceedings of the National Academy of Sciences 108(42), 17296-17301.

Zhang, Z. et al., 2010. Periodic climate cooling enhanced natural disasters and wars in China during AD 10–1900. Proceedings of the Royal Society B: Biological Sciences 277(1701), 3745-3753.